

Receptors and Synapses in the MSO

Dissertation of the
Graduate School of Systemic Neurosciences of
Ludwig-Maximilians-Universität München

Submitted by
Kiri Couchman
München, February 2011

Oral Defense
May 6th 2011



First reviewer / supervisor

Dr. Felix Felmy

Second reviewer

Prof. Dr. Mark Hübener

Supervisor

Prof. Dr. Benedikt Grothe

Supported by the GRK 1091

*Yes, to dance beneath the diamond sky with one hand waving free
Silhouetted by the sea, circled by the circus sands*

-Bob Dylan

Contents

Summary	9
I Introduction.....	13
Sound localisation in mammals	16
Cellular and synaptic specialisations in the auditory pathway	19
Coincidence detection: strategies and cellular adaptations	23
Structure / function relationships in the MSO	26
Aims of this study	28
II Materials and Methods.....	33
Slice preparation	33
Electrophysiology	33
Electroporation	36
Immunohistochemistry and confocal microscopy	37
UV uncaging	37
Picospritzer pressure-application	39
Data and statistical analysis	41
III Quantifying synaptic input to adult MSO neurons.....	45
Excitatory and inhibitory inputs are large with fast kinetics	45
Synaptically evoked action potential threshold is unexpectedly high	48
Single inhibitory fibres contain many synaptic varicosities	50

IV Functional receptor and synapse distributions in the mature MSO 55

AMPA and NMDA receptors are differentially expressed.....	55
Excitatory inputs are predominantly AMPA receptor mediated	58
Glycine receptor distributions are developmentally invariant.....	59
Functional synaptic input to glycine receptors refines during development	61
Extra-synaptic glycine receptors are $\alpha\beta$ -heteromers	63
GABA _A receptors are present but lack synaptic input on mature MSO neurons	65

V NMDA receptors in the mature MSO 69

NMDA receptors can be synaptically activated	69
Synaptically released glycine potentiates NMDA receptors	72

VI Discussion 75

Size and strength of single inputs to MSO neurons.....	76
Functional mapping of receptors and synapses in the MSO.....	79
AMPA receptors and their inputs	82
The development of glycine receptors and their inputs.....	83
NMDA receptors and their role in the mature MSO circuit	83
GABA receptors and their role in the mature MSO circuit.....	85
Coincidence detection in MSO neurons	86
Consequences for ITD coding and sound localisation	88
List of acronyms and initialisms	93
List of Figures	97
Reference List	99

Summary

The ability to localise sound sources is vital to the survival of a species, as an important cue for identifying and responding to predators and prey and for intraspecies interactions. In mammals, the location of sound sources in the horizontal plane is processed in the auditory brainstem by a series of specialised nuclei. There are two neural pathways specialised to deal with the interaural cues that are created at different frequency ranges. High frequency sounds (>1.5 kHz for humans) are effectively ‘shadowed’ by the head, so that the amplitude of the sound at the ear closest to the sound source is larger. This cue, called the interaural level difference (ILD), is coded for by neurons in the lateral superior olive (LSO). For sounds at lower frequencies (<1.5 kHz), this shadowing effect is minimal, so the cue used instead involves a comparison between the arrival times of the sounds at the two ears. Even for sounds with a comparatively long wavelength, this interaural time difference (ITD) cue can be as short as tens of microseconds. The neural circuit underlying ITD coding is therefore one of the most temporally precise in the mammalian brain, containing highly specialised nuclei and recruiting some of the largest and fastest synapses in the brain. This circuit culminates in the neurons of the medial superior olive (MSO) which encode ITDs via a coincidence detection mechanism. As yet, the synaptic and cellular strategy underlying this uniquely precise coincidence detection mechanism is not fully understood.

From previous studies, it is known that MSO neurons code for ITDs by integrating a set of binaural excitatory and inhibitory inputs. Anatomical evidence suggests that these inputs are segregated, with excitatory inputs contacting dendritic segments and inhibitory inputs somatically targeted. In the mature circuit, these inputs are mediated by fast AMPA and glycine receptors to maintain temporal precision. Post-synaptically, MSO neurons have a low input resistance and fast membrane time constants which effectively limit input integration windows and may underlie much of the precision of this nucleus. Morphologically, MSO neurons are simple bipolar cells, with relatively short (~ 100 μ m), spineless dendrites with few major branch points at adult stages. Given the tight structure / function relationships typical in the auditory brainstem, the stereotyped input arrangement and simple morphology of MSO neurons may well influence the function of this nucleus.

In this study, an *in vitro* functional anatomical approach has been used to investigate the coincidence detection strategy employed by neurons of the MSO. Firstly, to determine the synaptic basis for coincidence detection in this nucleus, the size and strength of single excitatory and inhibitory inputs to adult MSO neurons was measured. In keeping with the general size and strength of auditory brainstem synapses, large single fibre currents were recorded for both excitatory and inhibitory inputs. However, to counter the fast leaky MSO membrane, the simultaneous activation of 2 - 4 excitatory fibres is required for action potential generation. Each MSO neuron was estimated to receive at least 4 - 8 excitatory inputs, and a detailed reconstruction of inhibitory inputs revealed that each neuron receives a total of 2 - 3 inhibitory inputs. Coincidence detection in the MSO is therefore possible with the integration of a minimal number of large synaptic inputs.

On the post-synaptic membrane, the distribution of AMPA, NMDA, glycine (Gly) and GABA_A receptors (Rs) and their synaptic inputs were investigated, producing several novel findings. Firstly, excitatory and inhibitory inputs are not strictly segregated as both target the soma and proximal dendrites. The profile of GlyRs remains developmentally constant despite a refining synaptic input, exposing an extra-synaptic population of GlyRs on the dendrites of mature MSO neurons. The maintenance of NMDARs and GABA_{AR}s in the mature MSO was uncovered, although likely in extra-synaptic roles. Additionally, the potentiation of NMDAR currents at the MSO soma by synaptically released glycine is demonstrated.

These findings add a further level of complexity to our understanding of MSO function as a model for both general coincidence detection mechanisms and fast synaptic transmission. In terms of sound localisation, the integration of fewer, larger synaptic inputs may provide the system with the necessary precision to encode ITDs on the microsecond time scale. The presence of possible extra-synaptic modulators suggests that further, more subtle modulation of the circuit may be possible. The behavioural role of such modulation is discussed in the context of the transition between quiet and noisy environments with the simultaneous maintenance of hard-wired ITD coding in individual MSO neurons.

I

Introduction

The ability to quickly and accurately localise sound underlies behaviours from basic predator / prey interactions to more complex mating and social behaviours. The neural representation of sound source location is an interesting challenge as unlike in other sensory systems such as vision or somatosensation, auditory input can not be directly represented as a receptor surface map. Instead, the brain must decode a combination of frequency, timing and intensity information to reconstruct auditory space. This is no easy task as sound waves travel in air at ~ 340 m/s, and single sound sources typically produce complex signals modulated both in frequency and amplitude. Once more than one sound source is present, the task becomes much more difficult to complete, with added complexity if the environment is reverberant. Nonetheless, sound localisation systems throughout the animal kingdom are incredibly accurate. Humans are capable of identifying differences in the location of pure tone sound sources down to a single degree (Mills, 1958; Perrott and Saberi, 1990). This level of acuity is due to our ability to exploit position-specific cues arising from spectral interference created by the head and ears of the listener. These minute cues are decoded by extremely precise neuronal circuits. For localising sounds in the vertical plane (elevation), listeners exploit the differential modulation of the sound by the external ear (pinna) which creates ‘notches’ in sound spectra unique to a vertical location (Gardner and Gardner, 1973; Rice et al., 1992). In the horizontal (azimuthal) plane, two binaural cues are used for sound localisation: the intensity and time differences between sounds arriving at the two ears. In mammals, differences between the relative intensity and timing of sounds at the two ears are processed in parallel streams in the auditory brainstem. These principles were united into a duplex theory of azimuthal

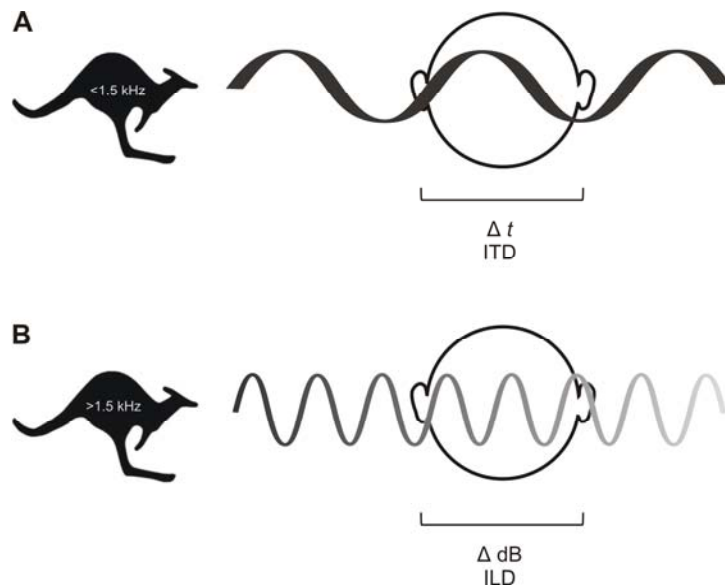


Figure 1.1 ITDs and ILDs

A: For low frequency sounds the interaural level difference (ILD) is used as a sound localisation cue. This system takes advantage of the microsecond-scale differences in the arrival times of the sounds between the two ears (Δt). **B:** For high frequency sounds, sound intensity is significantly attenuated by the head. These sounds are localised using the interaural loudness difference (ILD), or the difference in the intensity of the sounds between the two ears (ΔdB).

sound localisation in Lord Rayleigh's seminal paper 'On our perception of sound direction' (Rayleigh, 1907).

At the simplest level, when a distant sound source emits a single pure tone, the function of these two systems can be largely separated. For human listeners, at low frequencies (<1.5 kHz), the main cue utilised for sound source location is the interaural time difference (ITD), or the difference between the arrival times of a sound at the two ears (Rayleigh, 1907). This system relies on identifying individual phases in the sound wave between the two ears, so the wavelength of the tone must be larger than the width of the head (Figure 1.1A). For humans, the physiological range of ITDs is therefore up to $\sim 700 \mu\text{s}$. For pure tones at higher frequencies, this strategy is no longer available, likely due to limitations in the temporal precision of the peripheral auditory system (Palmer and Russell, 1986). Instead, the interaural level difference (ILD), or the relative difference between the loudness of a sound at the two ears, is exploited (Thompson, 1882). ILDs are created as the head shadows sounds originating from contralateral sources, thereby creating a relative

difference in amplitude between the two ears (Figure 1.1B). These localisation systems are incredibly precise, with human listeners being able to distinguish ITDs of 10 μ s and ILDs of 0.5 dB (Mills, 1958; Perrott and Saberi, 1990). There are exceptions to the strict ITD/ILD dichotomy. Although in general low frequency sounds travel farther and fail to generate significant ILDs, in the near-field, (<1 - 2 m) significant ILDs can be produced and used for localisation (Brungart and Rabinowitz, 1999; Shinn-Cunningham et al., 2000). ITDs can also be used for localising high frequency sounds if they are amplitude modulated at low frequencies, by taking advantage of these ‘envelope’ ITDs (Batra et al., 1993; Joris and Yin, 1995; Griffin et al., 2005).

In 1948, Jeffress published a model for ITD processing that dominated thinking in the auditory community for the next 50 years. This elegant model relied firstly on the premise that ITD processing involves the integration of binaural inputs that are capable of firing precisely and repetitively to specific phases of a sound wave (‘phase-locking’). Further, that these phase locked inputs would culminate in an array of coincidence detector neurons connected with a series of axonal delay lines that could compensate for the delay between the ears, causing maximal firing when this ‘characteristic delay’ occurred between the binaural inputs (Jeffress, 1948). This elegant arrangement has been demonstrated in the avian auditory brainstem, where axons of nucleus magnocellularis (NM) neurons form ladder-like innervations to the coincidence detector neurons of the nucleus laminaris (NL) (Parks and Rubel, 1975; Carr and Konishi, 1990; Overholt et al., 1992; Joseph and Hyson, 1993), which fire maximally to coincident inputs (Reyes et al., 1996). It is increasingly apparent, however, that mammals possess an analogous system employing an entirely different strategy (for review, see Grothe, 2003 and McAlpine and Grothe, 2003). In this model, delay lines are replaced by a fast, phasic inhibitory input which precedes the excitation, shifting the overall PSP to bring inputs into coincidence. There are several lines of evidence to suggest that mammals are employing a different strategy. Firstly, there is little evidence for systematic axonal delay lines to the coincidence detector neurons in the medial superior olive (MSO) of the mammalian auditory brainstem. Further, in addition to the binaural excitatory inputs present in the NL, MSO neurons require a phase-locked inhibitory input in order to code for a range of ITDs (Brand et al., 2002; Pecka et al., 2008). Finally, MSO neurons often fire maximally outside of the physiologically relevant range of ITDs (Fitzpatrick et al., 2000; McAlpine et al., 2001; Brand et al., 2002), making it unlikely that they use peak firing rates to code for sound source location. The result is

that unlike in the avian NL, where ITDs are represented by a topographic ‘place code’ (Jeffress, 1948; Carr and Konishi, 1990), the mammalian system relies on a comparison between a more diffuse ‘population code’ produced by the MSO in each brain hemisphere (McAlpine et al., 2001).

Sound localisation in mammals

The mammalian sound localisation pathway begins with a number of specialised structures that detect and filter sound information, converting it from physical waves in a medium to electrical impulses the brain can understand (Figure 1.2). The process of sound localisation starts when sound waves impinge upon the head and ears of the listener, refracting and reflecting in unique ways according to the shape and size of the head and the convolutions of the pinna. Sound is then funneled into the ear canal where all of the temporal and spectral complexities of multiple sound sources are simplified to a 2-dimensional movement of the tympanum; in and out. These vibrations are conducted to the ossicles, three small bones located in the gas-filled cavum tympani, linking the tympanic membrane to the smaller oval window of the cochlea. The ossicles allow for the efficient transfer of vibrations from air to the fluid endolymph of the cochlea without the massive loss in amplitude that might otherwise accompany such a change in medium viscosity (Figure 1.2).

The next step in sound processing involves frequency decomposition at the level of the cochlea, and the establishment of a spatial map of frequencies, or ‘tonotopic’ map (Von Békésy, 1960). The cochlea itself is an elegant cone-shaped spiral structure, much like a snail shell, filled with a relatively non-compressible endolymphatic fluid. Two membranes at the base of the cochlea, the oval and round windows, move in concert to convert sound waves from the outer ear to pressure waves which travel along the length of the cochlea. These pressure waves cause vibrations in the basilar membrane, suspended along the longitudinal axis of the cochlea. The basilar membrane is graded in both width and stiffness, decreasing progressively from the base of the cochlea to the tip. It is this gradient that creates a tonotopic map of resonant frequencies along the length of the membrane, with higher frequencies causing resonant vibrations at the base of the cochlea, and lower frequencies at the thinner end (Von Békésy, 1960). Membrane deflections at resonant

points are detected by the hair cells, which act as mechanotransducers, converting the mechanical energy of these deflections into graded electrochemical potentials. Large, specialised, ‘ribbon’ synapses at the base of the inner hair cells (IHCs) transfer these graded responses to binary action potential (AP) responses in type 1 spiral ganglion neurons (SGNs). This first synapse of the auditory pathway is the first of many unique specialisations in this sensory system that allows for the transmission of synaptic activity at extremely high frequencies. The axons of SGNs form the 8th (auditory) cranial nerve which transfers sound information, now filtered into narrow frequency channels, to the cochlear nucleus (CN) in the auditory brainstem (De No, 1933; Warr, 1966; Osen, 1969).

There are two fairly distinct nuclei in the auditory brainstem of mammals for dealing with ITD and ILD information, each receiving a characteristic set of inputs driven by neurons in the CN (Figure 1.3). In the anterior-ventral part of the CN (AVCN), SGN axons form large endbulb of Held synapses on globular and spherical bushy cells (Osen, 1969; Warr, 1972). These bushy cells provide input to the superior olivary complex (SOC). Spherical bushy cells provide excitatory input to both the MSO and LSO (Osen, 1969; Warr, 1972; Cant and Casseday, 1986), where binaural sound localisation cues are processed. Globular bushy cells drive an indirect inhibitory input into the MSO and LSO, via a one-to-one specialised synaptic connection with MNTB neurons (Held, 1893; Spangler et al., 1985; Kuwabara et al., 1991; Smith et al., 1991). MNTB neurons then provide a strong inhibitory input to both the MSO and LSO (Cant and Hyson, 1992). Generally speaking, neurons of the MSO produce an output code for ITDs whilst LSO neurons code for ILDs (Boudreau and Tsuchitani, 1968).

The neurons of the MSO process ITDs using a coincidence detection mechanism (Goldberg and Brown, 1969; Yin and Chan, 1990; Brand et al., 2002). Operating on microsecond timescales, these neurons perform the most precise coincidence detection in the mammalian brain. Principal neurons of the MSO integrate excitatory inputs arising from the AVCN of both ears (Stotler, 1953; Clark, 1969; Kil et al., 1995), as well as a substantial inhibitory input from the contralateral MNTB (Clark, 1969; Cant and Hyson, 1992; Kuwabara and Zook, 1992; Kapfer et al., 2002). The LNTB provides an additional, though likely minor, inhibitory input (Cant and Hyson, 1992; Grothe and Sanes, 1993; Couchman et al., 2010). In comparison, neurons of the LSO receive excitatory ipsilateral input from the AVCN (Stotler, 1953; Cant and Casseday, 1986; Thompson and Thompson,

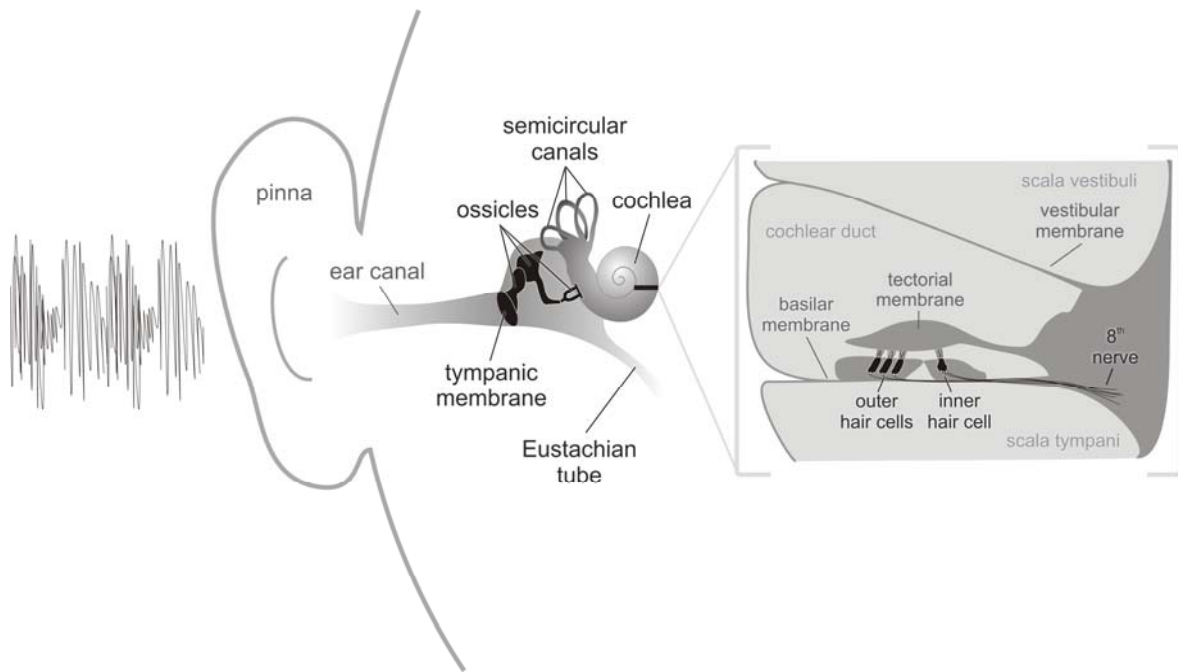


Figure 1.2 The ear

Diagram showing the major steps in the transfer of sound from the environment (left) through the outer and inner ear to the auditory nerve (right). Airborne sounds interact with the pinna, and are funnelled into the ear canal (external auditory meatus) to the tympanic membrane. Movements of this membrane are transferred via the ossicles (malleus, incus and stapes) to the round window of the cochlea. The semicircular canals are responsible for tracking head movements in three directions, whilst the Eustachian tube allows mucus drainage and pressure equalisation by connecting the middle ear with the pharynx. Inset: In the cochlea, pressure waves cause the basilar membrane to vibrate, activating inner and outer hair cells as their stereocilia bend on contact with the tectorial membrane. Incoming sounds are decomposed into narrow frequency bands at this stage as resonant points on the basilar membrane map frequency into a spatial tonotopic map along spiral of the cochlea. Graded responses from the hair cells are then transferred to the dendrites of spiral ganglion neurons, whose axons form the 8th (auditory) nerve that then innervates brainstem structures.

1987), and a contralateral inhibitory input via the MNTB (Moore and Caspary, 1983; Kuwabara and Zook, 1992). Simply put, ILD coding therefore relies on a comparison of the relative strengths of the input from the two ears so that the input driven by the ear with the largest sound amplitude will determine the response of the neuron (Galambos et al., 1959; Tsuchitani and Boudreau, 1966; Boudreau and Tsuchitani, 1968; Caird and Klinke, 1983).

From the SOC, neurons of MSO and LSO both project to the inferior colliculus (IC) (Zook and Casseday, 1982; Caird and Klinke, 1987) via the nuclei of the lateral lemniscus (NLL)

(Adams, 1979; Glendenning et al., 1981; Benson and Cant, 2008). The precise functions of the NLL are only poorly understood, though it is known that each nucleus has differing temporal response properties and input patterns (Covey and Casseday, 1991; Batra, 2006; Kuwada et al., 2006). The IC is a complex structure whose precise computations, though long studied, are also little understood. In general, the IC is a main processing hub for ascending (Adams, 1979) and descending (Saldana et al., 1996) auditory projections, containing neurons sensitive to monaural or binaural auditory cues (Rose et al., 1966). Broadly speaking, neurons of the IC play an important role in converting the precise temporal code of auditory information from brainstem nuclei into a slower rate code for further processing in higher centres (for review, see Joris et al., 2004). From the IC, auditory information is sent to the medial geniculate nucleus (MGN) in the thalamus (Moore and Goldberg, 1966), which in turn has strong reciprocal connections with the auditory cortex (AC) (Ryugo and Weinberger, 1976; Clerici and Coleman, 1990; Budinger et al., 2000; Budinger et al., 2008).

Cellular and synaptic specialisations in the auditory pathway

The binaural sound localisation system, from the very first synapse in the inner ear, possesses unique synaptic and cellular specialisations required for the temporally precise coding of auditory information. These neurons and their output synapses are all configured to respond to the challenges of processing and transmitting timing information: they are highly precise across large gain ranges, whilst transferring information rapidly and with extremely high fidelity. One of the recurring motifs in the auditory brainstem is the ability of neurons and synaptic inputs to ‘phase-lock’, often at a specific or ‘best’ frequency, responding precisely at a consistent phase of the stimulus often up to several hundred hertz. Additionally, SGNs (Chen, 1997; Szabo et al., 2002; Rusznak and Szucs, 2009), bushy cells (Oertel, 1983; Manis and Marx, 1991), MNTB neurons (Banks et al., 1993; Johnston et al., 2010), maintain precision through rapid membrane kinetics shaped by low-voltage activated potassium channels (K_{LVA}) and the hyperpolarisation-activated depolarising current, I_h (Koch et al., 2004). High-voltage activated potassium currents (K_{HVA}) are also widely expressed, shortening AP half-widths and speeding up membrane repolarisation between APs (Perney and Kaczmarek, 1997). Additionally, the synapses of the ITD pathway are highly specialised, often with large single fibre quanta and fast

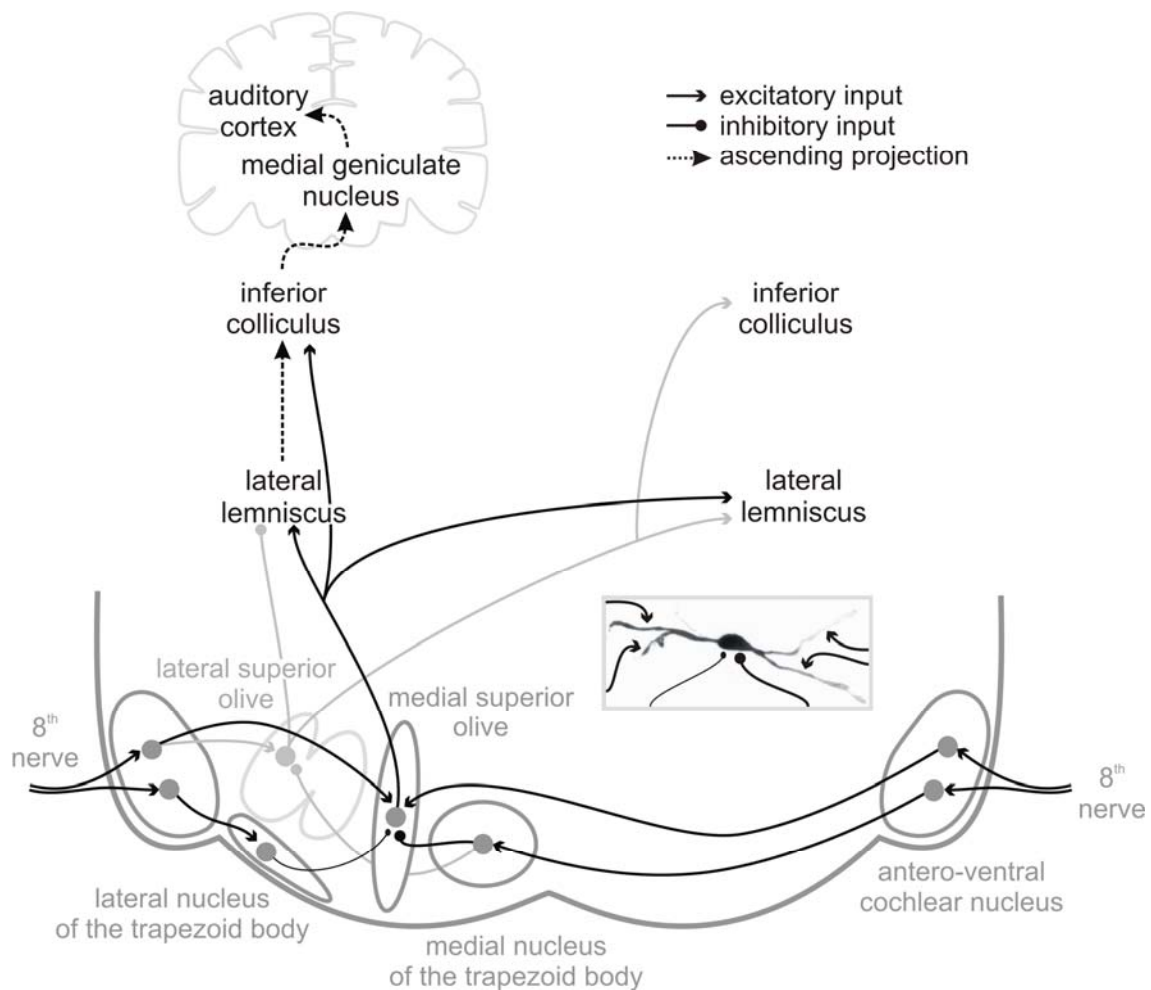


Figure 1. 3 Mammalian ascending auditory pathways for ITD and ILD processing

The major nuclei and their connectivity in the ascending auditory pathways responsible for ITD (in black) and ILD (in grey) processing. Only one side of the pathway is shown, and only the major nuclei and connections. The 8th nerve innervates the cochlear nucleus, including the antero-ventral part (AVCN). Here, spherical bushy cells provide input to excitatory brainstem nuclei (lateral and medial superior olives; LSO and MSO) while globular bushy cells provide an input to inhibitory nuclei (lateral and medial nuclei of the trapezoid body; LNTB and MNTB). Inset: Reconstructed principal MSO neuron showing major input locations. Neurons in the MSO use a coincidence detection mechanism on bilateral excitatory inputs (from the AVCN), which are segregated onto the dendrite of the side of origin. An additional major inhibitory input from the ipsilateral MNTB targets the soma and is vital for ITD coding. Both the LSO and MSO then project to the nuclei of the lateral lemniscus and the inferior colliculus. Auditory information is then passed to higher centres in the thalamus, specifically the medial geniculate nucleus, and then on to the primary auditory cortex in the temporal lobe

synaptic kinetics which compensate for high post-synaptic current (PSC) thresholds.

These specifications help to transfer timing, frequency and intensity cues along divergent auditory pathways each specialised for specific computational tasks. In the following, specialisations in neuronal and synaptic properties are surveyed in the circuit encoding ITDs.

The first neurons in the ITD pathway, the IHCs, produce a tonic, graded output (Sewell, 1984; Robertson and Paki, 2002) that must precisely maintain both intensity and timing information. In order to do this, IHCs dynamically modulate their membrane kinetics through voltage-dependent conductances, favouring either modulation speed or sensitivity depending on the sound environment (Kros et al., 1998; Fuchs, 2005). Inner hair cells provide an excitatory glutamatergic synaptic input synapse onto type 1 SGNs (Kellerhals, 1967; Godfrey et al., 1976; Drescher and Drescher, 1992). Each post-synaptic SGN may form synapses with multiple inner hair cells (Berglund and Ryugo, 1987; Liberman et al., 1990), but is innervated by only a single massive release site from each one (Kiang et al., 1982; Spoendlin, 1985). At a single release site, a pool of \sim 100 synaptic vesicles is stabilised to a ribbon tether (Smith and Sjostrand, 1961; Liberman et al., 1990; Lenzi et al., 1999) to generate a readily-releasable pool of anywhere between \sim 15 - 50 vesicles (Moser and Beutner, 2000; Spassova et al., 2004; Khimich et al., 2005). The constant release of synaptic vesicles produces bursts of PSCs each on the order of \sim 150 pA, mediated almost entirely by fast 2-amino-3-(5-methyl-3-oxo-1,2-oxazol-4-yl) propanoic acid receptors (AMPARs) (Matsubara et al., 1996; Ruel et al., 2000; Glowatzki and Fuchs, 2002). This synapse also exhibits short-term depression (STD), leading to a rapid adaptation in the SGN response which is thought to be important for the processing of complex sounds (Moser and Beutner, 2000; Spassova et al., 2004). This combination of pre- and post-synaptic specialisations allows this first synapse in the auditory system to maintain both precise timing and intensity information (Rose et al., 1967), and transfer this information in narrow frequency filters into the auditory brainstem.

At the next synapse in the ITD pathway, type 1 SGNs produce large endbulb of Held synaptic terminals onto bushy cells in the AVCN (Brawer and Morest, 1975). Each endbulb contains 100 - 200 synaptic specialisations (Cant and Morest, 1979; Nicol and Walmsley, 2002). Post-synaptically, AMPARs containing fast GluR2 (Gardner et al., 2001), and likely also GluR4 (Caicedo and Eybalin, 1999) subunits mediate excitatory post-synaptic currents (EPSCs) with peak amplitudes of up to 10 - 20 nA (Gardner et al., 2001; Wang and Manis,

2008; Chanda and Xu-Friedman, 2010). These currents are produced by a readily-releasable pool of at least 100 vesicles in each endbulb (Oleskevich et al., 2004). Although this synapse maintains precise timing information so that *in vivo* most bushy cells have firing properties almost indistinguishable from SGNs (Pfeiffer, 1966; Rhode et al., 1983), it is more than just a relay. Between 2 and 4 endbulb terminals innervate each bushy cell (Sento and Ryugo, 1989; Ryugo and Sento, 1991; Chanda and Xu-Friedman, 2010) and their integration has been shown to increase phase locking precision (Oertel, 1985; Rothman et al., 1993; Joris et al., 1994; Spirou et al., 2005; Xu-Friedman and Regehr, 2005). The input/output function of these neurons may also be dynamic, with evidence that signalling through gamma aminobutyric acid receptors (GABARs) could convert the circuit from a relay at low stimulus rates to a coincidence detector at higher rates (Chanda and Xu-Friedman, 2010). These characteristics allow bushy cells to integrate substantial synaptic inputs using fast membrane kinetics to maintain and in some circumstances sharpen the temporal precision of auditory information.

At the next synapse in the ITD pathway, globular bushy cells innervate MNTB neurons with one of the largest synapses in the mammalian brain (Held, 1893). Each MNTB neuron receives only one calyx of Held synapse which covers around half of the soma surface and contains several hundred active zones which support a readily releasable pool of ~1000 vesicles (Schneggenburger et al., 1999; Wu and Borst, 1999; Taschenberger and von Gersdorff, 2000; Satzler et al., 2002; Taschenberger et al., 2002). This calyx of Held synapse is extremely secure, driving MNTB neurons with almost perfect efficacy at extremely high rates (Forsythe, 1994; Smith et al., 1998; Englitz et al., 2009; Lorteije et al., 2009). When activated, the calyx rapidly drives the cell to threshold with a synaptic delay of around 500 μ s (Taschenberger and von Gersdorff, 2000; Englitz et al., 2009; Typlt et al., 2010). At mature stages, EPSCs reach peaks of ~10 - 30 nA, and are mediated almost exclusively by fast GluR2 and GluR4 subunit-containing AMPA receptors (Futai et al., 2001; Joshi and Wang, 2002; Koike-Tani et al., 2005). These specialisations allow MNTB neurons to rapidly invert their phase-locked excitatory input to produce an inhibitory glycinergic output that maintains much of this timing information.

There has been some investigation into the inputs to MSO neurons, although much of this data is anatomical, or limited to the developing system. It is known that neurons in the MSO have a membrane time constant on the order of hundreds of microseconds an input

resistance of 5 - 7 MΩ (Magnusson et al., 2005; Scott et al., 2005; Chirila et al., 2007; Couchman et al., 2010), meaning that small or asynchronous currents can be rapidly shunted. MSO neurons set their resting membrane potential with a dynamic balance between I_h (Koch et al., 2004; Golding et al., 2009) and K_{LVA} conductances (Scott et al., 2005; Mathews et al., 2010). As both of these conductances are already open at rest (-60 mV) (Golding et al., 2009; Mathews et al., 2010), this neuron is able to respond extremely rapidly to voltage deflections, meaning that the post-synaptic potential (PSP) is almost as fast as the underlying PSC, further tightening the coincidence detection window by limiting summation of PSCs (Couchman et al., 2010). This also means that large synaptic currents are likely required for AP generation and for inhibitory inputs to have a significant impact. Indeed, there is ultrastructural evidence for multiple active zones on both excitatory and inhibitory synaptic boutons contacting the MSO (Clark, 1969; Lindsey, 1975; Kiss and Majorossy, 1983; Brunso-Bechtold et al., 1990; Kapfer et al., 2002).

All synapses upstream to the MSO are highly specialised for high fidelity transmission at extremely high frequencies. These calyceal synapses maintain timing information and reduce synaptic jitter by providing a large synaptic drive to the post-synaptic neuron with few failures. Post-synaptically, neurons in the ITD pathway are specialised for speed with fast membrane time constants and low input resistances, partly due to the widespread expression of K_{LVA} and I_h conductances. *In vivo* studies show that MSO neurons, as the output of the ITD circuit, maintain the ability to fire at very high frequencies (Yin and Chan, 1990), locking precisely to the phase of pure tones (Brand et al., 2002). It is therefore expected that synaptic input to MSO neurons would maintain these strategies for ensuring temporal precision and high fidelity information transfer. The hypothesis is therefore that the recruitment of a set of strong and fast synaptic inputs establishes the pre-synaptic basis for the exquisite coincidence detection in MSO neurons.

Coincidence detection: strategies and cellular adaptations

Coincidence detector neurons employ different input strategies to establish and maintain fine temporal precision. Coincidence detection, in terms of input timing, is a common mechanism in the brain, although it operates across vastly different timescales and in different functional roles in different areas. Coincidence detector neurons must essentially

limit the integration of inputs, either spatially in different cellular compartments, or temporally by limiting the time window of integration. In the auditory system, high temporal precision is maintained using short integration windows. This means that these neurons discard non-coincident excitatory post-synaptic potentials (EPSPs) in order to maintain timing information, whereas on the other end of the scale, ‘integrator’ neurons would sum EPSPs over long time periods, with a loss of fine timing information (for review, see Konig et al., 1996). The integration of inputs can be regulated by passive properties such as neuron and input morphology, or active, activity-dependent processes such as voltage-dependent or second-messenger activating channels, as elaborated in the following.

In the cortex, the idea of pyramidal neurons acting as spatio-temporal coincidence detectors, both at the whole neuron level and within specific cellular compartments, is not a new one. Morphologically, pyramidal neurons are complex, allowing for the electrical compartmentalisation of inputs, especially at distal dendritic sites. Thus, the generation of APs in pyramidal neurons depends on coincidence detection at many levels. Within dendritic branches, the production of dendritic Na^+ or Ca^{2+} spikes in single branches relies on the simultaneous activation of multiple input sites (Schiller et al., 1997; Stuart et al., 1997; Polsky et al., 2004; Kampa and Stuart, 2006). The large-scale activation of distal inputs to pyramidal neurons can further modulate coincidence detection by facilitating propagation (Losonczy et al., 2008), or effectively silencing entire dendritic compartments (Jarsky et al., 2005). A further level of coincidence detection occurs at the interaction between dendritic and somatic compartments. For example, somatic synaptic inputs can trigger back-propagating action potentials which excite large parts of the dendritic tree, in turn causing Ca^{2+} spikes that invade the soma, where they can again interact with somatic synaptic inputs to generate APs (Larkum et al., 1999). Input integration in pyramidal neurons is therefore strongly influenced by their complex morphology and tightly regulated channel expression patterns, creating complex structure/function interactions. Similar interactions between dendritic structure and function in coincidence detection have been shown in granule cells in the dentate gyrus (Schmidt-Hieber et al., 2007). Aside from morphology, the complex interactions in pyramidal neurons can be modulated by a number of other mechanisms. Neuromodulators such as serotonin, GABA (through GABA_B receptors) and glutamate (through mGluRs), acetylcholine and norepinephrine (by modulating I_h) have been shown to influence input integration and therefore pyramidal

neuron activity (for review, see Sjostrom et al., 2008). Coincidence detection in cortical areas therefore involves often complex interplays between thousands of synaptic input sites to complete complex computational operations between distinct cellular compartments.

In comparison with cortical neurons, coincidence detector neurons in the auditory brainstem are generally simpler, both in terms of morphology and electrical compartmentalisation. The interactions between inputs are therefore more straightforward, although there is still great variation in the number, strength, relative timing and modulation of inputs to coincidence detector neurons in the auditory system. For example, octopus cells in the CN (Golding et al., 1995; Oertel et al., 2000) and neurons in the chick NL (Reyes et al., 1996; Agmon-Snir et al., 1998; Kuba et al., 2002a; Cook et al., 2003; Kuba et al., 2006) integrate a large number of small, independent fibre inputs. In contrast, the endbulb of Held synapses on bushy cells operate with a minimal number of large excitatory input fibres (Joris and Yin, 1995; Xu-Friedman and Regehr, 2005). As yet, the synaptic basis for coincidence detection in the MSO is unknown. This lack of precise biophysical data on mammalian binaural coincidence detection has resulted in computational models with diverse estimates of input number and strength (Kempter et al., 1998; Brand et al., 2002; Cook et al., 2003; Grau-Serrat et al., 2003; Kuba et al., 2006; Ashida et al., 2007). This uncertainty has hampered the development of an in-depth cellular understanding of this circuit.

In the auditory brainstem, in terms of post-synaptic properties, coincidence detection at the whole cell level operates on much shorter timescales than in cortical areas, relying on essentially simpler computations regarding input timing. For example, octopus cells have fast membrane kinetics and express K_{LVA} (Ferragamo and Oertel, 2002) and I_h conductances (Bal and Oertel, 2000) to sharpen coincidence detection. In the NL, although ITD coding is achieved through a different circuit mechanism than that of mammals (for review, see Grothe, 2003), similar cellular mechanisms are employed in coincidence detection (Kuba, 2007). As in the analogous MSO, neurons of the NL express fast AMPA receptor isoforms to speed up the EPSP time-course (Ravindranathan et al., 2000) and limit summation (Kuba et al., 2003). NL neurons also have a low input resistance, and express K_{LVA} (Kuba et al., 2005) and I_h (Yamada et al., 2005) conductances that activate near the resting potential to shorten coincidence detection windows (Kuba et al., 2002b). Thus despite their markedly different circuit function, coincidence detector neurons in the

auditory brainstem employ similar post-synaptic strategies to reach microsecond scale coincidence detection resolutions.

Structure / function relationships in the MSO

The unique morphological specialisations of synaptic connections strongly influence the precision of temporal computations in the auditory brainstem. As in other nuclei, the main input to MSO neurons appears highly stereotyped, and this morphological arrangement is thought to have functional consequences (Agmon-Snir et al., 1998; Zhou et al., 2005). Specifically, glutamatergic excitation is supposed to be largely dendritic, with ipsilateral input targeting the lateral dendrite and contralateral input the medial (Stotler, 1953; Clark, 1969; Smith et al., 1993; Kil et al., 1995). In contrast, glycinergic inhibitory inputs are thought to target the soma and proximal dendrites (Clark, 1969; Kuwabara and Zook, 1992; Kapfer et al., 2002; Couchman et al., 2010). Given the relationship between structural and functional specialisations typical in the auditory brainstem, this apparent segregation of input location could well be important for determining input integration rules, thereby setting coincidence detection windows.

In the auditory brainstem, the major neurotransmitter systems are glutamate, glycine and GABA. Early in postnatal development, N-methyl-D-aspartate glutamate receptors (NMDARs) can be synaptically activated (Smith et al., 2000) but are strongly down-regulated at synapses of the mature superior olivary complex (SOC) (Zhou and Parks, 1993; Kotak and Sanes, 1996; Futai et al., 2001). Functional expression of GABA_ARs also undergoes a developmental down regulation and these receptors are thought to be absent from synapses in the mature ITD pathway (Kotak et al., 1998; Smith et al., 2000; Nabekura et al., 2004). Therefore, at mature stages, glutamatergic input from the AVCN is thought to be mediated exclusively by AMPARs, whilst inhibitory inputs from the MNTB are solely glycinergic. The transfer of synaptic transmission to ‘faster’ AMPARs and glycine receptors (GlyRs) is thought to be important for developing temporal precision in the MSO (Smith et al., 2000).

In addition to a general switch in transmitter and receptor types, the molecular identity of both AMPARs and GlyRs is developmentally modulated. Specifically, the subunit

composition of heterotetrameric AMPARs (Sobolevsky et al., 2009) switches from GluR1 and GluR2 to predominantly GluR4 subunits during development (Caicedo and Eybalin, 1999), with a concomitant speeding up of channel kinetics (Koike-Tani et al., 2005) and an increase in single channel conductance (Swanson et al., 1997). GlyRs are heteropentameric channels, with synaptic receptors generally consisting of three α pore-forming and two β scaffolding subunits (Langosch et al., 1988; Kuhse et al., 1993). During development, α subunits change from embryonic $\alpha 2$ to $\alpha 1$ forms (Friauf et al., 1997), resulting in a decrease in channel open times (Takahashi et al., 1992). GlyRs in general change rapidly between several conductance states, with the main state in $\alpha 2/\beta$ receptors (54 pS) slightly larger than $\alpha 1/\beta$ (44 pS) (Bormann et al., 1993). This subunit change also decreases the affinity of GlyRs for glycine (Handford et al., 1996), an important adaptation for the high concentrations encountered in the synaptic cleft. This developmental speeding up of channel kinetics during development should result in faster PSC kinetics, further reducing the effective coincidence detection window in mature MSO neurons.

As well as imposing direct excitatory or inhibitory drive, neurotransmitter systems interact on various levels on the post-synaptic neuron. On the whole cell level, inhibition and excitation interact to balance their overall strength (Haider et al., 2006; Couchman et al., 2010; Dorrn et al., 2010; Sun et al., 2010). On the receptor level, accessory neurotransmitters modulate responses to the primary agonist neurotransmitter (Liu et al.; Malenka and Nicoll, 1993; Farrant and Nusser, 2005; Li et al., 2009). These accessory neurotransmitters can originate from direct synaptic transmission, synaptic spillover or ambient volume transmission. Neurotransmitter accumulating from these sources can act on receptors both in the PSD and across the entire surface of a neuron. The actions of accumulated neurotransmitter are difficult to detect in *in vitro* preparations, but can have profound effects on synaptic transmission and cellular computation (Chen et al.; Semyanov et al., 2004).

On the post-synaptic membrane, neurons express a multitude of neurotransmitter receptors. Ionotropic neurotransmitter receptors for glutamate, glycine and GABA can be highly mobile, often only transiently clustering at post-synaptic densities (PSDs) (Srinivasan et al., 1990; Meier et al., 2001; Borgdorff and Choquet, 2002). Classical electrical stimulation of synaptic inputs typically describes only those receptors in the vicinity of a synapse, thereby neglecting the physiology of a large proportion of the total population of receptors

inserted into the membrane. In contrast, UV ‘uncaging’ of neurotransmitters can be used to develop subcellular functional maps of neurotransmitter receptors across the entire neuronal membrane (Callaway and Katz, 1993). Knowledge of such distributions provides insight into synaptic input location and relative efficacy (Pettit and Augustine, 2000), as well as post-synaptic integration mechanisms and possible interactions between neurotransmitter systems (Eder et al., 2001; Eder et al., 2003).

Other than the primary neurotransmitters mediating direct synaptic transmission in the auditory brainstem, it has become apparent that a number of secondary neurotransmitters act as activity dependent modulators throughout the ITD circuit. In the cochlear nucleus of the mouse, GABARs are expressed both pre-synaptically on the endbulb of Held and post-synaptically on bushy cells and may differentially modulate high-frequency firing (Chanda and Xu-Friedman, 2010). In the bat cochlear nucleus, noradrenaline application reduces spontaneous activity and increased onset responses by decreasing latency jitter (Kossl and Vater, 1989). At the calyx of Held synapse in the rat, pre-synaptic cannabinoid (Kushmerick et al., 2004) and adrenergic (Leao and Von Gersdorff, 2002) receptors decrease glutamate release, thereby supporting high frequency firing. Post-synaptically, in rat MNTB neurons, cAMP and norepinephrine modulate I_h currents and therefore the resting membrane potential (Banks et al., 1993). Though minimal, NMDAR signalling is also maintained into maturity in the mouse MNTB where it may activate second messenger systems by regulating calcium influx (Steinert et al., 2010). In the LSO, GABA released by the dendrites of LSO neurons dynamically modulates ILD sensitivity *in vivo* (Magnusson et al., 2008). Finally, at the MNTB to MSO synapse of gerbils, pre-synaptic GABA_BRs can modulate glycine release (Hassfurth et al., 2010). The presence of such diverse neuromodulators in the auditory brainstem points to their importance in auditory processing.

Aims of this study

To elucidate the presence and distribution of ionotropic receptors and synaptic inputs and their potential interactions, a neuronal system with low morphological complexity and well defined inputs is an advantage. Neurons in the MSO are ideal candidates for functional neurotransmitter receptor mapping using UV uncaging, with a simple and stereotyped

morphology, and a well defined synaptic input pattern (Grothe, 2003). Typically bipolar, the dendrites of MSO neurons are short ($\sim 150 \mu\text{m}$), spineless and remain largely uniform in diameter along their length (Rautenberg et al., 2009). Once leak currents are minimised with pharmacology or a Cs^+ -based internal solution, these short, stumpy dendrites limit dendritic filtering during recording (Williams and Mitchell, 2008). The lack of spines makes the identification of synaptic input sites extremely difficult, but conversely makes the mapping of receptors using coarse single-photon techniques more useful, as synaptic ‘hot-spots’ that may skew receptor maps are somewhat smoothed out. These morphological specifications make the comparison between both different dendritic locations and different cells easy, and make MSO neurons ideal for the development of receptor and synaptic input maps.

This study aims to contribute to a thorough understanding of the function of MSO neurons as the output of the most temporally precise mammalian coincidence detector circuit. To provide insight into the pre- and post-synaptic strategies employed by MSO neurons, I have completed an *in vitro* analysis of MSO neurons and their synaptic inputs from the Mongolian gerbil (*Meriones unguiculatus*). The gerbil is an excellent model for ITD research as, unlike mice and rats, it has excellent low frequency hearing, and a well developed MSO. Gerbil hearing thresholds (Ryan, 1976; Heffner and Heffner, 1988) and ITD sensitivity (Lesica et al., 2010) are also strikingly similar to humans (Klumpp and Eady, 1957; Mills, 1958). Additionally, like other rodents, hearing onset in gerbils occurs postnatally, around postnatal day (P) 10 - 12, making them an ideal model for studying hearing development. A thorough study of this unique circuit, which essentially pushes the limits of neuronal computation in terms of speed and accuracy, can provide insights into both general mechanisms of coincidence detection, and mammalian ITD coding in particular.

Despite widespread study of upstream nuclei in the auditory brainstem and the function of the MSO *in vivo*, there is as yet no thorough investigation into the cellular characteristics that underlie the ability of MSO neurons to code so precisely for ITDs. Indeed, the mechanism by which the MSO is able to represent sound source location is still unclear. In order to develop a sense of which coincidence detection strategy MSO neurons might employ (i.e. integrating few or many inputs), single excitatory and inhibitory synaptic inputs are described and their post-synaptic effects investigated in Chapter III. The

stereotyped morphology and input pattern of MSO neurons likely holds clues to how these cells have adapted to their unique role. The presence and distribution of several major post-synaptic receptor types and their synaptic input was therefore assayed and described in Chapter IV. These distributions uncover the maintenance of ‘immature’ neurotransmitter types in the mature MSO, namely NMDAR and GABA_AR signalling, and provide evidence for modulatory roles for these largely extra-synaptic populations. The contribution of NMDARs to synaptic signalling in the mature MSO and their modulation by synaptically released glycine is described in Chapter V. This description of some of the pre- and post-synaptic properties of MSO neurons provides a solid basis on which to postulate about the cellular mechanisms underlying ITD coding in the MSO.

II

Materials and Methods

Slice preparation

All experiments complied with institutional guidelines, national and regional laws. Slices were prepared from male and female Mongolian gerbils (*Meriones unguiculatus*). Animals were decapitated and brains were removed in dissection solution containing (in mM) 50 sucrose, 25 NaCl, 25 NaHCO₃, 2.5 KCl, 1.25 NaH₂PO₄, 3 MgCl₂, 0.1 CaCl₂, 25 glucose, 0.4 ascorbic acid, 3 myo-inositol and 2 Na-pyruvate (pH 7.4 when bubbled with 95% O₂ and 5% CO₂). Subsequent to the removal of the brain, horizontal (for electrophysiology; 90 - 120 µm) or transverse (for fibre tracing; 240 µm) brainstem slices containing the medial superior olive (MSO) and the medial nucleus of the trapezoid body (MNTB) were taken with a VT1200S vibratome (Leica, Wetzlar, Germany). In the horizontal preparation the most ventral section was discarded to restrict recordings to the low frequency region of the MSO. Slices were incubated in recording solution (same as slice solution but with 125 mM NaCl, no sucrose and 2 mM CaCl₂ and 1 mM MgCl₂) at 36 °C for 45 minutes, bubbled with 5% CO₂ and 95% O₂.

Electrophysiology

Electrophysiology: Chapter III

The electrophysiological properties of MSO neurons and the time course of their inputs are developmentally regulated and a dependency on the recording temperature has been reported (Smith et al., 2000; Magnusson et al., 2005; Scott et al., 2005; Chirila et al.,

2007). In order to obtain quantitative estimates comparable to the function described by *in vivo* physiology, we restricted our *in vitro* circuit analysis to acute horizontal brain slices from adult (P60 - P100) Mongolian gerbils. Unless otherwise stated, all experiments were carried out at near physiological temperature (34 – 36 °C), maintained by an in-line (SF-28) and bath chamber heater (PH-1, Warner Instruments, Biomedical Instruments, Zöllnitz, Germany) and monitored with a temperature probe placed directly by the slice. After incubation, slices were transferred to a recording chamber attached to a microscope (BX50WI, Olympus, Hamburg, Germany) equipped with gradient contrast illumination (Luigs and Neumann, Ratingen, Germany) and continuously perfused with recording solution. Cells were visualized and imaged with a TILL Photonics system (Gräfelfing, Germany) composed of an Imago CCD camera, a monochromator and its control unit. Voltage-clamp whole-cell recordings were performed using an EPC10/2 amplifier (HEKA Elektronik, Lambrecht, Germany) on visually identified MSO neurons. Access resistance was compensated to a residual of 2.5 – 3 MΩ; data was acquired at 20 – 50 kHz and filtered at 3 – 4 kHz.

Electrophysiology: Chapters IV & V

Slices were prepared from Mongolian gerbils (*Meriones unguiculatus*) at from two age groups. Animals aged postnatal day (P) 10 were used to investigate the development of GlyRs and their synaptic inputs at a pre-hearing stage. For the other receptor and synaptic mapping experiments, animals aged P20 - 35 were used as MSO neurons have reached their adult morphology at this stage (Rautenberg et al., 2009), and are electrophysiologically nearly indistinguishable from adult neurons (compare Scott et al., 2005 and Couchman et al., 2010). Receptor mapping was carried out at room temperature (22 - 25 °C); fibre stimulation experiments investigating the interaction between neurotransmitter systems were carried out at near physiological temperature (34 - 36 °C). Bath temperature was maintained using an in-line and bath chamber heater feedback controlled with a reference electrode located in the heating block (slice mini chamber I with TC05 temperature controller, Luigs & Neumann, Ratingen, Germany). The temperature was additionally monitored for consistency in between slices using a hand-held digital thermometer (Mini-K thermocouple thermometer with probe, Temperature Products GmbH, Freigericht, Germany). After incubation, slices were transferred to a recording chamber attached to a microscope (BX51W1, Olympus, Germany) equipped with gradient contrast illumination (Luigs & Neumann, Ratingen, Germany). For UV

uncaging experiments, 10 mL of 1 mM uncaging compound dissolved in normal recording solution was re-circulated throughout the experiment. For all other experiments, slices were continuously perfused with fresh recording solution. Dye loaded cells were visualized and imaged with either a TILL Photonics imaging system (Gräfelfing, Germany) or a TILL Photonics IR camera (VX 55) with fluorescence lamp (Xcite, Olympus, Germany) under the control of custom-written visual acquisition and microscope control software (Bendels et al., 2008). Voltage-clamp whole-cell recordings were performed using an EPC10/2 amplifier (HEKA Elektronik, Lambrecht, Germany) on visually identified MSO neurons. Access resistance was compensated to a residual of $3\text{ M}\Omega$; data was acquired at 20 kHz and filtered at 3 kHz.

Electrophysiology: general

The intracellular solution used to record EPSCs was (in mM): 130 Cs-gluconate, 10 Cs-HEPES, 20 TEA-Cl, 3.3 MgCl₂, 2 Na₂-ATP, 0.3 Na₂-GTP, 3 Na₂-Phosphocreatine, 5 Cs-EGTA and 5 QX-314 with 50-70 μM Alexa488 and for IPSCs (in mM): 105 Cs-gluconate, 26.7 CsCl, 10 Cs-HEPES, 20 TEA-Cl, 3.3 MgCl₂, 2 Na₂-ATP, 0.3 Na-GTP, 3 Na₂-Phosphocreatine, 5 Cs-EGTA and 5 QX-314 with 50-70 μM Alexa488, leading to 50 mM final Cl⁻ concentration. Intracellular solutions were adjusted to pH 7.2 with CsOH. For current clamp recordings the internal solution consisted of (in mM): 145 K-gluconate, 5 KCl, 2 Mg-ATP, 2 K-ATP, 0.3 Na₂-GTP, 7.5 Na₂-phosphocreatine, 15 HEPES and 5 K-EGTA with 50-70 μM Alexa568. In general, no liquid junction potential correction was made. The conductance (G) of synaptic currents was calculated using the equation $G = I/V$ where I is the recorded current (both mPSC and PSC) and V is the driving force. Since cells were held at -60 mV during recordings we calculate a 70 mV driving force for AMPAR mediated currents. For glycinergic Cl⁻ currents we measured the reversal potential at ~ -15 mV, resulting in a 45 mV driving force (data not shown).

Postsynaptic receptor currents through AMPA, NMDA, glycine, GABA_A and kainate receptors were isolated using the appropriate mix of DNQX (20 μM , Tocris), D-APV (50 μM , Tocris) or (R)-CPP (CPP, 10 μM , Biotrend), strychnine hydrochloride (STR, 0.5 or 1 μM , Sigma), SR 95531 (10 μM , Biotrend), and GYKI 53655 (GYKI, 50 μM , Axon Medchem). For receptor mapping experiments, ZD 7288 (50 μM , Biotrend), Tetrodotoxin (0.5 μM , Alomone), 4-aminopyridine (2 mM, Aldrich) and tetraethylammonium chloride (10 mM, Sigma) were added. For mapping the AMPAR distribution (Figure 3.1),

cyclothiazide was added to prevent desensitization (CTZ, 100 μ M, Biotrend). Picrotoxin (PTX, 100 μ M) was used to distinguish between α -homomeric and $\alpha\beta$ -heteromeric glycine receptors (Pribilla et al., 1992; Schofield et al., 1996).

Synaptic currents were evoked by local stimulation of available afferent fibers with a glass electrode filled with incubation solution. We then probed the vicinity (40 – 150 μ m) of a patched MSO neuron with a monopolar stimulation electrode for stably activatable input sites. To stimulate fibers a 200 μ s biphasic voltage pulse was triggered by the EPC10/2 amplifier (HEKA Elektronik, Lambrecht, Germany) and delivered either through an isolated pulse stimulator (2100; A-M Systems, Inc., USA) or post amplified 10 times by a linear stimulus isolator (A395; World precision instruments, Berlin, Germany).

For receptor/synapse mapping experiments, all protocols were repeated 4-8 times at each location. For fiber stimulation, protocols were repeated at least 3 times. To allow for the full recovery of the response, repetitions of single pulses were delivered at 7 s intervals and stimulus trains with intervals of 15 - 20 s (Couchman et al., 2010). For UV uncaging, laser pulses were delivered at least 15 seconds apart to allow for re-equilibration of the caged compound at the uncaging site.

Electroporation

Single cell electroporation was performed as described recently (Rautenberg et al., 2009) on transverse brain slices (240 μ m thickness) containing the MNTB and MSO of P20 - 25 day old gerbils. A patch pipette (size corresponding to 4 - 5 $M\Omega$), loaded with either Alexa FluorTM 488 sodium hydrazide or its 568 analog (1 mM, Molecular Probes) was pressed onto the surface of visually identified MNTB neurons and a single 18 - 22 ms long voltage pulse (15 - 22 V) was applied. The voltage pulse was generated by an EPC10/2 amplifier (HEKA Elektronik, Lambrecht, Germany) and post amplified 10 times by a linear stimulus isolator (A395; World Precision Instruments, Berlin, Germany). After ~1 minute the dye appeared evenly distributed within the cell soma and dendrites. During electroporation the slices were perfused continuously with incubation solution at room temperature. Slices containing labeled cells were fixed in 4% paraformaldehyde and left overnight. After two 5 minute washes with phosphate buffered saline (PBS, pH 7.4), sections were stained for

Nissl. After confocal reconstruction of the area in question, the fibers were traced off-line from their terminus in the MSO to the originating cell in 3D through high-resolution Z-stacks.

Immunohistochemistry and confocal microscopy

Immunohistochemistry was carried out in tissue from animals aged between P22 and P30. The animals were anesthetized (0.5% chloral hydrate, 0.2 ml / 10 g bodyweight) and perfused with PBS containing 0.1% Heparin and 155 mM NaCl for about 10 minutes before switching the perfusion to 4% paraformaldehyde. After a 45 minute perfusion the brains were removed and post-fixed overnight. Brains were washed twice in PBS and coronal brain slices of 40-60 μ m thickness were taken with a VT1000S vibratome (Leica, Wetzlar, Germany). Standard immunohistochemistry procedures were carried out on free floating slices. Sections containing electroporated MNTB neurons (Alexa 568) were colabelled using either Neurotrace® 500/525 green-fluorescent Nissl (Molecular Probes, Invitrogen, Karlsruhe, Germany) or with primary antibodies (AB) for synaptic vesicle protein 2 (SV2; monoclonal mouse AB, DSHB, Iowa City, IO) and MAP-2 (polyclonal anti-chicken AB, Neuromics, Acris Antibodies, Hildesheim, Germany). Secondary ABs were applied the following day for 2 hours at room temperature. These were conjugated with Alexa488 (SV2; Molecular Probes, Invitrogen, Karlsruhe, Germany) or Cy5 (MAP2; Dianova, Hamburg, Germany). Slices were mounted in Vectashield medium (H-100, VectorLaboratories Inc., AXXORA, Lörach, Germany) and confocal scans were taken with a Leica SP System (Leica, Wetzlar, Germany). Images were acquired with a 25x or 63x objective (0.75 NA or 1.32 NA respectively), leading to a pixel size between 0.781 nm^2 and 310 nm^2 .

UV uncaging

In vitro recordings to calibrate laser intensity and duration

Single-photon focal laser uncaging of caged MNI-caged-L-glutamate (MNI-Glu, 1mM, Tocris) and O-CNB-caged GABA (CNB-GABA, 1mM, Invitrogen) was carried out using a double-pumped solid state UV laser shuttered with an acousto-optic modulator (DPSL-355/1000 Rapp Optoelectronics, Germany) connected to the microscope using a 50 μ m

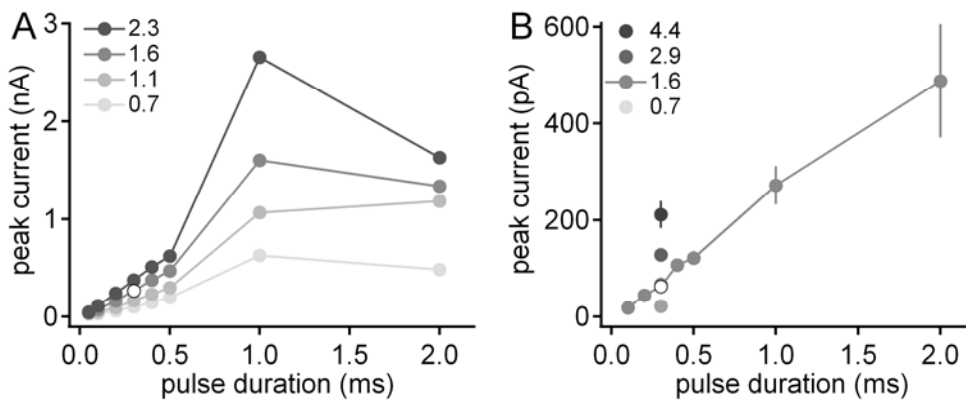


Figure 2.1 Calibration of laser intensity and duration

A: Peak amplitudes of AMPAR mediated currents in response to uncaging of MNI-Glu at varying pulse durations and as a function of laser intensity. Different laser intensities (in mW) represented by filled circles in shades of grey. **B:** As in A, for peak amplitudes of GABAAR mediated currents, plotted as a response to the uncaging of CNB-GABA for different durations. White circle (1.6 mW for 300 ms) was selected for use during mapping experiments as it lies within the linear range of responses for both uncaging compounds, and neurons tolerate this well.

quartz light guide and spot illumination adaptor (OSI-BX, Rapp Optoelectronics, Germany). At the sample site, this setup produces a spot size with an approximate diameter of $2 - 3 \mu\text{m}$. The duration and intensity of laser pulses were calibrated to ensure cell survival and reproducibility of the responses (Figure 2.1). For this calibration, AMPAR mediated responses to UV-uncaging of MNI-Glu were measured in whole-cell voltage-clamp mode at room temperature. Average peak responses to changes in laser pulse duration and intensity revealed a non-linearity in the response to pulses between 0.5 and 2 ms (Figure 2.1A). A 300 μs laser pulse was selected to ensure data was collected in a linear range and an intensity of 1.6 mW was found to produce with sizable and reproducible currents without any apparent damage to the cell (Figure 2.1A, open circle). For the calibration of CNB-GABA, GABA_AR mediated responses to UV uncaging were also measured in whole-cell voltage-clamp mode at room temperature (Figure 2.1B). Again, a 300 μs pulse with an intensity of 1.6 mW was chosen to ensure responses were sizable, reproducible and in the linear range of photolysis of the caged compound without damaging the cell (Figure 2.1B, open circle).

In vitro recordings to determine effective uncaging spot size

As two different caged groups with different properties (Wieboldt et al., 1994; Sarkisov and Wang, 2006) were used in this study, a separate calibration of the effective uncaging spot size at full width of the half maximal response (FWHM) was necessary (Figure 2.2). The FWHM was determined as the half-maximal current response to uncaging pulses at successively distant points from the proximal dendrite of an MSO neuron under a 60 X / 0.9 NA objective (Figure 2.2). Normalised peak current responses to uncaging pulses for both MNI-Glu and CNB-GABA were plotted as a function of lateral distance from the dendrite. The distance at the half-maximal response was then measured from a sigmoidal fit to the peak responses and used to calculate the effective uncaging spot size, or FWHM (Figure 2.2B). For MNI-Glu, a 300 μ s laser pulse at 1.6 mW resulted in a FWHM of 6.8 μ m ($n = 6$); for the CNB-GABA, the FWHM was 16.8 μ m ($n = 6$). We mapped and binned the receptor responses for MNI-Glu in 15 μ m bins, and for the CNB-GABA responses the data was binned in 30 μ m increments. When the 40 X / 0.8 NA objective was used (Figure 5.3), we estimate that the larger objective increased the uncaging spot size by about 1/3 to ~10 μ m FWHM.

UV uncaging of glutamate and GABA

For AMPAR and GABA_{AR} mediated currents, a 300 μ s laser pulse at ~1.6 mW was applied to visually identified neuronal segments. Due to their slower single channel kinetics and relatively sparse distributions, a 500 μ s pulse was required to elicit reliable NMDAR mediated currents. For receptor distributions, a 60 X objective (NA 0.9, LUMPlanFI, Olympus) was used to minimise the effective uncaging spot size. In the experiment shown in Figure 5.3, a 40 X objective (NA 0.8, LUMPlanFI, Olympus) was used to increase the uncaging spot size to encompass as much of the somatic region as possible.

Picospritzer pressure-application***Glycine***

To determine the sub-cellular location of Gly-Rs, glycine was pressure-applied. A patch pipette was loaded with 1 mM glycine and 50-100 μ M Alexa 488 or 568 dissolved in water. This was placed within 5 μ m of the cell membrane and a 4 ms puff at 4 psi given via picospritzer. The puff of solution was visualized using a TILL Photonics imaging system to

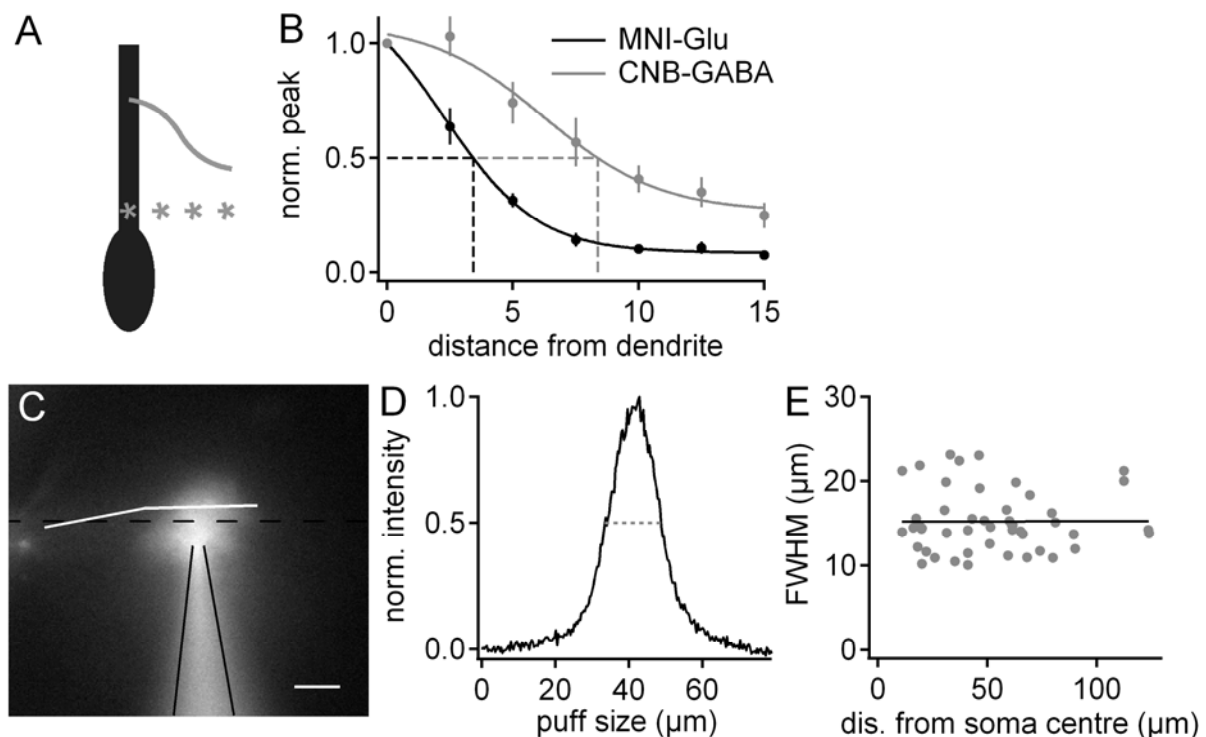


Figure 2.2 FWHM calibrations

A: UV-uncaging: Schematic of experimental paradigm; uncaging pulses were delivered in 2.5 μm steps successively distant from the proximal dendrite of an MSO neuron. **B:** Normalised peak AMPAR and GABA_{AR} responses to uncaging pulses delivered at locations as indicated in (A). The FWHM was calculated from doubling the distance at 50 % of peak from sigmoidal fits to the data (solid lines). Data are presented as average \pm SEM. **C:** Picospritzer pressure-application: Fluorescence image showing pipette (bottom) and the full extent of a puff (4 ms at 4 psi) of 1 mM glycine, visualised by the inclusion of 100 μm Alexa 568 in the puff solution. Image of MSO dendrite is overlaid, indicated with a solid white line. The dotted line indicates the position at which the FWHM was calculated. Scale bar is 20 μm . **D:** Normalised plot of fluorescence intensity from dotted line in (C). Grey dotted line corresponds to the FWHM of this puff. **E:** Line fit to FWHMs of 50 randomly selected puffs from 12 cells plotted against distance from the soma centre. The FWHM remained stable between experiments and along the dendrite length.

ensure the tip did not become blocked and the puff was of a consistent size (Figure 2.2C & E). Using normalized images taken at the maximum extent of the puff (Figure 2.2C), we estimate the average full width at half maximum (FWHM) was \sim 16 μm (Figure 2.2D & E). The presented data were pooled and binned in 20 μm increments.

High $[K^+]$ solution

In order to functionally locate synaptic inputs, a patch pipette was loaded with a solution

containing (in mM) 40 KCl, 3 CaCl₂, 100 NaCl, 10 Na-HEPES, 20 Glucose with 50 µM Alexa 568. This was then placed 10-50 µm of the cell membrane and a 50 - 150 ms puff at 4 psi given via picospritzer. Given the large size of the puff (~50 - 100 µm effective diameter) this experiment was only used to identify differences between the somatic and distal dendritic regions of an MSO neuron. These puffs were again visualized using a TILL Photonics imaging system (Gräfelfing, Germany) to ensure the tip did not become blocked.

Data and statistical analysis

Peak-scaled non-stationary fluctuation analysis

Peak-scaled non-stationary fluctuation analysis was carried out on mIPSCs as described in Silver et al. (1996). Briefly, for each cell, mIPSCs from 50 pA about the mean were selected and peak-aligned. The background variance was calculated from a time window immediately preceding each mIPSC. The mean mIPSC waveform was then scaled to the peak of each individual mIPSC and the two waveforms subtracted. The resulting difference waveform was then binned in time according to equally sized amplitude bins of the average mIPSC. An average overall variance was calculated for each time bin and the background variance subtracted. The remaining variance, corresponding mainly to channel noise during the mIPSC, was plotted versus the average mIPSC amplitude. The peak-scaled variance σ_{p-s}^2 is a parabola and is calculated from the equation:

$$\sigma_{p-s}^2 = i \bar{I} - \bar{I}^2 / N_p + \sigma_b^2 \quad (\text{Silver et al., 1996})$$

where i is the average single channel current of all channels opened during the mIPSC, \bar{I} is the mean mIPSC amplitude and N_p is the number of channels open at the peak of the mIPSC. σ_b^2 is the background variance, set to zero as this is earlier subtracted from the variance bins. An estimate of the average single channel conductance (G_i) can then be calculated from Ohm's law by dividing the single channel current by the ionic driving force (V_d):

$$G_i = i / V_d$$

General data and statistical analysis

Confocal image stacks were processed with ImageJ, MetaMorph (Universal Imaging Corp., Visitron System GmbH, Puchheim, Germany) and Neurolucida (MBF Bioscience Inc., Magdeburg, Germany) to extract varicosity number and synaptic number by eye. Currents were analyzed using custom-written functions written in IGOR Pro (WaveMetrics Inc, Lake Oswego, OR). Miniature IPSCs were extracted by a custom written template matching routine provided by Dr. Holger Taschenberger (Taschenberger et al., 2005). Results are presented as mean \pm standard error of the mean. Unless otherwise stated, statistical significance was determined using an unpaired, two-tailed, student's t-test with a significance threshold of $p < 0.05$.

III

Quantifying synaptic input to adult MSO neurons

In this chapter, a classical minimal stimulation paradigm was used to estimate the size and kinetics of single excitatory and inhibitory fibres to principal MSO neurons, providing insight into the relative importance of these inputs and their temporal integration. The post-synaptic impact of excitatory inputs was quantified, in terms of the action potential current threshold using synaptically elicited currents, to estimate the minimal number of excitatory inputs to each MSO neuron. Using single-cell electroporation, it was also possible to determine the total number of inhibitory fibre inputs that innervate an MSO neuron, and therefore their post-synaptic impact in terms of synaptic conductance. This work represents the first characterisation of the inputs to MSO neurons from adult (P60 - 100) gerbils.

Excitatory and inhibitory inputs are large with fast kinetics

In the first experiment, whole-cell voltage-clamp mode was established on visually identified MSO neurons, and currents through AMPA receptors (R_s) were pharmacologically isolated. A stable fibre stimulation site was then established in the vicinity of the patched neuron, and the stimulus strength roved in 1 V steps (Figure 3.1A & B). A peak histogram of the peak amplitude of evoked EPSCs generally showed distinct peaks (Figure 3.1C, grey bars) that corresponded to different stimulation strengths in Figure 3.1A & B. Individual peaks in the distribution of the EPSC peak amplitudes were fit with a Gaussian function to estimate the average amplitude of each stimulated fibre (Figure

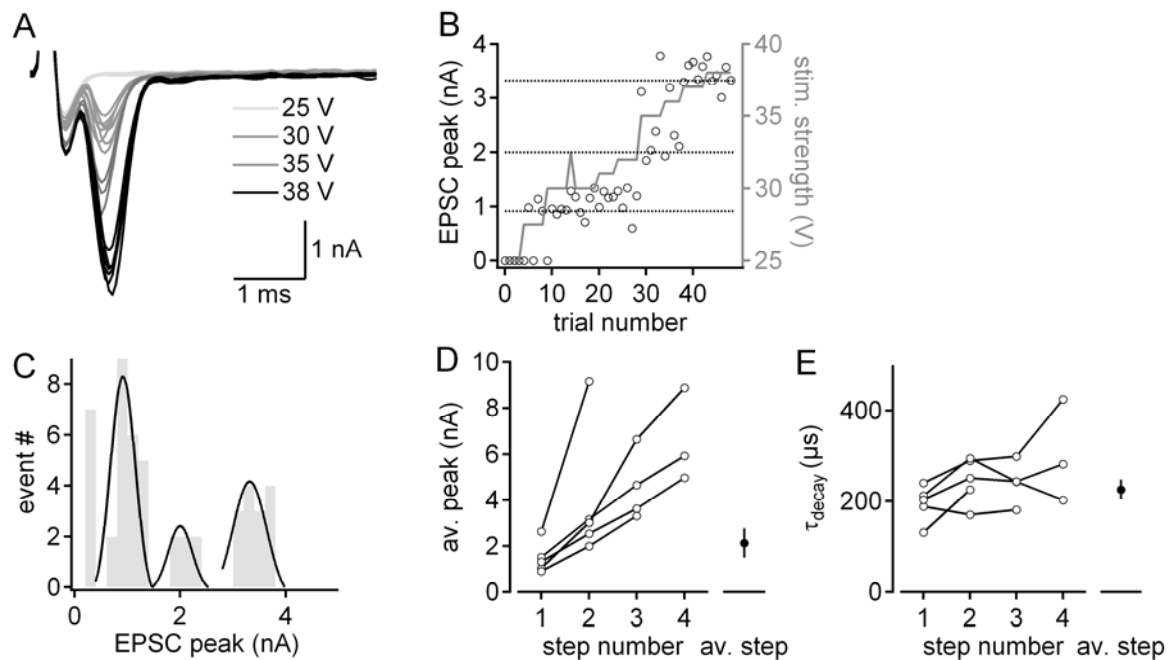


Figure 3.1 Excitatory fibre inputs to MSO neurons estimated with classical minimal stimulation

A: AMPAR mediated EPSCs stimulated at different voltage intensities roving in 1 V steps. **B:** Left axis: EPSC amplitudes plotted versus trial number (open black circles). Right axis: corresponding stimulus intensities used to elicit EPSCs (grey line). Clear amplitude steps corresponding to the recruitment of single excitatory fibres are elicited to graded stimuli. **C:** Histogram of EPSC peaks from (B) (grey bars) were fit with Gaussian functions (black lines) to estimate the amplitude of single fibres. **D:** Summary of single fibre steps estimated from the peaks of Gaussian functions as in (C). **E:** Summary of average decay time constant measured with a single exponential function (τ_{decay}) for EPSCs at each step. Single fibre steps elicited in single cells (open circles) are joined. Filled circle is overall average step \pm SEM, corresponding to the average AMPAR mediated single fibre current or decay time constant.

3.1C, black lines). The average peak amplitude of all apparent excitatory fibres was 2.13 ± 0.64 nA, with single fibres ranging from 0.91 nA to 6.52 nA (Figure 3.1D, $n = 5$ cells, 17 fibres). At a given stimulation site, an average of 6.45 ± 1.13 nA total current could be elicited, ranging from 3.32 to 9.16 nA from between 2 and 4 individual fibres. EPSCs were fast, with an average decay time constant of 226 ± 22 μ s (Figure 3.1E), when fit with a single exponential function. These results confirm that with this technique multiple fibres could be elicited at each location, providing a good estimate of the average single fibre current for each cell.

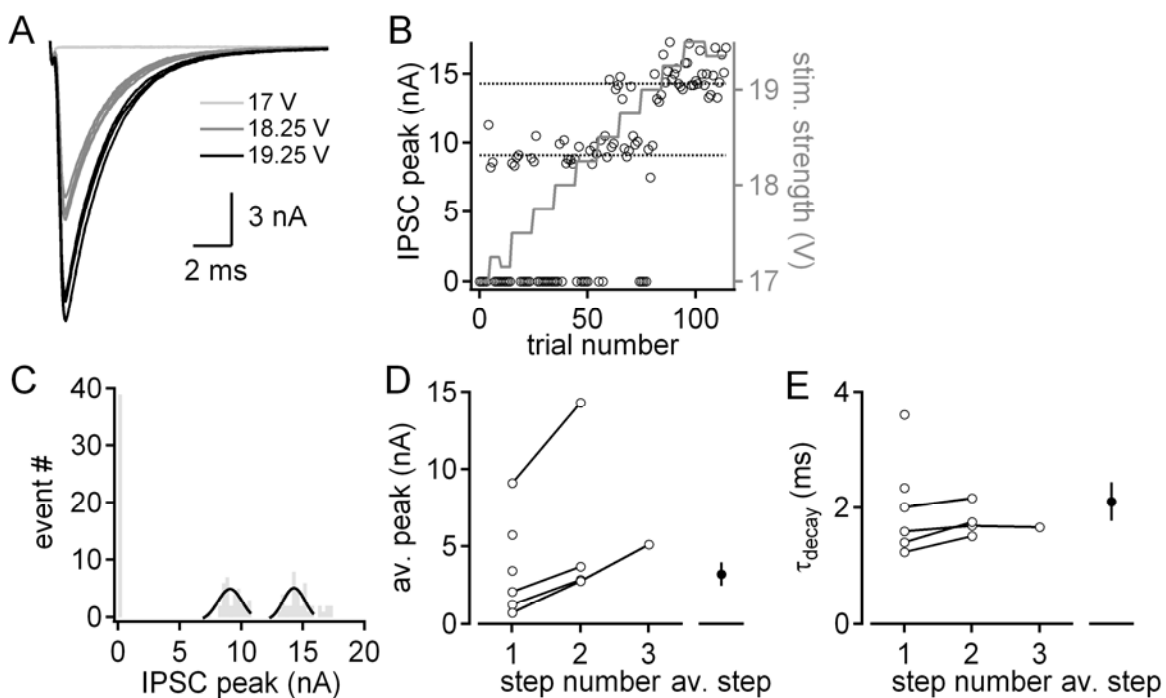


Figure 3.2 Inhibitory fibre inputs to MSO neurons estimates with classical minimal stimulation

A: GlyR mediated IPSCs stimulated at different voltage intensities roving in 0.25 – 1 V steps. **B:** Left axis: IPSC amplitudes plotted versus trial number (open black circles). Right axis: corresponding stimulus intensities used to elicit IPSCs (grey line). Clear amplitude steps corresponding to the recruitment of single inhibitory fibres are elicited to graded stimuli. **C:** Histogram of IPSC peaks from (B) (grey bars) were fit with Gaussian functions (black lines) to estimate the amplitude of single fibres. **D:** Summary of single fibre steps estimated from the peaks of Gaussian functions as in (C). **E:** Summary of average decay time constant measured with a single exponential function (τ_{decay}) for IPSCs at each step. Single fibre steps elicited in single cells (open circles) are joined. Filled circle is overall average step \pm SEM, corresponding to the average GlyR mediated single fibre current or decay time constant

The strength of an average inhibitory fibre was also investigated using the same experimental paradigm. Pharmacologically isolated glycinergic currents were recorded in MSO neurons in whole-cell voltage-clamp mode. A stable stimulation site was established and fibres were stimulated using 0.25 - 1 V steps in stimulus amplitude (Figure 3.2A & B). At each site, IPSC amplitudes increased in distinct steps with increasing stimulus amplitude (Figure 3.2A & B). From a peak histogram of IPSC amplitudes, each single fibre peak was fit with a Gaussian function to estimate the average amplitude of each stimulated fibre (Figure 3.2C). The average peak amplitude of all apparent inhibitory fibres was 3.5 ± 0.98 nA, with single fibres ranging from 0.72 to 9.10 nA (Figure 3.2D, $n = 6$ cells, 10 fibres). At a given stimulation site, 1 to 3 individual fibres could be elicited, with total

currents at each location ranging from 2.83 to 14.30 nA with an average total of 5.85 ± 1.75 nA. IPSCs were fit with a single exponential function resulting in an overall average decay time constant of 2.11 ± 0.33 ms (Figure 3.2D).

The synaptic currents presented here are the product of substantial synaptic conductances, which often interact and can have further modulatory effects not immediately obvious at the current level. Therefore, in order to develop a physiologically relevant comparison of excitatory and inhibitory fibre strengths, the average synaptic conductance imposed by single fibre inputs was estimated using the driving force for the respective synaptic currents (see Materials and Methods) and the actual current amplitudes. For excitatory currents, the driving force calculated from the electrochemical reversal potential between the intracellular recording solution and the external recording solution was approximately 70 mV. The average single excitatory fibre produced an average AMPAR mediated current of 2.13 ± 0.64 nA resulting in an average single fibre conductance of 35 ± 1 nS. In comparison, inhibitory currents had a driving force of 45 mV, and single fibre inputs produced an average GlyR mediated current of 3.5 ± 0.98 nA, resulting in an average single fibre conductance of 79 ± 2 nS. The presence of such substantial inhibitory input to MSO neurons points to their importance in coincidence detection computation.

Synaptically evoked action potential threshold is unexpectedly high

In order to determine the physiological post-synaptic impact of the large single fibre excitatory currents to MSO neurons (Figure 3.1), the current threshold for AP generation and the corresponding number of excitatory fibres was estimated. Both on-cell and whole-cell recordings were obtained from the same neurons to measure the size of pharmacologically isolated AMPAR mediated currents that correlate with AP generation in adult MSO neurons.

In on-cell configuration a stable, phasic stimulation site was isolated, and the stimulation intensity varied (Figure 3.3A). In the example in Figure 3.3, a 45 V stimulus elicited ‘EPSP’ waveforms with a small peak and after-hyperpolarisation (AHP) amplitude. A 50 V stimulus intensity reliably elicited larger voltage deflections, exhibiting a small kink in the rising phase (Figure 3.3A, arrow), a faster repolarisation and larger AHP amplitude.

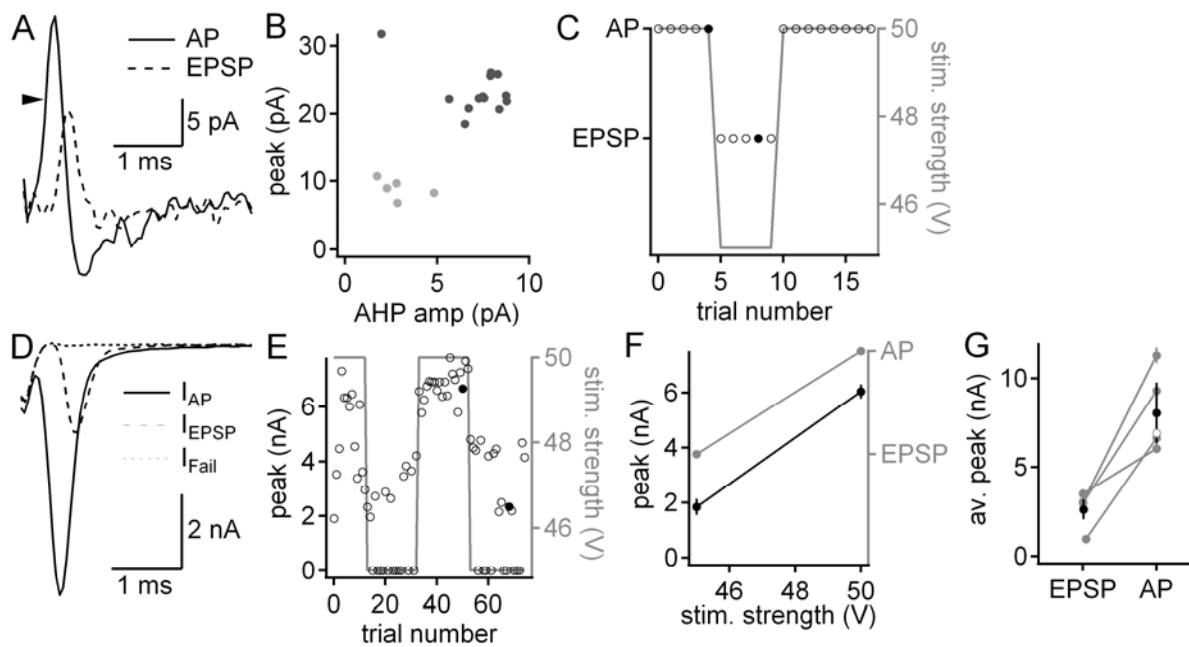


Figure 3.3 Functional consequences of large excitatory fibres

A: On-cell recording of synaptic inputs evoked at different stimulation intensities. Arrow indicates inflection during rise of the largest response type (AP event). **B:** Plot of peak vs. AHP amplitude for all currents recorded from this cell. Black circles were classified as AP, grey circles as EPSP events. **C:** Event type as a function of trial number (circles). Stimulation strength is shown as a solid grey line. Filled symbols correspond to the traces shown in (A). **D:** Whole-cell voltage clamp response of the same cell, stimulation site and strength as in (A to C). **E:** EPSC peak amplitude and the corresponding stimulation strength are plotted as a function of trial number. Solid symbols correspond to the traces shown in (D). **F:** Average EPSC peak amplitude and event type from (C) and (E) given as a function of stimulation strength. **G:** Average EPSC amplitude corresponding to EPSP and AP events. Gray circles correspond to single cells; black circles represent the population average ($n = 5$). Open circle is one cell where no EPSP events could be isolated (i.e. all trials were AP events).

In order to classify these events, we plotted, for each cell, the peak vs. AHP amplitude of the voltage deflections (Figure 3.3B). According to their clustering in this plot, these different waveforms were termed fail, EPSP, and AP accordingly (Figure 3.3B and C). Plotting the elicited event type and the stimulation strength against the trial number for the example cell in Fig. 4 revealed that AP events occur at 50 V stimulation strength and EPSP events occur at 45 V (Figure 3.3C). Once this stimulation threshold for evoking AP events was established in the on-cell configuration, whole-cell mode was established in the same neuron. AMPAR mediated EPSCs elicited by the same stimulus intensities at the same stimulation site were recorded in whole-cell voltage-clamp mode. In these recordings, step like increases in EPSC amplitude were observed. These were termed I_{fail} , I_{EPSP} and I_{AP}

accordingly (Figure 3.3D). When plotting the EPSC peak amplitude and the event type as a function of the stimulation strength, the EPSCs between 2 and 5 nA correlate predominantly with EPSP events. For the example cell in Figure 3.3, some stimulus trials failed to activate fibre inputs during the recordings in whole-cell mode. To reliably elicit AP events only, a 6 nA EPSC was required.

In a total of 5 such recordings, EPSP events were correlated to an average EPSC peak of 2.6 ± 0.5 nA (Figure 3.3G, $n = 4$). To elicit an AP event, an average EPSC of 8.0 ± 1.7 nA was evoked with the same stimulus intensity (Figure 3.3G, $n = 5$). In one cell no EPSP events could be obtained, consistent with the fact that no EPSC smaller than 5.2 ± 0.1 nA could be recorded in whole-cell mode (Figure 3.3G, open circle). On average, the EPSC required to reliably elicit an AP corresponds to an estimated 2 - 4 excitatory fibres. Therefore, with an average single fibre conductance of 35 nS, action potential threshold in the MSO is reached with ~ 70 - 140 nS of AMPAR mediated conductance. Note that this number represents a lower bound of required excitatory inputs to this system.

Single inhibitory fibres contain many synaptic varicosities

To correlate the physiological estimates of the inhibitory input strength with synaptic anatomy, the morphology of MNTB inputs to MSO neurons was analysed. Consistent with substantial single fibre inhibitory input, electron microscopy (EM) studies have identified up to three active zones in a single inhibitory bouton / varicosity (Clark, 1969; Lindsey, 1975; Kiss and Majorossy, 1983; Brunso-Bechtold et al., 1990; Kapfer et al., 2002). To develop an estimate of the number of synaptic varicosities per inhibitory fibre, single MNTB neurons were electroporated with Alexa dyes and their axons reconstructed with confocal microscopy. Single visually identified MNTB neurons were electroporated in slice and later identified by their calyceal input with immunohistochemistry (Figure 3.4C). In total, 8 MNTB axons were reconstructed, terminating with a total of 28 final branch segments in the MSO (Figure 3.4).

All terminal segments targeted to the MSO were axon collaterals of larger fibres that, save one, passed ventrally or dorsally the MSO. These collaterals terminated in several branches of ~ 85 μ m in length, often in an arrangement parallel to the dendritic axis (medial-lateral)

of the MSO (Figure 3.4B, C). Final branches had an inter-tip distance of ~ 35 μm (Figure 3.4D), suggesting that each branch terminated on a single MSO neuron, since MSO somas are perpendicularly spaced (dorsal-ventral) ~ 15 μm apart (Rautenberg et al., 2009). Axon terminals were dotted with swellings that appeared identical to those identified as pre-synaptic varicosities in other regions of the brain (Shepherd et al., 2002; Zeilhofer et al., 2005). We counted 24 to 93 varicosities in the MSO region per fibre, with an average of 18 \pm 1.2 per final branch (Figure 3.4E). Assuming these swellings are pre-synaptic varicosities, and together with the ultrastructural evidence for multiple release sites per synapse (Clark, 1969; Lindsey, 1975; Kiss and Majorossy, 1983; Brunso-Bechtold et al., 1990; Kapfer et al., 2002), this anatomical analysis supports the electrophysiological results indicating large single inhibitory fibre inputs to MSO neurons (Figure 3.2). Furthermore, we confirmed that one MNTB axon innervates between 1 and 7 MSO neurons (Werthat et al., 2008).

From immunohistochemical evidence (Couchman et al., 2010), it is known that each MSO neuron receives a total of ~ 50 inhibitory varicosities. From the single fibre reconstruction presented here, MNTB inputs to the MSO exhibit an average ~ 18 varicosities per final branch, likely containing multiple release sites. It can therefore be calculated that each MSO neuron receives input from 2 - 3 inhibitory fibres, with a combined total inhibitory conductance of ~ 160 - 240 nS. Thus the combined inhibitory input to an MSO neuron has at any time ~ 45 readily releasable vesicles. This represents a significant inhibitory drive to MSO neurons that can be rapidly stimulated, leaving no doubt as to the importance of fast inhibition to the MSO circuit *in vivo* (Brand et al., 2002; Pecka et al., 2008).

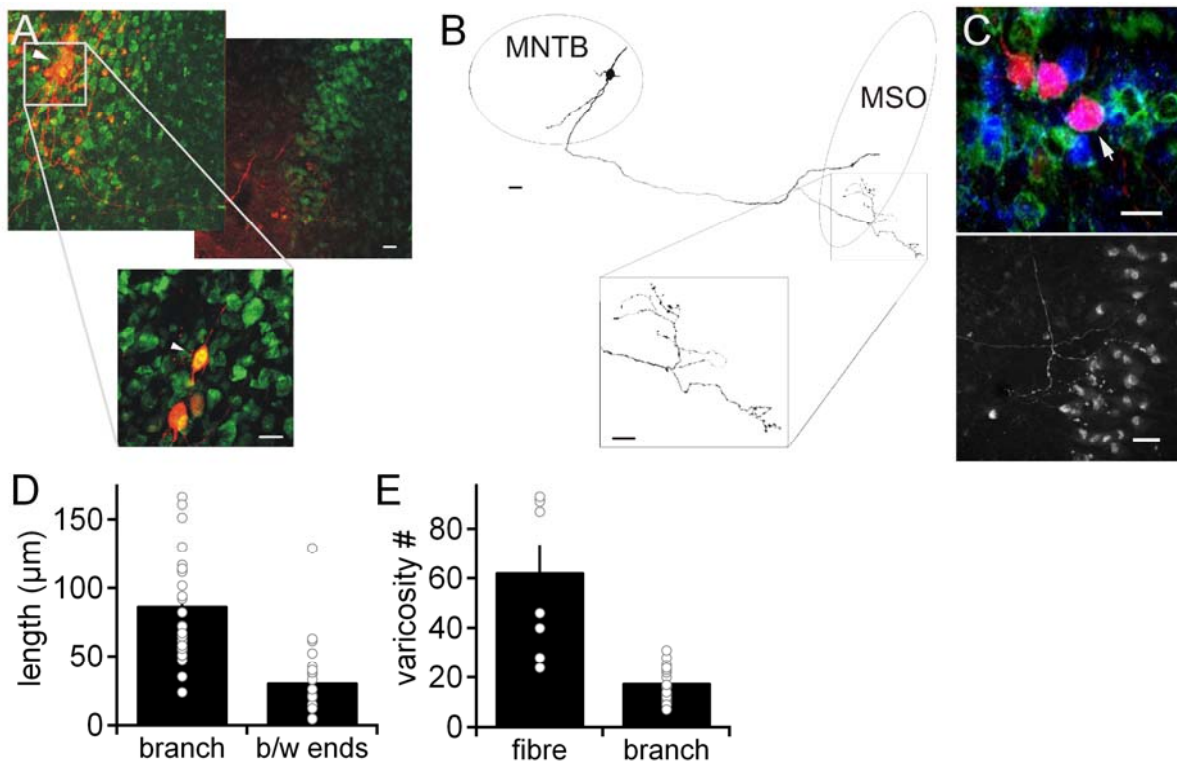


Figure 3.4 Quantification of pre-synaptic varicosities on single MNTB inputs to MSO neurons

A: Single Alexa568 electroporated MNTB neuron (arrow) that projects to the MSO region (inset: cell body of MNTB neuron in a subsequent Z-stack with 63 x magnification). Cell bodies are stained with Nissl-green. Scale bar equals 20 μ m. **B:** Reconstruction of the labelled neuron shown in (A). Nuclei boundaries are indicated; scale bar equals 20 μ m. Inset: magnification of the axon branch in the MSO and its adjacent region. Note varicosities on axon branches. **C:** Upper panel shows principal MNTB neuron (arrow) labelled with Alexa568 by single cell electroporation and processed with standard immunohistochemistry to highlight the calyx of Held with SV2 labelling (green). Lower panel shows termination of axon collateral from this neuron in the MSO. Nuclei of MSO neurons are apparent with auto-fluorescence. **D:** Final branch length of reconstructed fibres (left; branch), and the closest distance between the terminal tip of neighbouring final branches (right; b/w ends). **E:** The number of visually identified varicosities on reconstructed fibres (left; n = 8 fibres) and on the final branches of these fibres (right; n = 28 final branches).

IV

Functional receptor and synapse distributions in the mature MSO

In this chapter, the functional expression of neurotransmitter receptors in the mature MSO was thoroughly mapped. Using UV uncaging and pressure-application, the subcellular distribution of AMPARs, kainate (KA)-Rs, NMDARs, GlyRs and GABA_ARs and their synaptic input was described. To complement these maps, and as there has been no pharmacological investigation of synaptic receptors in the mature MSO, the subunit types of both glutamate- and GlyRs were characterised. The functional mapping of receptors and their inputs uncovered the expression of extra-synaptic receptors and raises the possibility of new kinds of circuit modulation in the MSO.

AMPA and NMDA receptors are differentially expressed

The excitatory input to mature MSO neurons is thought to be almost exclusively AMPAR mediated (Kotak and Sanes, 1996) and dendritically targeted (Stotler, 1953; Clark, 1969). UV-uncaging of MNI-caged-L-glutamate (MNI-Glu) was used to see whether this anatomical arrangement and receptor subtype identity is reflected in functional AMPAR, KAR and NMDAR distributions. Pharmacologically isolated AMPAR or NMDAR mediated currents were elicited along the length of MSO dendrites, and currents recorded in whole-cell voltage-clamp mode. In both cases, somatic responses were always present, but were not included in the receptor distributions (Figure 4.1) because of the large difference in surface area and shape compared to the dendrites. The functional expression

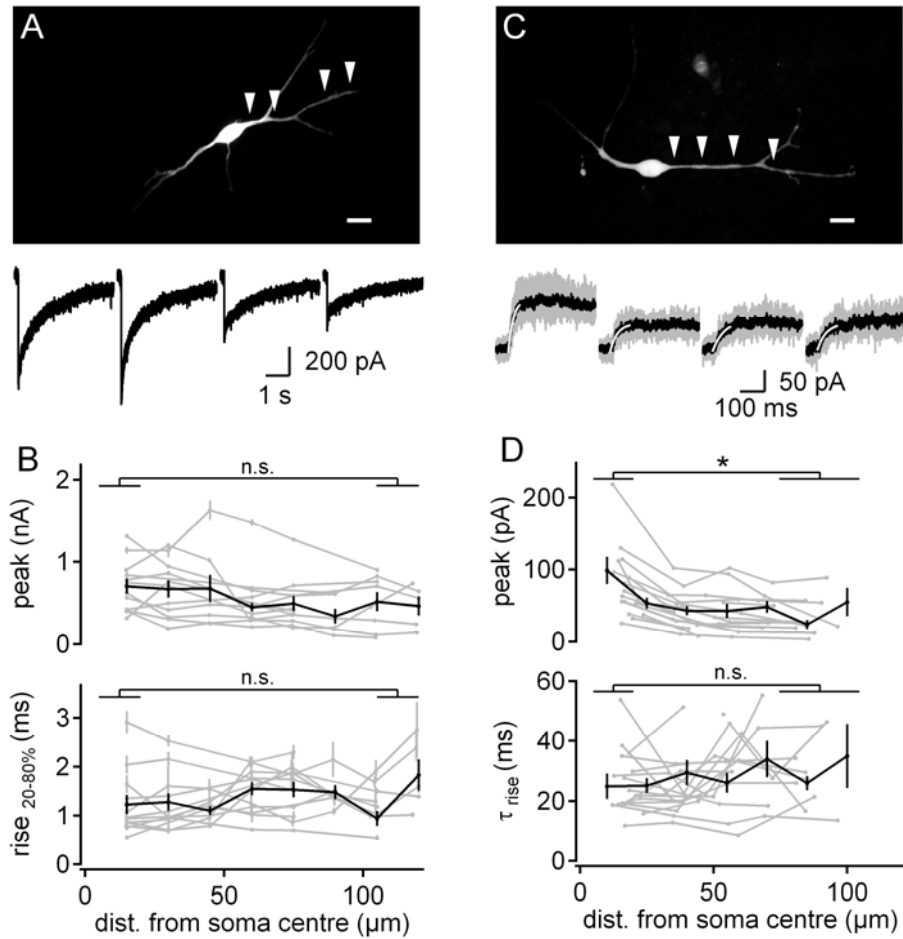


Figure 4.1 Functional AMPAR and NMDAR distributions

A: Top: MSO neuron filled with Alexa568, arrows indicate MNI-Glu uncaging positions. Bottom: corresponding AMPAR mediated currents elicited (left to right) at 20 μm, 40 μm, 59 μm and 79 μm from the soma centre. **B:** Summary of peak (top) and 20 - 80 % rise times (bottom) of AMPAR mediated currents plotted versus the distance from the soma centre of the uncaging position. Individual cells in grey, average in 20 μm bins overlaid in black. **C:** Top: MSO neuron filled with Alexa 568, arrows indicate MNI-Glu uncaging positions. Bottom: corresponding NMDAR mediated currents elicited (left to right) at 16 μm, 37 μm, 59 μm and 84 μm from the soma centre. Grey traces are individual trials, black average overlaid. White trace is single exponential fit to rising phase used to calculate peak and τ_{rise} . **D:** Summary of peak (top) and τ_{rise} (bottom) of NMDAR mediated currents plotted versus the distance from the soma centre of the uncaging position. Individual cells in grey, average in 20 μm bins overlaid in black. Scale bars are 20 μm, all average values \pm SEM. Star denotes significance ($p < 0.05$); n.s. is not significant.

of KARs was also assayed, but no KAR mediated currents could be elicited using MNI-Glu uncaging in the presence of GYKI and CPP ($n = 7$ cells; data not shown).

AMPAR mediated currents were elicited along the dendrites of a total of 12 MSO neurons

(Figure 4.1A and B). At the proximal dendrite (10 - 20 μ m from the soma centre), an average AMPAR mediated peak current of 705 ± 89 pA could be evoked, compared to 497 ± 81 pA at distal locations (105 - 120 μ m from the soma). This decrease in AMPA peak current was not significant ($p > 0.05$), indicating a uniform distribution of AMPARs on the dendrites of MSO neurons.

In order to rule out distortion effects originating from the diffusion of uncaged glutamate, variations in light scatter with stimulation depth and space clamp errors, the rise time (20 - 80%) of the receptor currents were determined (Figure 4.1B, lower panel). At the proximal dendrite (10 - 20 μ m from the soma), rise times were 1.23 ± 0.19 ms. The data collected 105 - 120 μ m from the soma (average 1.49 ± 0.17 ms) was not significantly different ($p > 0.05$). Overall, we could not identify a systematic effect of dendritic distance on current kinetics, indicating that distortion effects are unlikely to affect our results.

Generally, the contribution of NMDARs to signalling in the mature auditory brainstem is thought to be minimal (Zhou and Parks, 1993; Caicedo and Eybalin, 1999; Futai et al., 2001) although their functional presence has recently been shown (Steinert et al., 2010). In order to investigate a possible contribution to the mature MSO circuit, functional NMDAR expression was mapped along MSO dendrites using UV uncaging of MNI-Glu ($n = 14$). As the currents elicited were small, 4 - 8 trials at each location were averaged (Figure 4.1C, black traces), and the peak of the current was determined using the maximum of a single exponential fit to the rise of the response (Figure 4.1C, white traces). Overall, NMDARs appear somatically biased, though they were present even on distal dendritic segments (Figure 4.1D, upper panel). This bias was significant as the proximal dendritic NMDA currents (10 - 15 μ m from the soma centre) were on average 99 ± 18 pA compared to 33 ± 8 pA at 75 - 105 μ m ($p < 0.05$). The rise times of these currents were measured from the single exponential fit (Figure 4.1C, white traces). The τ_{rise} of proximal dendritic currents (10 - 15 μ m) was 25 ± 1.7 ms; the average at 75 - 105 μ m was 29 ± 3.8 ms (Figure 4.1D, lower panel). As before, the τ_{rise} did not differ significantly ($p > 0.05$) between proximal and distal sites, indicating currents are not distorted.

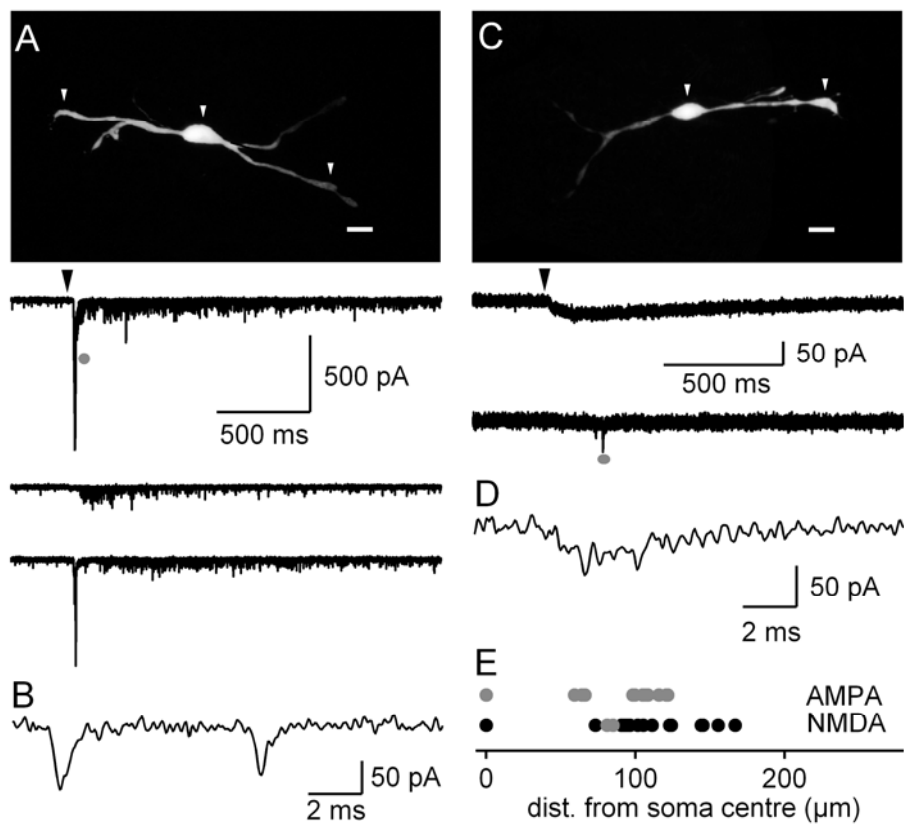


Figure 4.2 Functional AMPA and NMDA synapse distributions

A: Top: MSO neuron filled with Alexa 568, arrows indicate position of pressure-application of 40 mM K⁺. Bottom: corresponding currents elicited (top to bottom) at 108 μm, 0 μm and 122 μm from the soma centre. Response to large-scale release of vesicles indicates the presence of excitable synaptic inputs at these sites. Black arrowhead marks stimulus onset. Grey circle enlarged in (B). **B:** Synaptic AMPAR mediated EPSCs elicited by the pressure-application of 40 mM K⁺. Extended time course from grey circle in (A). **C:** Top: MSO neuron filled with Alexa 568, arrows indicate position of pressure-application of 40 mM K⁺. Bottom: corresponding currents elicited at 0 μm (top) and 85 μm (bottom) from the soma centre. We found a DAPV sensitive response (grey circle) at the dendrite of only 2/10 cells. Black arrowhead marks stimulus onset. Grey circle enlarged in (D). **D:** Synaptic NMDAR mediated event elicited by the pressure-application of 40 mM K⁺. Extended time course from grey circle in (C). **E:** Summary of synaptic input sites to AMPARs (top) and NMDARs (bottom). Grey circles indicate the presence of an input; black circles are positions where no input could be elicited. Scale bars are 20 μm, all average values ± SEM.

Excitatory inputs are predominantly AMPA receptor mediated

The presence of somatic AMPARs and widespread NMDAR expression led us to investigate the location of synaptic inputs to these receptors. Pre-synaptic terminals were

depolarised using the local pressure-application of a high $[K^+]$ (40 mM) solution for 50 - 150 ms. Given the limited resolution of such stimuli (FWHM \sim 50 - 100 μ m) the solution was applied only to cell somata and distal dendritic sites, thereby localising synaptic input only to either the somatic or dendritic cellular compartment.

AMPAR mediated responses were measured after pressure-application of 40 mM potassium solution to a total of 8 cell somata and 21 dendritic sites located 59 - 121 μ m from the soma centre (Figure 4.2A & E). At all tested locations, both on dendrites and somata, the stimulation elicited bursts of fast postsynaptic AMPAR responses of varying sizes (Figure 4.2B & E). To determine possible synaptic activation patterns to NMDARs, Mg^{2+} was omitted from the recording solution and cells were held at -60 mV while input sites were probed. In total, the somata of 10 cells and 16 dendritic locations ranging from 73 - 167 μ m were stimulated (Figure 4.2E). A synaptic input to NMDARs could only be stimulated at the dendrites of 2/10 cells (one such cell in Figure 4.2C). Part of the response is magnified in Figure 4.2D (from grey circle in Figure 4.2C). In both cells this response was blocked by D-APV, confirming that it was mediated by NMDARs. However, the magnitude of this response indicates that synaptic input to the functional NMDARs identified in Figure 4.1 may be limited.

Glycine receptor distributions are developmentally invariant

Anatomically, the restriction of inhibitory inputs to the soma and proximal dendrites of mature MSO neurons is well documented (Kuwabara and Zook, 1992; Kapfer et al., 2002; Couchman et al., 2010). To date though, there has been no functional investigation to confirm this morphological arrangement, or its developmental refinement. The distribution of functional GlyRs on the dendrites of MSO neurons was therefore measured using a minimal (4 ms) focal pressure-application of a saturating concentration (1 mM) of glycine. A saturating concentration ensures that the peak of any elicited currents reflects the maximal response of receptors in the vicinity of the stimulation and minimises the relative effects of diffusion on the rise times of the currents. To track the developmental refinement of GlyRs, this experiment was carried out on animals both before hearing onset (P10; Figure 4.3A & B) and at more mature stages after hearing onset (P20 - 35; Figure 4.3C & D).

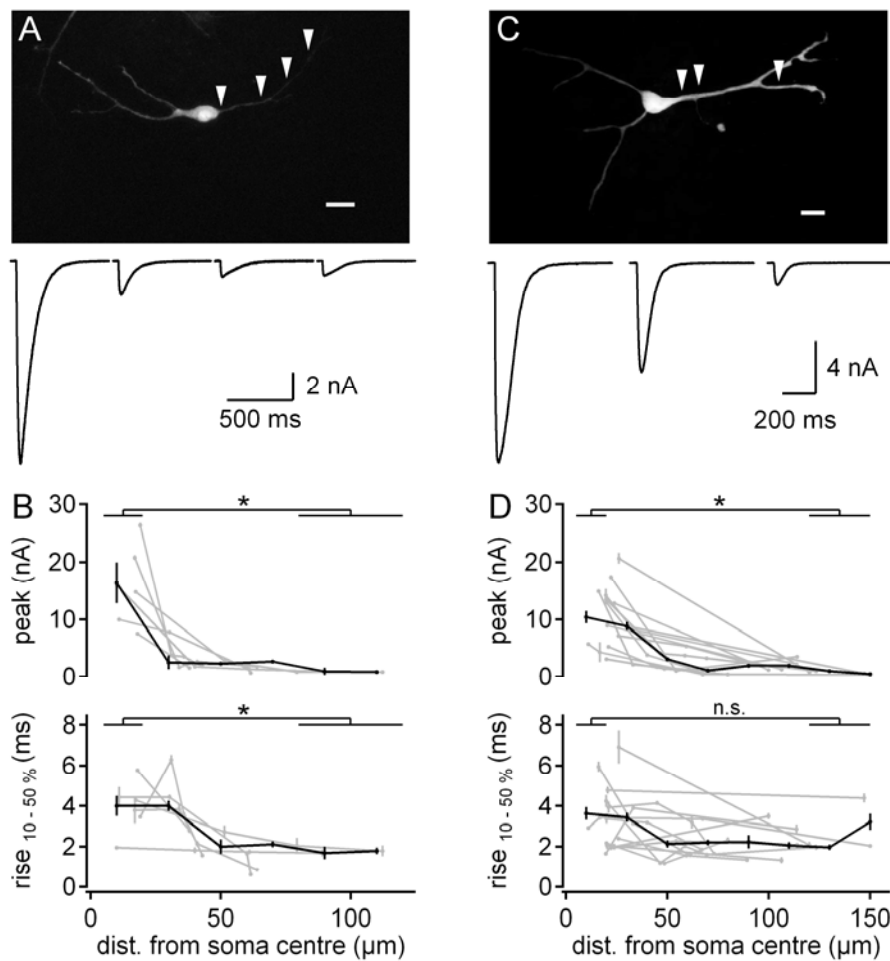


Figure 4.3 Comparison of GlyR distributions from P10 and P20 - 35 MSO neurons

A: Top: MSO neuron filled with Alexa 568, arrows indicate positions for pressure-application of 1 mM glycine. Bottom: corresponding GlyR mediated currents elicited (left to right) at 17 μ m, 51 μ m, 79 μ m and 112 μ m from the soma centre. **B:** Summary of peak (top) and 10 - 50 % rise times (bottom) of GlyR mediated currents plotted versus the distance from the soma centre of the stimulation position. **C:** Top: MSO neuron filled with Alexa 568, arrows indicate positions for pressure-application of 1 mM glycine. Bottom: corresponding GlyR mediated currents elicited (left to right) at 20 μ m, 33 μ m and 114 μ m from the soma centre. **D:** Summary of peak (top) and 10 - 50 % rise times (bottom) of GlyR mediated currents plotted versus the distance from the soma centre of the stimulation position. Individual cells in grey, average in 20 μ m bins overlaid in black. Star denotes significance ($p < 0.05$); n.s. is not significant.

Interestingly, already at P10, a sharp decrease in the GlyR mediated response from soma to dendrite was evident (Figure 4.3A & B; $n = 6$). Proximal dendritic GlyR currents (10 - 20 μ m from the soma centre) were on average 16.40 ± 1.23 nA; dendritic currents (80 - 120 μ m) were significantly smaller ($p < 0.05$), on average 873 ± 56 pA. The presence of a strongly biased receptor current in immature animals is surprising given that glycinergic

synaptic input is thought to be anatomically unrefined at this age (Kapfer et al., 2002). However, a sizable current (up to 1 nA) could be consistently elicited on dendritic end segments (Figure 4.3B, upper panel) indicating that this refinement process may not be fully complete. In general, for direct transmitter application, diffusion is a concern. However, an analysis of the 10 - 50 % rise times of these GlyR mediated currents showed a significant decrease ($p < 0.05$) in rise time from proximal locations (4.02 ± 0.26 ms) to distal ones (1.82 ± 0.16 ms). This decrease in rise time may reflect an overestimation of the proximal dendritic current, though it would not be enough to account for the order of magnitude difference in amplitudes evident in Figure 4.3B. The rise times also indicate that distally stimulated responses are likely mediated by distally located receptors.

As expected from anatomical results (Kapfer et al., 2002) and the GlyR gradient already evident at P10 (Figure 4.3B), GlyR mediated currents decreased significantly ($p < 0.05$) along the dendrite of MSO neurons at P20 - 35 (Figure 4.3C & D). The data were not significantly different between P20 and P35 (data not shown), so these data were pooled. At the proximal dendrite (10 - 20 μ m from the soma centre), an average current of 10.44 ± 1.05 nA could be elicited compared to 643 ± 67 pA at distal (120 - 150 μ m) sites (Figure 4.3D, upper panel). However, sizeable dendritic currents of up to 1 nA were still present, even distally, at this age (Figure 4.3D, upper panel). This indicates that either the GlyR gradient is fully mature by P10, or that there are a large number of extra-synaptic receptors throughout development which obscure a refinement of synaptic receptors. An analysis of the initial rise times (10 – 50 %) of the currents showed that those elicited proximally (3.63 ± 0.31 ms) and distally (2.8 ± 0.31 ms) were not significantly different ($p > 0.05$, Figure 4.3D, lower panel). This indicates that pressure-application of glycine along the MSO dendrite is affecting receptors over a consistently limited area, and confirms the presence of distally located GlyRs in the mature MSO.

Functional synaptic input to glycine receptors refines during development

To correlate the functional refinement of glycinergic synaptic inputs (Kapfer et al., 2002) with anatomical evidence (Kuwabara and Zook, 1992; Couchman et al., 2010), local pressure-application of a high $[K^+]$ solution was carried out at P10 and P20 - 35.

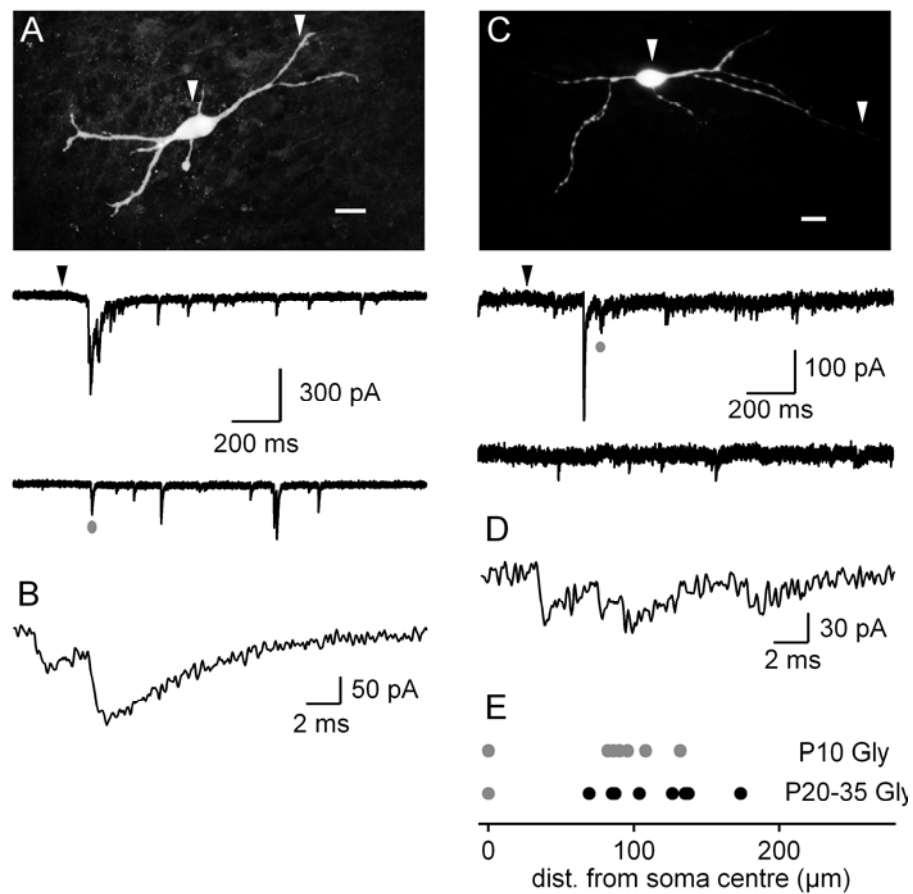


Figure 4.4 Comparison of synaptic input distributions to GlyRs from P10 and P20 - 35 MSO neurons

A: Top: MSO neuron filled with Alexa 488, arrows indicate position of pressure-application of 40 mM K⁺. Bottom: corresponding currents elicited at 0 μm (top) and 90 μm (bottom) from the soma centre. Response elicited by the release of multiple vesicles indicates the presence of excitatory synaptic inputs at both dendritic and somatic sites. Black arrowhead marks stimulus onset. Grey circle enlarged in (B). **B:** Synaptic GlyR mediated IPSCs elicited by the pressure-application of 40 mM K⁺. Extended time course from grey circle in (A). **C:** Top: MSO neuron filled with Alexa 568, arrows indicate position of pressure-application of 40 mM K⁺. Bottom: corresponding currents elicited at 0 μm (top) and 174 μm (bottom) from the soma centre. Response elicited by the release of multiple vesicles indicates the presence of excitatory synaptic inputs at somatic site only. Black arrowhead marks stimulus onset. Grey circle enlarged in (D). **D:** Synaptic GlyR mediated IPSCs elicited by the pressure-application of 40 mM K⁺. Extended time course from grey circle in (C). **E:** Summary of synaptic input sites to GlyRs at P10 (top) and P20 - 35 (bottom). Grey circles indicate the presence of an input; black circles are positions where no input could be elicited.

At P10, a total of 6 somatic and 6 dendritic locations (90 - 108 μm from soma centre) were probed (Figure 4.4E). At all locations tested, a burst of fast synaptic GlyR responses of varying sizes could be repeatedly stimulated (Figure 4.4A & B). This indicates that although GlyRs appear to have achieved their mature gradient, inhibitory synaptic input

targets all cellular compartments at P10, confirming previous anatomical findings (Werthat et al., 2008). In contrast, by P20 - 35, these responses were limited to the somatic region (Figure 4.4E). At the soma of all 8 cells tested, large bursts of synaptic GlyR responses could be repeatedly stimulated at the soma (Figure 4.4C - E). However, in a total of 10 dendritic locations ranging from 82 - 173 μ m from the soma, no synaptic input could be stimulated (Figure 4.4C & E). These results indicate that synaptic input is indeed functionally refined to the soma and proximal dendrites of mature MSO neurons. Additionally, the presence functional GlyRs on distal dendritic locations (Figure 4.3C & D), without a synaptic input (Figure 4.4C - E), demonstrates the presence of functional extra-synaptic receptors on the dendrites of mature MSO neurons. This finding also illustrates that the ‘background’ level of GlyRs evident at mature stages is sufficient to support functional synaptic inputs at P10.

Extra-synaptic glycine receptors are $\alpha\beta$ -heteromers

In other systems, the composition of synaptic and extra-synaptic GlyRs differs between those consisting of $\alpha\beta$ -heteromers and α -homomers, respectively (Deleuze et al., 2005b). To test if such heterogeneity exists in MSO neurons, we exploited the differential sensitivity of α -homomeric and $\alpha\beta$ -heteromeric GlyRs to Picrotoxin (PTX, (Pribilla et al., 1992; Schofield et al., 1996). When added to the bath solution at 100 μ M, PTX has significant antagonistic effect only on α -homomeric GlyRs. In 3 cells, distal pressure-application (106 - 147 μ m from the soma centre) of 1 mM glycine evoked 345 ± 100 pA of current. The addition of PTX did not significantly affect the currents ($p > 0.05$), which were on average 300 ± 89 pA (Figure 4.5A, lower panel & B). The subsequent bath application of 0.5 μ M STR abolished all GlyR currents (Figure 4.5A, lower panel), indicating that these distal extra-synaptic GlyRs are likely normal synaptic-type $\alpha\beta$ -heteromers.

In order to further characterise the composition of GlyRs in the MSO, peak-scaled non-stationary variance analysis was performed on mIPSCs recorded from 8 cells (Figure 4.5C & D). This analysis, when performed on mIPSCs, provides a global estimate for the average single channel current and average conductance state of all receptors activated during the mIPSCs (see Materials and Methods). mIPSCs were recorded and extracted.

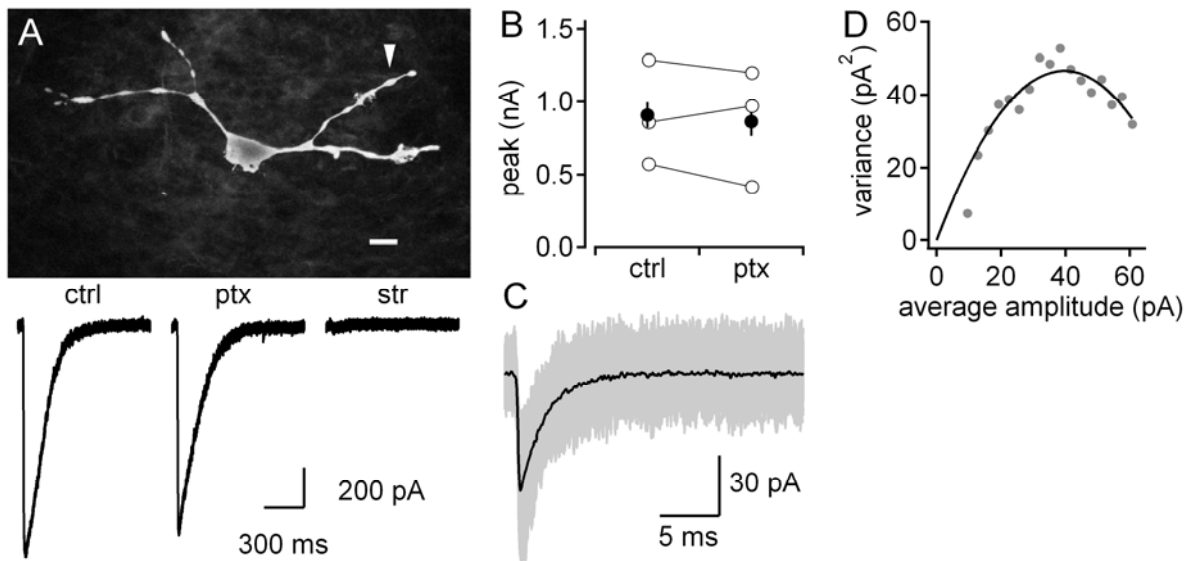


Figure 4.5 Characterisation of GlyRs

A: Top: MSO neuron filled with Alexa 488, arrow indicates location of pressure-application of 1 mM glycine. Scale bar is 20 μ m. Bottom: GlyR mediated currents elicited at 120 μ m from the soma centre. From left to right, pharmacologically isolated GlyR control (ctrl), the same current after the addition of 100 μ M picrotoxin (ptx) and the subsequent addition of strychnine (str). **B:** Summary of peak currents before (ctrl) and after (ptx) the addition of 100 μ M picrotoxin; currents were not significantly affected. Open circles are individual cells, black filled circles are average \pm SEM. **C:** GlyR mediated mIPSCs selected from 50 pA about the cellular mean. Individual mIPSCs are in grey, black average overlaid. **D:** Peak-scaled non-stationary fluctuation analysis of the mIPSCs in (C). Averaged, binned variance of mIPSC decays plotted versus the average mIPSC amplitude (grey circles). Parabolic curve used to estimate the single channel current in black.

mIPSCs from within 50 pA of the mean were then selected (Figure 4.5C). The variance during the decay phase of these selected minis was then calculated, binned and plotted against the average mIPSC amplitude for each cell (Figure 4.5D, grey circles). The resulting curve was fit with a parabola to determine the average single channel current, then used to calculate the corresponding conductance for all GlyRs (Figure 4.5D, black line). In 8 cells, an average single channel current of 2.39 ± 0.12 pA, corresponding to an average single channel conductance of 53 ± 2.7 pS was measured. This large conductance is not unusual for GlyRs, and corresponds to that found in both the dorsal cochlear nucleus (Balakrishnan and Trussell, 2008) and hypoglossal motoneurons (Singer and Berger, 1999). Consequently, the GlyR conductance in MSO neurons is at least two-fold larger than that of GluR2 and GluR4 glutamate receptors (Swanson et al., 1997; Cathala et al., 2005), the primary excitatory synaptic receptors in the mature MSO (Caicedo and Eybalin,

1999). This large difference in the single channel conductance of excitatory and inhibitory receptors is likely responsible for the difference in single fibre conductance demonstrated in Figures 3.1 and 3.2.

From these results, an estimate of the average density of GlyRs in the mature MSO could be made. These calculations used the average current peaks at proximal and distal dendritic sites, the driving force for GlyR mediated currents (45 mV; data not shown), the measured FWHM of pressure-applied glycine (16 μm) and the calculated single channel conductance for mature GlyRs (53 pS) along with the quantification of dendrite diameter (Rautenberg et al., 2009). As the single GlyR channel conductance is likely similar at P10 (Takahashi, 2005), the approximate receptor density at this age is 57 receptors / μm^2 at the proximal dendrite and 5 receptors / μm^2 at the distal dendrite. At P20 - P35, taking into account an increase in dendrite diameter (Rautenberg et al., 2009), the approximate density of GlyRs is 29 receptors / μm^2 at the proximal dendrite and 2 receptors / μm^2 on distal dendrites. Note the relatively scarce average GlyR density at dendritic locations at P10 is sufficient to support functional synapses.

GABA_A receptors are present but lack synaptic input on mature MSO neurons

GABAR mediated synaptic transmission is strongly down-regulated during the development of MSO neurons (Smith et al., 2000). However, a modulatory role for pre-synaptic GABA_BRs in the mature MSO has recently been suggested (Hassfurth et al., 2010). In order to identify a possible post-synaptic effect, the presence of GABA_ARs was probed using UV-uncaging of CNB-GABA on the dendrites of mature MSO neurons ($n = 13$). Surprisingly, GABA_AR mediated currents were consistently elicited along the entire cellular extent. As these currents were small, 4 - 8 trials per location were averaged and the rising phase of the current fit with a single exponential function to estimate τ_{rise} and current peaks (Fig 2.6A). Proximal to the soma (10 - 30 μm from the soma centre), an average of 39.27 ± 5.27 pA of GABA_AR mediated current was elicited, and at distal dendritic segments (90 - 150 μm) only 18.18 ± 4.26 pA. This drop in GABA_AR mediated current along the dendrite was apparently linear and significant ($p < 0.05$; Figure 4.6B, upper panel). Importantly, the average τ_{rise} of these GABA_AR currents were not significantly

different ($p > 0.05$, Figure 4.6B, lower panel) between proximal (5.42 ± 0.81 ms) and distal dendrites (8.50 ± 1.50 ms, $90 - 150$ μm).

The presence of functional GABA_ARs together with the report of punctate glutamic acid decarboxylase positive staining in the MSO (Hassfurth et al., 2010), is suggestive of a GABAergic synaptic input to MSO neurons. As before, the pressure-application of a high $[\text{K}^+]$ solution at both somatic and distal dendritic locations was used to probe for synaptic inputs to GABA_ARs (Figure 4.6C). In total, the soma of 9 cells and a total of 15 dendritic locations ranging from $62 - 238$ μm from the soma centre were probed (Figure 4.6D). However, no GABA_AR mediated synaptic input could be elicited (Figure 4.6C). In a set of additional experiments, GABA_ARs were pharmacologically isolated in an attempt to detect GABA_AR mediated mIPSCs (Figure 4.6E). In all of these recordings, the addition of DNQX, D-APV and STR abolished all mIPSCs, indicating a lack of functional synaptic input to GABA_ARs in the mature MSO ($n = 5$, Figure 4.6E). Electrical stimulation of fibre inputs ($n = 9$ cells) also failed to produce any GABA_AR mediated responses (data not shown). We therefore hypothesise that, contrary to previous assumptions (Hassfurth et al., 2010), these receptors respond to ambient GABA levels and are not activated by a direct, fast synaptic input.

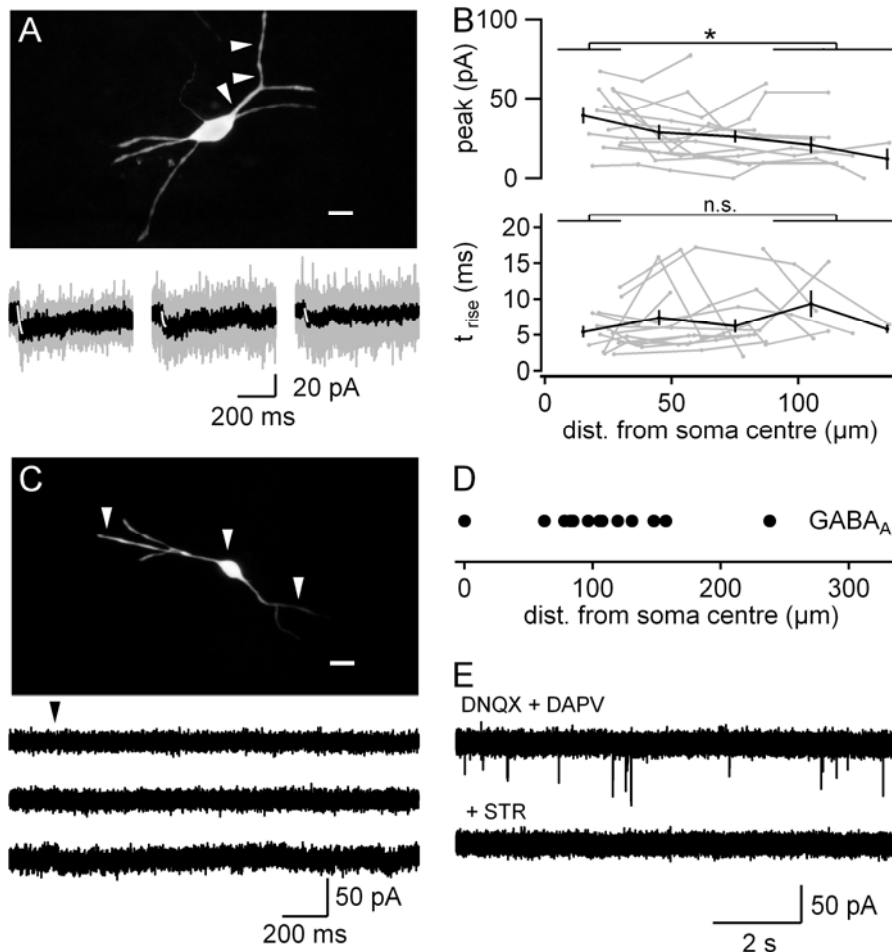


Figure 4. 6 GABA_A receptor and synapse distributions

A: Top: MSO neuron filled with Alexa568, arrows indicate CNB-GABA uncaging positions. Bottom: corresponding GABA_AR mediated currents elicited (left to right) at 23 μm, 62 μm and 81 μm from the soma centre. Grey traces are individual trials, black average overlaid. White trace is single exponential fit to rising phase used to calculate peak and τ_{rise} . **B:** Summary of peak (top) and τ_{rise} (bottom) of GABA_AR mediated currents plotted versus the distance from the soma centre of the uncaging position. Individual cells in grey, average in 20 μm bins overlaid in black. Star denotes significance ($p < 0.05$); n.s. is not significant. **C:** Top: MSO neuron filled with Alexa568, arrows indicate position of pressure-application of 40 mM K⁺. Bottom: corresponding currents elicited (top to bottom) at 105 μm, 0 μm and 85 μm from the soma centre. There was no response to the pressure-application of 40 mM K⁺, indicating a lack of excitatory inputs at these locations. Scale bars are 20 μm, all average values \pm SEM. **D:** Summary showing locations where we attempted to stimulate synaptic inputs to GABA_ARs. Black circles represent a failure to stimulate synaptic input at all positions tested. **E:** Example traces of mIPSCs recorded in the presence of DNQX and D-APV (top), the subsequent addition of strychnine (STR; bottom) abolished all mIPSCs. No GABA_AR mediated miniature events could be recorded.

V

NMDA receptors in the mature MSO

The experiments presented here deal with the questions raised in Chapter IV about the role of synaptic NMDARs in the mature MSO. Excitatory currents elicited by electrical fibre stimulation were pharmacologically characterised to determine the relative contribution of AMPARs, KARs, and NMDARs to mature synaptic signalling, including during ongoing activity. Additionally, the potentiation of NMDARs by synaptically released glycine is demonstrated, providing another mechanism by which coincidence detection in the MSO may be modulated.

NMDA receptors can be synaptically activated

The functional presence of NMDARs in neurons of the MSO from P30 - 35 animals is surprising. The contribution of NMDARs to excitatory synaptic currents was therefore measured in electrically stimulated fibre inputs. Both single pulse and train stimuli were applied to inputs to MSO neurons from mature animals at near-physiological temperature (35 – 36 °C). AMPAR and NMDAR mediated currents were recorded at -60 mV and +50 mV respectively. Single fibre shocks revealed substantial AMPAR mediated currents in MSO neurons (Figure 5.1A). On average, peak AMPAR mediated currents of 4.12 ± 0.76 nA were elicited at single stimulation sites (Figure 5.1D, $n = 13$). These currents had extremely fast decay time constants, on average 380 ± 43 μ s (data not shown). Again, no contribution from KARs was found during fibre stimulation in the presence of GYKI and

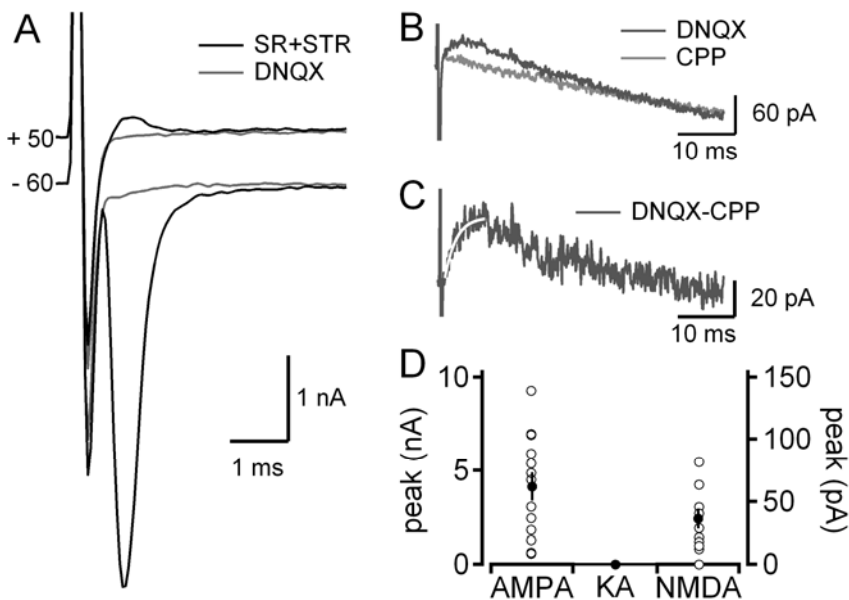


Figure 5. 1 NMDARs are recruited during fibre stimulation

A: Example traces of excitatory currents to MSO neurons elicited by electrical stimulation. Currents are recorded in whole-cell voltage clamp at +50 mV (outward currents) and -60 mV (inward currents). AMPAR mediated currents (dark grey traces) are blocked completely with DNQX (light grey traces). **B:** Extended timescale of average traces recorded at +50 mV. A slow NMDAR mediated component is blocked by CPP (light grey trace). **C:** Isolated NMDAR mediated current revealed after the subtraction of the average traces in B. White trace is a single exponential fit to the rising phase of the current used to calculate the peak of the NMDAR mediated response. **D:** Summary of peak AMPAR, kainate and NMDAR mediated currents. Circles are average currents from single cells; filled circle is average \pm SEM.

CPP ($n = 10$ cells; Figure 5.1D). Once a reliable excitatory input site was located (see Materials and Methods), AMPAR mediated currents were blocked with either DNQX or GYKI. For single fibre stimuli, a slow NMDAR mediated current was apparent in 9/13 cells after background subtraction, achieved by the subsequent application of CPP (Figure 5.1B and C). As these currents were small, 4 - 8 trials were averaged and a single exponential fit to the rising phase of the current used to calculate the τ_{rise} and peak of NMDAR mediated currents (white line in Figure 5.1C). In the 9 cells with an NMDA response, single fibre stimulation produced an average NMDAR mediated current of 36.3 ± 7.97 pA (Figure 5.1D) with an average τ_{rise} of 3.24 ± 0.43 ms (data not shown).

In order to describe the summation of these NMDA currents during ongoing activity, a 10-pulse stimulus train at 200 Hz was applied ($n = 10$; 5 of these cells were also used in the

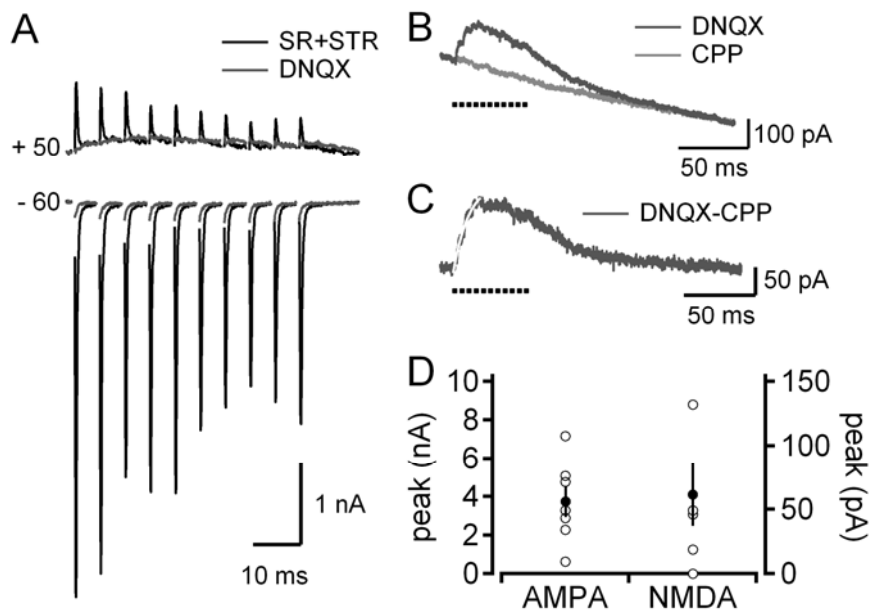


Figure 5.2 NMDAR currents accumulate during fibre stimulus trains

A: Example traces of excitatory currents to MSO neurons elicited by 200 Hz electrical stimulation for 10 pulses. Stimulus artefacts have been removed for clarity. Currents are recorded in whole-cell voltage clamp at +50 mV (outward currents) and -60 mV (inward currents). AMPAR mediated currents (dark grey traces) are blocked completely with DNQX (light grey traces). **B:** Extended timescale of average traces recorded at +50 mV. A slow NMDAR mediated component is blocked by CPP (light grey trace). **C:** Isolated NMDAR mediated current revealed after the subtraction of the average traces in (F). White trace is a single exponential fit to the rising phase of the current used to calculate the peak of the NMDAR mediated response. **D:** Summary of peak AMPAR and NMDAR mediated currents. Circles are average currents from single cells; filled circle is average \pm SEM. Dotted line indicates train duration.

single stimulus pulse recordings; Figure 5.2A). The average peak AMPAR mediated current from the first pulse of the train was 3.91 ± 0.63 nA (Figure 5.2D) and these currents decayed with a time constant of 349 ± 15 μ s (data not shown). In 4/10 of these cells, an NMDAR mediated current was present and built up over the course of the stimulus train (Figure 5.2B & C). The peak of this current was calculated from a fit to the average of 4 - 8 trials recorded after DNQX application (Figure 5.2B), subsequently baselined via the subtraction of an averaged trace recorded in the presence of CPP (Figure 5.2C). During the stimulus train, an average peak NMDA current of 61.6 ± 2.5 pA ($n = 4$) was elicited (Figure 5.2D). Thus, ongoing activity can generate a two-fold increase in the NMDAR mediated response.

Synaptically released glycine potentiates NMDA receptors

Given the similar distribution profiles of GlyRs and NMDARs on MSO neurons, an interaction between the glycinergic and glutamatergic (NMDAR) transmitter systems on the receptor level (Johnson and Ascher, 1987; Ahmadi et al., 2003; Li et al., 2009) is possible. As excitatory and inhibitory synapses and NMDA and Glycine receptors colocalise at MSO somata, any interaction between these systems would likely take place there. We therefore sought to potentiate somatic NMDAR responses to uncaging pulses with synaptically released glycine. During whole-cell voltage-clamp recordings at holding potentials of +50 mV at 35 - 36 °C, glycinergic inputs to MSO neurons were stimulated with a 10 pulse train at 200 Hz using a glass fibre stimulation electrode (n = 8; Figure 5.3A). 5 ms after the final stimulus pulse of the train, we uncaged MNI-Glu at the soma of the neuron using a 40 X objective for 500 μ s (Figure 5.3A: inset). To correct for background currents, interleaved recordings of either a glycinergic train alone or a simple step to +50 mV were subtracted from those with uncaging pulses (Figure 5.3B). NMDAR responses elicited by uncaging were potentiated significantly both in peak amplitude (117.9 ± 21.5 to 137.5 ± 25.7 pA) and charge (10.6 ± 2.5 to 13.2 ± 3.1 pS; $p < 0.05$, paired t-test; Figure 5.3C) when paired with the stimulation of glycinergic inputs. This potentiation of NMDARs by synaptically released glycine suggests a functional role for the colocalisation of glycinergic inputs and NMDARs at the MSO soma. Specifically, it indicates an interaction between excitatory and inhibitory neurotransmission systems on the somata of matured MSO neurons is possible during ongoing activity. It also demonstrates that at least *in vitro*, the glycine binding site on NMDARs is not saturated.

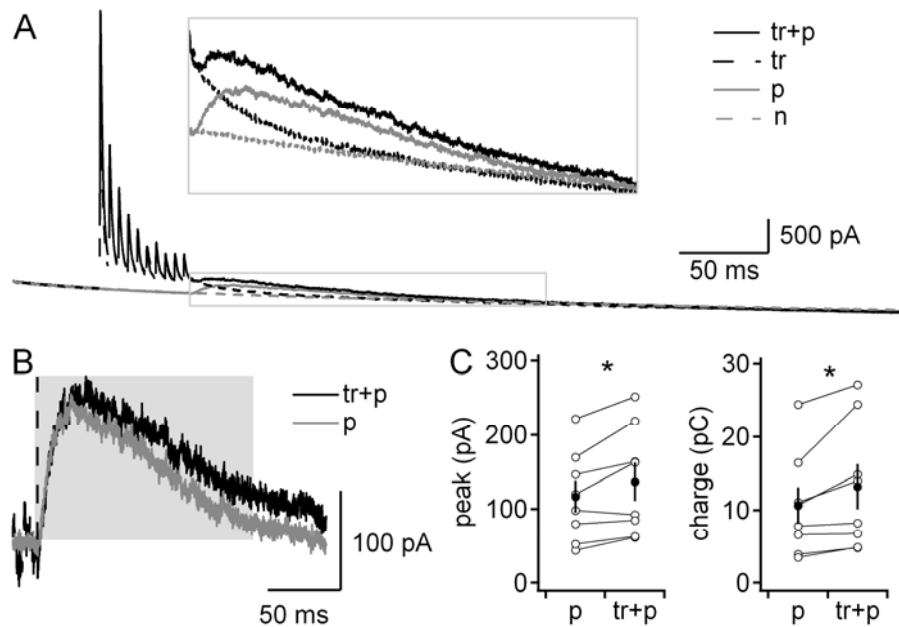


Figure 5.3 Synaptically released glycine acts on somatic NMDARs

A: Currents elicited by electrical stimulation of inhibitory inputs and/or glutamate uncaging on MSO neurons during a step to +50 mV. Solid traces contain a 500 μ s uncaging stimulus on the soma of the neuron; in the recordings in black the uncaging pulse was preceded by a 10-pulse train of glycinergic inputs at 200 Hz. Inset is an enlargement of the area indicated by the grey box. tr: glycinergic train; p: uncaging pulse, n: simple step to +50 mV to subtract background currents. **B:** NMDAR mediated currents resulting from the subtraction of traces in A; the dashed traces were subtracted from the respective solid traces to remove background leak currents, glycinergic currents and stimulus artefacts. Grey trace (p) is the NMDAR mediated current elicited by an uncaging pulse alone; black trace (tr+p) is the same current elicited 5ms after a 200 Hz glycinergic train. Dotted line indicates the onset of the uncaging stimulus, grey shaded area was used for calculation of the charge through NMDARs. **C:** Summary of peak (left) and charge (right) of the response to the uncaging pulse without (p) and with (tr+p) a preceding glycinergic train. Open circles are results from individual cells; filled circles are the average \pm SEM. Statistical significance was calculated with a paired *t*-test, star denotes significance ($p < 0.05$). All recordings were made at near physiological temperature (35 - 36 °C).

VI

Discussion

This work provides new insight into the functioning of the most temporally precise of all mammalian coincidence detectors, within an *in vitro* context. Chapter III details the significant strength of single excitatory and inhibitory inputs to MSO neurons from adult gerbils. Consequently, despite extremely fast membrane time constants and a very low input resistance, action potential threshold is reached from rest with the integration of only 2 - 4 excitatory inputs. Although individual inhibitory fibres to MSO neurons impose a two-fold larger conductance than excitatory fibres, we estimate from functional and anatomical data that each MSO neuron receives a minimum of 4 - 8 excitatory inputs and 2 - 4 inhibitory inputs, resulting in an equal overall post-synaptic conductance for both excitatory and inhibitory inputs (for summary see Figure 6.1).

From the functional mapping of neurotransmitter receptors and synaptic inputs described in Chapter IV, the importance of AMPAR and GlyR signaling at the synapse is confirmed although the strict segregation of excitatory and inhibitory inputs is challenged. In addition, this work uncovers the maintenance of NMDARs and GABARs in the mature MSO, and provides evidence for a shift to largely extra-synaptic roles for these receptors. Further involvement of NMDARs is revealed in Chapter V, both synaptically and in the cross-modulation of excitatory and inhibitory inputs, adding a further level of complexity to our understanding of MSO function (for summary see Figure 6.2).

Size and strength of single inputs to MSO neurons

The synaptic strength and size of excitatory and inhibitory inputs were compared, both in terms of post-synaptic currents and their accompanying conductances. From our data we estimate the overall inhibitory input and the minimally required amount of excitation for AP generation to an MSO neuron. We estimate from our anatomical data that 2 - 4 inhibitory fibres innervate each MSO neuron (Figure 3.4), conveying a total inhibitory conductance of 160 - 240 nS (Figure 3.2). We confirm that this inhibition is mainly targeted to the soma (Clark, 1969; Kapfer et al., 2002; Werthat et al., 2008). Excitation onto bipolar MSO neurons, on the other hand, is compartmentalized according to the side of origin; contralateral excitation contacts the medial and ipsilateral excitation the lateral dendrite (Stotler, 1953). It is known that the excitatory drive onto one of these dendrites can be sufficient to elicit an AP; (Goldberg and Brown, 1969; Yin and Chan, 1990; Grothe and Sanes, 1993), which we estimate requires the simultaneous activation of 2 - 4 fibres (Figure 3.3) with a total conductance of ~70 - 140 nS (Figure 3.1). Thus it follows that at least 4 - 8 excitatory fibres converge onto a single MSO neuron generating approximately 140 - 280 nS in total. The corresponding synaptic currents that are required for AP generation were found to be larger than previously estimated using step current injections (Scott et al., 2005; Chirila et al., 2007). This is likely due to the extremely rapid kinetics of EPSCs in the MSO which may not activate the same voltage-dependent conductances as would be activated during a long depolarisation (Couchman et al., 2010). These currents are produced by a pool of ~120 vesicles in each excitatory fibre (Couchman et al., 2010), similar to the readily releasable pool measured at the upstream endbulb of Held synapse (Oleskevich et al., 2004). The total excitatory drive to MSO neurons (from at least 4 - 8 fibres) is therefore likely larger than the endbulb input to bushy cells (from 2 - 4 endbulbs) (Sento and Ryugo, 1989; Ryugo and Sento, 1991; Chanda and Xu-Friedman, 2010), and results in a combined pool size that rivals the calyx of Held synapse (Schneggenburger et al., 1999; Wu and Borst, 1999; Taschenberger and von Gersdorff, 2000).

Neurons of the MSO are very electrically leaky, with an input resistance of 5 - 7 M Ω , and a membrane time constant likely faster than the 200 - 300 μ s reported so far (Magnusson et al., 2005; Scott et al., 2005; Chirila et al., 2007; Couchman et al., 2010). These neurons are therefore well equipped to rapidly and effectively shunt synaptic current, even without the

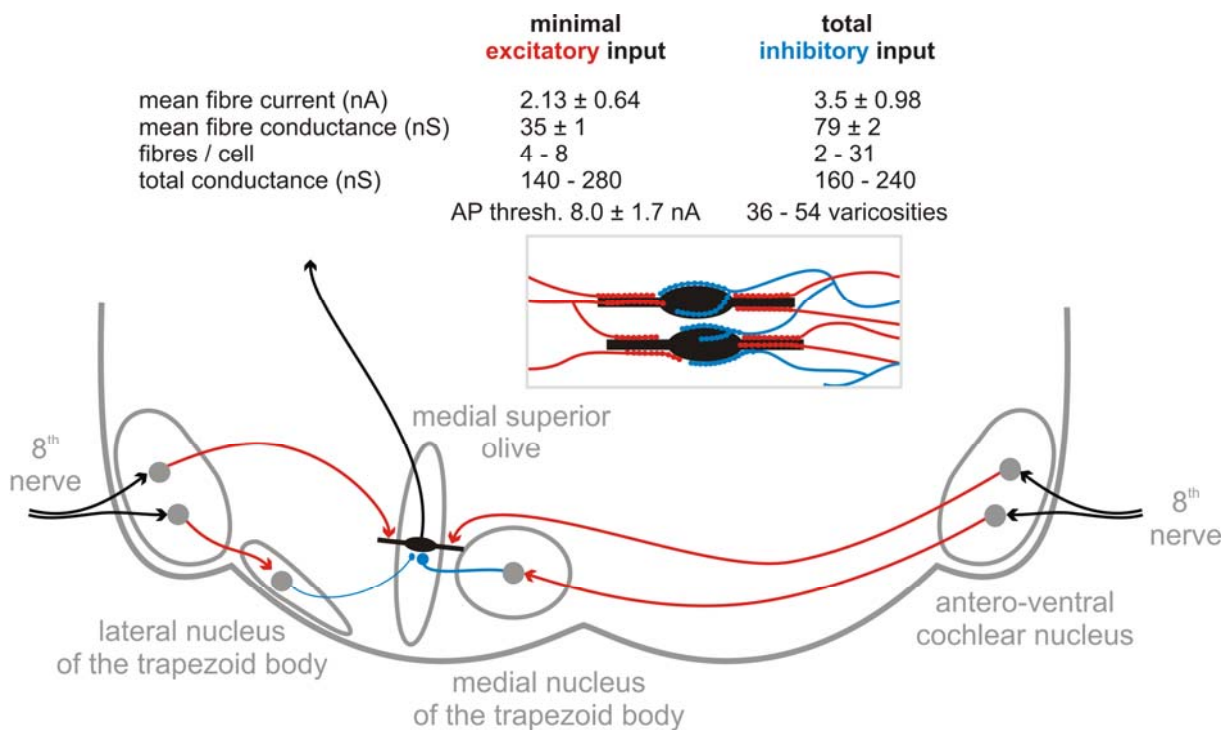


Figure 6. 1 Summary schematic of excitatory and inhibitory input statistics

Despite different single fibre currents and conductances, the overall impact of the minimal excitatory and total inhibitory input is similar. AP threshold in adult MSO neurons is reached from rest with the simultaneous activation of 2 - 4 excitatory fibres, and each MSO neuron receives a large number of inhibitory varicosities, likely containing multiple release sites.

additional conductance that accompanies the unusually large synaptic inputs that the MSO receives. Indeed, the conversion of EPSC to EPSP occurs with little chance for the activation of voltage-dependent potassium conductances during the time course of such rapid synaptic current kinetics (Couchman et al., 2010). This rapid shunting effectively shortens the coincidence detection window to the limits of synaptic kinetics, providing a means by which relatively slow APs can be converted into a code with microsecond accuracy.

Given the large resting leak of MSO neurons, large single fibre inputs may be a means of countering the resultantly high current thresholds for AP generation reported here, whilst minimising jitter between multiple single fibre inputs. This suggests that MSO neurons are utilising a coincidence detection strategy cogent with our current knowledge of fast auditory processing, i.e. a preference for fewer, larger single fibre inputs. Additionally, this circuit clearly relies on massive leak conductances (Scott et al., 2005; Golding et al., 2009)

to further limit coincidence detection windows. Therefore, the modulation of synaptic input through cross-talk or the presence of additional activity-dependent conductances could dynamically modulate timing, and in turn coincidence detection windows and ITD coding. However, it is important to note that inputs to the MSO undergo significant short-term depression, even at relatively low frequencies (Couchman et al., 2010), meaning that our estimates of excitatory input number are a lower bound for the total excitatory drive to MSO neurons. The estimate of AP threshold presented here is also in the absence of inhibition, which we know shapes ITD coding *in vivo* (Brand et al., 2002; Pecka et al., 2008). However, the consequences of this inhibitory input are difficult to predict. On the one hand, activation of inhibitory inputs would hyperpolarise the membrane whilst introducing a substantial synaptic conductance, thereby increasing AP current thresholds *in vivo*. Conversely, this hyperpolarisation may deactivate K_{LVA} and strongly activate I_h conductances, increasing the membrane resistance and strengthening the rebound depolarising current, thereby decreasing AP current threshold. The precise effects of inhibitory inputs on AP generation are likely to depend on the relative timing of excitatory and inhibitory inputs. Indeed, membrane potential rebound from a temporally precise inhibitory input precedent to the excitation is a likely mechanism for producing ITD coding *in vivo* (for review, see Grothe, 2003).

The unusual strength of the inhibitory input speaks to the fundamental importance of inhibition in this circuit (Brand et al., 2002; Pecka et al., 2008). In order to convey such an input, a single fibre would have to contain at least 50 active zones; however, reconstruction of these fibres indicates that less than half that number of synaptic varicosities is present (Figure 3.4). This apparent contradiction is resolved by ultra-structural evidence from EM studies that indicate multiple active zones in single excitatory and inhibitory varicosities (Clark, 1969; Lindsey, 1975; Kiss and Majorossy, 1983; Brunso-Bechtold et al., 1990; Kapfer et al., 2002). Therefore, if we assume that each of the varicosities counted in single fibre reconstructions is a synaptic input, then each must contain 2 - 3 active zones. This results in an apparent pool of ~70 vesicles in each individual inhibitory fibre to the MSO (Couchman et al., 2010). Such a specialisation is congruent with the large pool sizes of the excitatory input to the MSO, and of excitatory endbulb and calyx synapses located upstream in the ITD processing pathway.

Functional mapping of receptors and synapses in the MSO

Single photon UV laser uncaging is a useful tool for investigating functional morphology in terms of the distribution of neurotransmitter receptors. Neurons of the MSO are ideal to investigate receptor distributions using this tool given they have short, spineless dendrites (typically ~ 150 μm in length) aligned in a single focal plane with a relatively uniform diameter (Rautenberg et al., 2009). The suitability of these neurons was confirmed by an analysis of the rise times of uncaging-elicited currents. This indicated that experimental distortions such as space clamp and light scatter did not interfere substantially with our results. UV uncaging of caged glutamate and GABA was used to provide maps of the subcellular functional distributions of AMPARs, NMDARs and GABA_ARs. Due to the scarcity of biologically inert caged glycine compounds, GlyRs were mapped using a minimal pressure-application paradigm. Although this technique has a lower resolution, we were able to ensure the uniformity of the stimulus (Figure 2.2E), making this technique a fair match for comparison with UV uncaging methods.

The bipolar morphology of MSO neurons and their arrangement is suggestive of a segregation of function between the medial and lateral dendrites. Indeed, it has been suggested that a systematic asymmetry in dendritic properties could be present and computationally relevant for ITD coding in the MSO (Jercog et al., 2010). However, in the course of the study presented in Chapter IV, it was found that medial and lateral dendrites of MSO neurons express similar complements of neurotransmitter receptors with a similar pattern. All evidence to date also suggests that there is no difference in the expression of other important voltage-gated conductances on MSO dendrites (Mathews et al., 2010; Scott et al., 2010). *In vivo* evidence from the cat (Yin and Chan, 1990), gerbil (Spitzer and Semple, 1995), dog (Goldberg and Brown, 1969) and rat (Inbody and Feng, 1981) suggests that individual MSO neurons may be more strongly driven by either ipsilateral or contralateral inputs. In these studies, the proportions of ipsilaterally or contralaterally dominated neurons appear to be roughly even (contralaterally dominated neurons were more numerous only in Inbody and Feng, 1981). Thus it is not surprising that no systematic difference between medial and lateral MSO dendrites could be identified in the present study. However, it is not possible to conclude that MSO dendrites are symmetrical as the resolution of the functional receptor maps (FWHMs ranging from ~ 7 - 16 μm), was

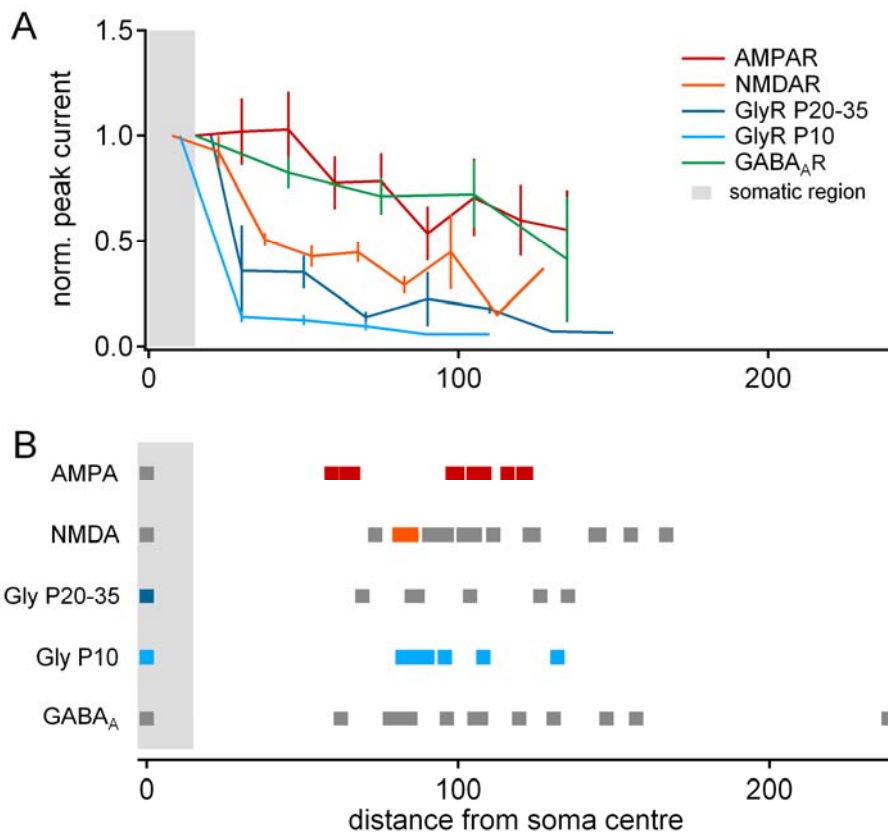


Figure 6.2 Summary of functional receptor and synapse distributions

A: Normalised functional receptor distributions as a function of distance from soma centre. Lines represent average peak currents SEM. **B:** Synaptic input locations probed using high $[K^+]$ solution as a function of distance from soma centre. Coloured points represent sites where synaptic input could be stimulated. At locations indicated with grey points no synaptic input could be stimulated.

not sufficient to analyse the receptor complements at individual synaptic input sites. Additionally, as these neurons lack dendritic spines, it is not possible to determine exactly how many synaptic input sites are affected by the mapping stimulus. It is therefore possible that there remains some synaptically defined difference between the medial and lateral dendrites of MSO neurons which may well have computational consequences (Jercog et al., 2010).

The difficulty in drawing conclusions about the synaptic involvement of receptors from the results presented in this study is highlighted in the mapping of functional GlyRs at different age groups. Although the distributions of GlyRs did not undergo a marked change between P10 and P20 - 35 (Figure 6.2A), the synaptic input was shown to undergo a

significant functional refinement during this period (Figure 6.2B). As an interesting side-note, estimates of the distal dendritic GlyR density (Chapter IV) combined with the presence of functional dendritic input at P10 indicate that only a relatively low overall receptor density (~ 2 receptors / μm^2) is required to maintain functional synaptic inputs. These findings also confirm that it is likely that the techniques used in this study provide far more information about extra-synaptic than synaptic receptors. However, this approach allowed us to identify extra-synaptic signalling processes, specifically the maintenance of GABA_ARs and possible circuit modulation by NMDARs.

The mapping of receptors, both in and outside of the synapse, can provide information on synaptic function, as both synaptic AMPARs (Borgdorff and Choquet, 2002; Groc et al., 2004) and GlyRs (Dahan et al., 2003; Levi et al., 2008) are often highly mobile in the membrane. This mobility is often activity-dependent and is a key regulator of synaptic plasticity and the maintenance of synaptic function through receptor cycling (Choquet and Triller, 2003). Thus, despite the limitations of a functional anatomical approach in terms of synaptic characterisation, it can provide unique insights into the behaviour of neurotransmitter receptors across the whole neuron.

To complement the receptor mapping approach, the cellular compartmentalisation of synaptic inputs to MSO neurons was also mapped (Figure 6.2B). From early anatomical studies, a strict segregation between excitatory dendritic input and inhibitory somatic input was proposed. However, this segregation likely only holds for dendritically targeted excitation, as the soma of MSO neurons receives both excitatory and inhibitory input (see Figures 4.2E & 4.4E). This arrangement is thought to be important for ITD computation by shaping the relative timing of the somatic integration of excitatory and inhibitory inputs (Agmon-Snir et al., 1998; Zhou et al., 2005). These neurons are morphologically compact (Rautenberg et al., 2009) and densely innervated by synaptic input (Stotler, 1953; Kapfer et al., 2002; Couchman et al., 2010), with excitatory inputs arranged to target the dendrite of the side of origin. It is therefore possible that this arrangement is a strategy for allowing for the massive synaptic innervation of MSO neurons whilst maintaining a simplified wiring pattern and minimal membrane complexity.

AMPA receptors and their inputs

This study confirms that AMPARs are the major excitatory neurotransmitter receptor both on the membrane and at excitatory synapses to mature MSO neurons. Specifically, AMPARs are evenly distributed across the entire dendritic surface of MSO neurons (Figure 6.2A), and conduct nearly all of the excitatory synaptic current (Figure 5.1 - 5.3) at synapses located at both somatic and dendritic locations (Figure 6.2B). These findings complement previous anatomical investigations (Stotler, 1953; Caicedo and Eybalin, 1999). Given the large single excitatory fibre currents reported here, it is likely that each fibre possesses large numbers of synaptic contacts with multiple active zones. It is therefore possible that morphologically, these inputs will resemble the inhibitory input morphology, i.e., that a single fibre input would contact multiple points of the post-synaptic dendrite, spread over a relatively large area (Figure 6.1). However, the morphology of these inputs in terms of fibre convergence has yet to be thoroughly described, so it is unknown exactly how many presynaptic neurons contribute to excitatory signalling in the MSO, and how they might be organised.

The rapid kinetics of AMPAR EPSCs at physiological temperature (Figure 3.1), with decay time constants on the order of ~ 200 μ s are similar to other reports (Couchman et al., 2010). There is only a small increase in the decay time constant as additional fibres are recruited, indicating that fibres are highly synchronous (Figure 3.1E). This small increase may be responsible for the slower kinetics reported in Figure 5.1 (~ 300 μ s), where multiple fibres may have been recruited asynchronously. It is also possible that the decay phase of these currents could be affected by an additional NMDAR mediated current, which was not pharmacologically blocked in these experiments. The pharmacological blockade of NMDARs is important in the auditory brainstem as these receptors are typically activatable at rest (-60 mV) (Smith et al., 2000; Steinert et al., 2010). In any case, any measurement of current kinetics in mature MSO neurons is likely to result in an underestimate of the true current speed, partly due to the difficulty in clamping such leaky cells at physiological temperature. However, the fast AMPAR mediated current kinetics reported here support immunohistochemical evidence for the inclusion of fast GluR4 subunits in AMPARs in the mature auditory brainstem (Caicedo and Eybalin, 1999).

The development of glycine receptors and their inputs

The inhibition in mature MSO neurons is mediated by α/β heteromeric GlyRs, which are widely present on the membrane with a strong somatic bias apparent already at P10 (Figure 6.2A). In contrast to the distribution of GlyRs, inhibitory synaptic inputs appear to refine between P10 and P20 - 35 and at mature stages target only the soma and proximal dendrites (Figure 6.2B). Although the developmental refinement of inhibitory inputs has been described previously in anatomical studies (Kuwabara and Zook, 1992; Kapfer et al., 2002), the stability of the GlyR distribution throughout development was surprising. It is possible that extra-synaptic GlyRs may play a trophic role, where taurine may act as an agonist, though this action is most common during neonatal development (Flint et al., 1998), or in brain areas where GABA is the main inhibitory synaptic neurotransmitter (Deleuze et al., 2005a). On the other hand, as mentioned previously, synaptic receptors often diffuse laterally in the neuronal membrane, and GlyRs have been shown to diffuse in and out of the synapse (Dahan et al., 2003). In spinal cord neurons, where glycine is also the major inhibitory neurotransmitter, as many as 50% of GlyRs are extra-synaptic, with a large proportion of these diffusing freely in the membrane (Srinivasan et al., 1990; Levi et al., 2008). In the MSO, the expression of the GlyR anchoring protein gephyrin is sharply down-regulated on the dendrites (Kapfer et al., 2002), meaning that dendritic GlyRs are less likely to form clusters. Thus the presence of extra-synaptic GlyRs on the dendrites of mature MSO neurons (Figure 4.3) is not entirely without precedent, and may serve simply to provide a pool of receptors to maintain synaptic stability during ongoing activity.

NMDA receptors and their role in the mature MSO circuit

NMDARs are functionally expressed on mature neurons of the MSO. Interestingly, they are biased to the soma, resulting in a distribution profile more similar to GlyRs than AMPARs. Using both the chemical (Figure 4.2E) and electrical (Figure 5.1) stimulation of excitatory inputs, NMDARs were found to contribute only minimally to excitatory currents in the MSO. When present, they produced currents that were fast in rise with apparently slow decay time constants. The maintenance of NMDAR signalling in the mature MSO joins other work in the MNTB which indicates that NMDARs may shift roles during

development from charge carriers to mediators of Ca^{2+} influx at mature stages (Steinert et al., 2010). Additionally, as NMDARs are gated only in the presence of both glutamate and glycine, they are strongly implicated in maintaining a balance between excitation and inhibition at the synapse level.

The mismatch between the expression pattern of NMDARs and AMPARs (Figure 6.2A), as well as their synaptic activation patterns (Figure 6.2B), led us to search for functional roles for NMDARs other than as synaptic charge carriers. In the mature AVCN, NMDARs may maintain firing and increase precision during ongoing activity (Pliss et al., 2009). NMDARs are also maintained in the mature MNTB, where they may contribute to Ca^{2+} influx (Steinert et al., 2010). However, in the MSO it appears that the majority of NMDARs were extra-synaptic, so other functional roles might be considered. The similarity between the distributions of NMDARs and GlyRs and mature inhibitory input patterns was particularly striking, especially given that glycine and NMDARs have been shown to interact in other systems (Johnson and Ascher, 1987; Kotak and Sanes, 1996; Berger et al., 1998; Ahmadi et al., 2003; Li et al., 2009). Using a combination of uncaging and electrical fibre stimulation, we show that synaptically liberated glycine potentiates currents through NMDARs located at the soma of mature MSO neurons (Figure 5.3). Although the purpose of this interaction remains speculative, we favour a role in activity-dependent signalling, where NMDARs may be activated during periods of strong excitatory and inhibitory drive.

NMDARs have a high affinity for glutamate, making them ideal for sensing low glutamate levels such as might be encountered extra-synaptically. In this case, the activation of a slow NMDAR mediated excitatory conductance will add additional leak to MSO neurons, increasing the precision of coincidence detection, especially when inputs are driven at a high frequency. It is also possible that the activation of NMDARs provides a slow, temporally summing excitatory drive to MSO neurons, thus slowing the overall speed of excitatory signalling. This might be a way to compensate for the kinetic imbalance between excitation and inhibition (Figure 3.1 and 3.2). However, as the NMDAR mediated currents reported here are not large, NMDARs in the MSO may be involved in other signalling processes.

As NMDARs are highly permeable to Ca^{2+} , they can indirectly modulate the state of

synaptic receptors through the activation of Ca^{2+} -dependent signalling processes (Bliss and Collingridge, 1993; Malenka and Nicoll, 1993). Amongst a myriad of other functions, Ca^{2+} influx can modulate the mobility of AMPARs (Borgdorff and Choquet, 2002). The same is true for GlyRs, whose mobility is controlled by cytoskeletal elements (Charrier et al., 2006), which are in turn modulated by Ca^{2+} influx through NMDARs in a mechanism that can boost inhibitory drive (Levi et al., 2008). Thus NMDARs provide a mechanism by which the receptor population at synapses in the MSO could be altered in an activity dependent manner. Unfortunately, little is known about Ca^{2+} signalling in the MSO as until now it was thought that the circuit operates with a relatively hard-wired set of inputs and the integration of direct ionic currents. Indeed, most forms of synaptic plasticity involving NMDARs would be disadvantageous in a system that needs to produce a consistent code for ITDs over time. Thus it cannot be discounted that NMDARs in the mature MSO represent some residual and unused signalling mechanism.

GABA receptors and their role in the mature MSO circuit

Finally, mapping of GABA_ARs revealed that they were consistently present along the entire extent of MSO neurons (Figure 4.6B). This is a surprising result given that no direct GABAergic input is described to these neurons at mature stages. Indeed, no fast GABA_AR mediated current could be synaptically stimulated, nor could any spontaneous GABA_Aergic events be observed (Figure 4.6C - E). This indicates that GABAergic inputs likely affect MSO neurons through volume transmission rather than through direct synaptic transmission. It has been reported that excitatory and inhibitory inputs to the MSO are subject to modulation via pre-synaptic GABA_BRs (Hassfurth et al., 2010). It is therefore possible that postsynaptic GABA_ARs might sense the spillover from the activation of pre-synaptic GABA_BRs, or be a direct target of this GABA source.

In bushy cells of the AVCN, synaptic current through GABARs is minimal, even while GABA_BRs modulate synaptic inputs pre-synaptically and GABA_ARs are expressed diffusely on the post-synaptic membrane (Lim et al., 2000). This combination of pre- and post-synaptic modulation can regulate the input/output function of bushy cells in an activity-dependent manner. Specifically, GABA_BRs on the pre-synapse decrease vesicular release, while GABA_ARs increase the AP current threshold post-synaptically (Chanda and

Xu-Friedman, 2010). Thus, strong GABAR activation converts these neurons from a relay that fires to asynchronous inputs into coincidence detectors, requiring the simultaneous activation of multiple inputs (Chanda and Xu-Friedman, 2010). Such a mechanism could well be operating in the MSO during sustained periods of activity, although unlike in the AVCN (Caspary et al., 1994; Kopp-Scheinpflug et al., 2002; Gai and Carney, 2008), an *in vivo* role for GABA signalling in the mature MSO has yet to be demonstrated.

Although the subunit structure of the GABA_ARs in the MSO has not been thoroughly characterised (Campos et al., 2001), extra-synaptic GABA_A receptors almost always contain δ subunits (Nusser et al., 1998; Wei et al., 2003). The incorporation of this subunit results in receptors with a high affinity for GABA and minimal desensitisation, making them ideal sensors for ambient GABA levels (Saxena and Macdonald, 1994, 1996; Mody, 2001). Functionally, these receptors have diverse roles. In the dentate gyrus, δ subunit containing GABA_ARs prevent epileptic seizures by controlling hyper-excitability (Spigelman et al., 2002; Peng et al., 2004). These receptors are also a major target for neurosteroids (Mihalek et al., 1999; Belelli et al., 2002; Wohlfarth et al., 2002). Extra-synaptic GABA_ARs are also implicated in the modulation of cellular computation (Chen et al., 2010) and neuronal gain control (Semyanov et al., 2004; Farrant and Nusser, 2005). These receptors are therefore involved in a number of extra-synaptic processes that maintain circuit stability through homeostatic mechanisms, and we suggest such a role for them in the MSO. Additionally, the activation of GABA_ARs would add a diffuse activity-dependent conductance. This could well be part of a mechanism to dynamically adjust the leak of MSO neurons, thereby modulating coincidence detection windows.

Coincidence detection in MSO neurons

Neurons of the MSO are highly specialised for precision and speed, allowing them to produce an output code that represents microsecond scale changes in sound information. The circuit that feeds into this nucleus is wired for speed from the first synapses at the inner ear, and culminates at the MSO with extremely large and densely packed synaptic inputs mediated by fast AMPA and glycine receptors. The simple morphology of MSO neurons, combined with an extremely fast membrane time constant and low input resistance adapt this neuron for remarkable precision. The presence of additional, slower

NMDA and GABA receptors may provide a mechanism for modifying activity both on the single neuron and nucleus level. These specialisations mean that MSO neurons may be able to operate as a single electrical compartment, rapidly and repeatedly performing coincidence detection computations, even on a cycle-by-cycle basis. If this is the case, then MSO neurons may be thought of electrotonically as a ‘point’ neuron.

In order for MSO neurons to accurately and rapidly integrate synaptic inputs, it has been reported that somatically biased gradients of Na^+ and K_{LVA} conductances in MSO neurons actively linearise excitatory inputs arriving at different dendritic locations (Mathews et al., 2010; Scott et al., 2010). However, recent evidence has suggested that EPSPs in the MSO are too brief to allow for the activation of any voltage-dependent potassium conductances (Couchman et al., 2010), making such linearisation processes unnecessary. The question then arises as to how such a leaky neuron could act as a single electrical compartment. The answer to this may lie in the morphology of the excitatory inputs. The reconstruction of inhibitory inputs to the MSO (Figure 3.4) reveals a pearl-on-a-string morphology as synaptic contacts from a single axon stretch along a large part of the membrane surface. If the multiple input sites for excitatory fibres are similarly spaced along a dendrite, then rather than a local depolarisation of dendritic segments, excitatory fibre activation may depolarise large segments of the dendrite at once. This configuration might also better maintain input timing information, if excitatory inputs can simultaneously depolarise the entire dendrite rather than innervating small segments.

The large single fibre inputs to the MSO are indicative of a coincidence detection strategy that closely resembles that at upstream synapses in this circuit such as the endbulb of Held (Oleskevich et al., 2004; Xu-Friedman and Regehr, 2005). The large post-synaptic currents supported by large vesicular pools are typical of the specialised synaptic inputs throughout the ITD pathway. This strategy is in stark contrast to strategies employed by coincidence detector neurons in other auditory regions. Octopus cells in the AVCN and neurons of the avian analogue NL circuit instead rely on the integration of larger numbers of smaller inputs (Golding et al., 1995; Oertel et al., 2000). The findings presented here in terms of cellular coincidence detection strategies complement previous findings describing the mammalian ITD pathway, and further distinguish it from its avian analogue. Indeed, the finding that different biophysical strategies are employed by the MSO and its NL analogue is unsurprising given the independent evolution of the avian and mammalian ITD circuits

(Grothe, 2003).

On the cellular level, the presence of GABA and NMDA signalling raises the possibility of modulating the MSO circuit across different time ranges. On the near-instantaneous level, the additional conductances imposed by these receptors can modify the coincidence detection windows of MSO neurons. This may be especially relevant for NMDAR activation, as the axon of MSO neurons arises from the soma (Rautenberg et al., 2009) where these receptors are located and might provide a shunting conductance. On the slightly longer term, the activation of extra-synaptic GABA_ARs by ambient GABA release could act to modulate general excitability in the MSO. Further, the activation of NMDARs may modulate synaptic inputs to MSO neurons on an even longer time-scale, for example through the modulation of neurotransmitter receptor mobility both across the neuron and at the synapse specifically. It is therefore apparent that the additional signalling pathways in the MSO may have subtle but important modulatory roles.

Consequences for ITD coding and sound localisation

The thorough *in vitro* characterisation of MSO neurons, to which this work contributes, provides us with some insights into MSO function *in vivo*. As a general strategy, MSO neurons produce a code used for sound localisation based largely on the integration of a set of extremely strong, fast, excitatory and inhibitory synaptic inputs. This inhibitory input is important to adjust the firing rate of MSO neurons such that the steepest slope of the ITD function lies in the physiologically relevant range of ITDs (Brand et al., 2002; Pecka et al., 2008). Within the physiologically relevant range, the firing rate of individual MSO neurons is monotonically modulated according to ITD, providing an output that may be precise enough to directly account for the microsecond accuracy of behavioural results (Skottun, 1998). This precision is present behaviourally only in terms of the ‘just noticeable difference’ between two sound sources, allowing listeners to identify a difference, but not accurately localise sound sources. Precise sound localisation is a computationally much more difficult task and in mammals it is likely achieved via a comparison between the firing rates of a large population of MSO neurons in each brain hemisphere, and not via the maximal firing rates of individual MSO neurons (for review, see McAlpine and Grothe, 2003). In this context, it is perhaps easier to imagine how modulating the coincidence

detection windows of MSO neurons both individually and across a population might influence sound localisation.

One of the most direct forms of modulation occurs at the level of input adaptation, where both excitatory and inhibitory inputs to MSO neurons display strong STD (Couchman et al., 2010). Consequently, even in periods of relative quiet, inputs to the MSO may be substantially depressed. Further, given that endogenous Ca^{2+} levels *in vivo* are likely to be lower than those typically used in *in vitro* recordings, lower synaptic release probabilities and therefore smaller synaptic currents would be expected (for review, see Borst, 2010). Functionally, this reduction in release probability is thought to maintain high fidelity signalling at high frequencies (Kuba et al., 2002a; Cook et al., 2003; Yang and Xu-Friedman, 2008). The balanced STD of excitatory and inhibitory inputs in the MSO (Couchman et al., 2010) ensures that these inputs adapt synchronously, allowing for a stable input / output function during ongoing activity. This is reflected *in vivo* where ITD coding is consistent throughout the onset and ongoing component of responses (Pecka et al., 2008). Thus, when the system is driven hard, as in a noisy environment, these inputs continue to fire faithfully at very high frequency (Brand et al., 2002). As described, the rapid and substantial depression of these inputs via STD (Couchman et al., 2010) means that the full range of input adaptation by STP mechanisms may be already encountered at relatively low frequencies. Thus, as at higher frequencies, the circuit could be modulated through other means. MSO neurons are densely covered with synaptic inputs (Stotler, 1953; Kapfer et al., 2002; Couchman et al., 2010), making the spill-over of neurotransmitter from the synchronous activation of hundreds of release sites a real possibility. It is in this case that further circuit modulation, this time by extra-synaptically located receptors, becomes feasible and even likely.

Behaviourally, it is possible to envisage several instances where the modulation of MSO input / output functions may be important for sound localisation. For example, to localise a specific sound source, it may be advantageous to increase the relative contribution of MSO neurons representing certain frequencies to the overall output signal of the MSO. This might allow for the effective localisation of relevant sound sources against broadband background noises. The most likely mechanism for this would require efferent input which has not been demonstrated in the MSO. The most convincing evidence for efferent input is the presence of punctate GAD65 staining, indicating possible GABAergic input (Hassfurth

et al., 2010). As discussed, the activation of extra-synaptic GABA_ARs on MSO neurons could create a slow, shunting inhibition to modulate membrane resistance. Depending on the overall impact of the limited GABA_AR population, strong GABA_AR activation could cause membrane hyperpolarisation and a decrease in membrane resistance by deactivating K_{LVA}. In the preceding inhibition model of ITD coding (Grothe, 2003), this could increase the rebound effects of synaptic glycinergic inhibition.

In another case, the transition from quiet to noisy environments could be rapidly accommodated by adjusting the overall gain of the MSO. Specifically, lower synaptic activity levels in a quiet environment likely result in lower GABA_AR / NMDAR activation, as these receptors lie largely outside the synapse. This, combined with a lower synaptic conductance, makes MSO neurons more electrically ‘tight’ meaning they are more likely to fire in response to stimuli that fall outside of their normal response range. The transition to a noisier environment could rapidly invert this process, as the MSO neurons become much leakier due to significant synaptic conductances, and the activation of GABA and NMDA signalling pathways. This would maximise localisation acuity when attempting to segregate a specific sound source amongst many similar sound sources. As an overall strategy, this type of modulation would represent a trade-off between localisation acuity in noisy environments and the ability to produce a significant neuronal response across the population when in quiet. One major problem with this hypothesis is that it would mean that ITD coding in MSO neurons varies during ongoing activity, which has been shown not to be the case in anaesthetised gerbils *in vivo* (Pecka et al., 2008). However, if GABAR activation is controlled through an efferent pathway that can be activated during attention, then in the behaving animal such modulation might still be possible.

In addition to the modulation of MSO function by leak conductances, modulation by secondary effects, including Ca²⁺ influx through NMDARs is a distinct possibility. Interestingly, a reciprocal modulation of GlyRs by glutamate is also possible as a recent study shows that glutamate potentiates currents through synaptic GlyRs (Liu et al., 2010). Additionally, any other activity-dependent mechanism that sharpens coincidence detection during periods of high activation would conversely allow for a higher sensitivity during quieter periods by shifting the gain of the system (Chanda and Xu-Friedman, 2010). In any case, it is clear that the once simple picture of mammalian ITD processing, limited to the recruitment of exclusively excitatory inputs, is rapidly becoming complicated by the

possibility of complex interactions with significant inhibitory inputs and secondary modulators both within and without the synapse.

List of acronyms and initialisms

AB	antibody
AC	auditory cortex
AHP	after-hyperpolarisation
AMPA	2-amino-3-(5-methyl-3-oxo-1,2-oxazol-4-yl) propanoic acid
AP	action potential
AVCN	antero-ventral cochlear nucleus
CN	cochlear nucleus
CNB-GABA	O-CNB-caged GABA
CPP	3-((R)-2-Carboxypiperazin-4-yl)-propyl-1-phosphonic acid
DAPV	D-(-)-2-Amino-5-phosphonopentanoic acid
DNQX	6,7-Dinitroquinoxaline-2,3-dione
EM	electron microscopy
EPSC/P	excitatory post-synaptic current / potential
FWHM	full width at half-maximum
GABA	gamma aminobutyric acid
GABA _{A/B} R	gamma aminobutyric acid A or B receptor
Gly	glycine
GYKI	5-(4-Aminophenyl)-8-methyl-8,9-dihydro-1,3-dioxa-6,7-diaza-cyclohepta[f]indene-7carboxylic acid methylamide
IC	inferior colliculus
IHC	inner hair cell
ILD	interaural level difference
IPSC/P	inhibitory post-synaptic current / potential
ITD	interaural time difference
I _h	hyperpolarisation-activated cation current
KA	kainate
K _{HVA/LVA}	high- / low-voltage activated potassium current
LNTB	lateral nucleus of the trapezoid body
LSO	lateral superior olive
MGN	medial geniculate nucleus
mIPSC	miniature inhibitory post-synaptic current

MNI-Glu	MNI-caged-L-glutamate
MNTB	medial nucleus of the trapezoid body
MSO	medial superior olive
NL	nucleus laminaris
NLL	nuclei of the lateral lemniscus
NM	nucleus magnocellularis
NMDA	N-Methyl-D-aspartic acid
PBS	phosphate-buffered saline
PSC/P	post-synaptic current / potential
P	post-natal day (age)
PTX	picrotoxin
R	receptor
SGN	spiral ganglion neuron
SOC	superior olivary complex
STD	short-term depression
STP	short-term plasticity
STR	strychnine hydrochloride

List of Figures

Figure 1. 1 ITDs and ILDs	14
Figure 1. 2 The ear.....	18
Figure 1. 3 Mammalian ascending auditory pathways for ITD and ILD processing	20
Figure 2. 1 Calibration of laser intensity and duration.....	38
Figure 2. 2 FWHM calibrations.....	40
Figure 3. 1 Excitatory fibre inputs to MSO neurons estimated with classical minimal stimulation	46
Figure 3. 2 Inhibitory fibre inputs to MSO neurons estimates with classical minimal stimulation	47
Figure 3. 3 Functional consequences of large excitatory fibres	49
Figure 3. 4 Quantification of pre-synaptic varicosities on single MNTB inputs to MSO neurons	52
Figure 4. 1 Functional AMPAR and NMDAR distributions.....	56
Figure 4. 2 Functional AMPA and NMDA synapse distributions	58
Figure 4. 3 Comparison of GlyR distributions from P10 and P20 - 35 MSO neurons	60
Figure 4. 4 Comparison of synaptic input distributions to GlyRs from P10 and P20 - 35 MSO neurons.....	62
Figure 4. 5 Characterisation of GlyRs	64
Figure 4. 6 GABA _A receptor and synapse distributions.....	67
Figure 5. 1 NMDARs are recruited during fibre stimulation	70
Figure 5. 2 NMDAR currents accumulate during fibre stimulus trains	71
Figure 5. 3 Synaptically released glycine acts on somatic NMDARs.....	73
Figure 6. 1 Summary schematic of excitatory and inhibitory input statistics	77
Figure 6. 2 Summary of functional receptor and synapse distributions	80

Reference List

Adams JC (1979) Ascending projections to the inferior colliculus. *J Comp Neurol* 183:519-538.

Agmon-Snir H, Carr CE, Rinzel J (1998) The role of dendrites in auditory coincidence detection. *Nature* 393:268-272.

Ahmadi S, Muth-Selbach U, Lauterbach A, Lipfert P, Neuhuber WL, Zeilhofer HU (2003) Facilitation of spinal NMDA receptor currents by spillover of synaptically released glycine. *Science* 300:2094-2097.

Ashida G, Abe K, Funabiki K, Konishi M (2007) Passive soma facilitates submillisecond coincidence detection in the owl's auditory system. *J Neurophysiol* 97:2267-2282.

Bal R, Oertel D (2000) Hyperpolarization-activated, mixed-cation current ($I(h)$) in octopus cells of the mammalian cochlear nucleus. *J Neurophysiol* 84:806-817.

Balakrishnan V, Trussell LO (2008) Synaptic inputs to granule cells of the dorsal cochlear nucleus. *J Neurophysiol* 99:208-219.

Banks MI, Pearce RA, Smith PH (1993) Hyperpolarization-activated cation current (Ih) in neurons of the medial nucleus of the trapezoid body: voltage-clamp analysis and enhancement by norepinephrine and cAMP suggest a modulatory mechanism in the auditory brain stem. *J Neurophysiol* 70:1420-1432.

Batra R (2006) Responses of neurons in the ventral nucleus of the lateral lemniscus to sinusoidally amplitude modulated tones. *J Neurophysiol* 96:2388-2398.

Batra R, Kuwada S, Stanford TR (1993) High-frequency neurons in the inferior colliculus that are sensitive to interaural delays of amplitude-modulated tones: evidence for dual binaural influences. *J Neurophysiol* 70:64-80.

Belelli D, Casula A, Ling A, Lambert JJ (2002) The influence of subunit composition on the interaction of neurosteroids with GABA(A) receptors. *Neuropharmacology* 43:651-661.

Bendels MH, Beed P, Leibold C, Schmitz D, Johenning FW (2008) A novel control software that improves the experimental workflow of scanning photostimulation experiments. *J Neurosci Methods* 175:44-57.

Benson CG, Cant NB (2008) The ventral nucleus of the lateral lemniscus of the gerbil (*Meriones unguiculatus*): organization of connections with the cochlear nucleus and the inferior colliculus. *J Comp Neurol* 510:673-690.

Berger AJ, Dieudonne S, Ascher P (1998) Glycine uptake governs glycine site occupancy at NMDA receptors of excitatory synapses. *J Neurophysiol* 80:3336-3340.

Berglund AM, Ryugo DK (1987) Hair cell innervation by spiral ganglion neurons in the mouse. *J Comp Neurol* 255:560-570.

Bliss TV, Collingridge GL (1993) A synaptic model of memory: long-term potentiation in the hippocampus. *Nature* 361:31-39.

Borgdorff AJ, Choquet D (2002) Regulation of AMPA receptor lateral movements. *Nature* 417:649-653.

Bormann J, Rundstrom N, Betz H, Langosch D (1993) Residues within transmembrane segment M2 determine chloride conductance of glycine receptor homo- and hetero-oligomers. *EMBO J* 12:3729-3737.

Borst JG (2010) The low synaptic release probability in vivo. *Trends Neurosci* 33:259-266.

Boudreau JC, Tsuchitani C (1968) Binaural interaction in the cat superior olive S segment. *J Neurophysiol* 31:442-454.

Brand A, Behrend O, Marquardt T, McAlpine D, Grothe B (2002) Precise inhibition is essential for microsecond interaural time difference coding. *Nature* 417:543-547.

Brawer JR, Morest DK (1975) Relations between auditory nerve endings and cell types in the cat's anteroventral cochlear nucleus seen with the Golgi method and Nomarski optics. *J Comp Neurol* 160:491-506.

Brungart DS, Rabinowitz WM (1999) Auditory localization of nearby sources. Head-related transfer functions. *J Acoust Soc Am* 106:1465-1479.

Brunso-Bechtold JK, Henkel CK, Linville C (1990) Synaptic organization in the adult ferret medial superior olive. *J Comp Neurol* 294:389-398.

Budinger E, Heil P, Scheich H (2000) Functional organization of auditory cortex in the Mongolian gerbil (*Meriones unguiculatus*). IV. Connections with anatomically characterized subcortical structures. *Eur J Neurosci* 12:2452-2474.

Budinger E, Laszcz A, Lison H, Scheich H, Ohl FW (2008) Non-sensory cortical and subcortical connections of the primary auditory cortex in Mongolian gerbils: bottom-up and top-down processing of neuronal information via field AI. *Brain Res* 1220:2-32.

Caicedo A, Eybalin M (1999) Glutamate receptor phenotypes in the auditory brainstem and mid-brain of the developing rat. *Eur J Neurosci* 11:51-74.

Caird D, Klinke R (1983) Processing of binaural stimuli by cat superior olivary complex neurons. *Exp Brain Res*

Caird D, Klinke R (1987) Processing of interaural time and intensity differences in the cat inferior colliculus. *Exp Brain Res* 68:379-392.

Callaway EM, Katz LC (1993) Photostimulation using caged glutamate reveals functional circuitry in living brain slices. *Proc Natl Acad Sci U S A* 90:7661-7665.

Campos ML, de Cabo C, Wisden W, Juiz JM, Merlo D (2001) Expression of GABA(A) receptor subunits in rat brainstem auditory pathways: cochlear nuclei, superior olivary complex and nucleus of the lateral lemniscus. *Neuroscience* 102:625-638.

Cant NB, Morest DK (1979) The bushy cells in the anteroventral cochlear nucleus of the cat. A study with the electron microscope. *Neuroscience* 4:1925-1945.

Cant NB, Casseday JH (1986) Projections from the anteroventral cochlear nucleus to the lateral and medial superior olivary nuclei. *J Comp Neurol* 247:457-476.

Cant NB, Hyson RL (1992) Projections from the lateral nucleus of the trapezoid body to the medial superior olivary nucleus in the gerbil. *Hear Res* 58:26-34.

Carr CE, Konishi M (1990) A circuit for detection of interaural time differences in the brain stem of the barn owl. *J Neurosci* 10:3227-3246.

Caspary DM, Backoff PM, Finlayson PG, Palombi PS (1994) Inhibitory inputs modulate discharge rate within frequency receptive fields of anteroventral cochlear nucleus neurons. *J Neurophysiol* 72:2124-2133.

Cathala L, Holderith NB, Nusser Z, DiGregorio DA, Cull-Candy SG (2005) Changes in synaptic structure underlie the developmental speeding of AMPA receptor-mediated EPSCs. *Nat Neurosci* 8:1310-1318.

Chanda S, Xu-Friedman MA (2010) Neuromodulation by GABA converts a relay into a coincidence detector. *J Neurophysiol* 104:2063-2074.

Charrier C, Ehrenspurger MV, Dahan M, Levi S, Triller A (2006) Cytoskeleton regulation of glycine receptor number at synapses and diffusion in the plasma membrane. *J Neurosci* 26:8502-8511.

Chen C (1997) Hyperpolarization-activated current (I_h) in primary auditory neurons. *Hear Res* 110:179-190.

Chen X, Shu S, Schwartz LC, Sun C, Kapur J, Bayliss DA (2008) Homeostatic regulation of synaptic excitability: tonic GABA(A) receptor currents replace I(h) in cortical pyramidal neurons of HCN1 knock-out mice. *J Neurosci* 30:2611-2622.

Chen X, Shu S, Schwartz LC, Sun C, Kapur J, Bayliss DA (2010) Homeostatic regulation of synaptic

excitability: tonic GABA(A) receptor currents replace I(h) in cortical pyramidal neurons of HCN1 knock-out mice. *J Neurosci* 30:2611-2622.

Chirila FV, Rowland KC, Thompson JM, Spirou GA (2007) Development of gerbil medial superior olive: integration of temporally delayed excitation and inhibition at physiological temperature. *J Physiol* 584:167-190.

Choquet D, Triller A (2003) The role of receptor diffusion in the organization of the postsynaptic membrane. *Nat Rev Neurosci* 4:251-265.

Clark GM (1969) The ultrastructure of nerve endings in the medial superior olive of the cat. *Brain Res* 14:293-305.

Clerici WJ, Coleman JR (1990) Anatomy of the rat medial geniculate body: I. Cytoarchitecture, myeloarchitecture, and neocortical connectivity. *J Comp Neurol* 297:14-31.

Cook DL, Schwindt PC, Grande LA, Spain WJ (2003) Synaptic depression in the localization of sound. *Nature* 421:66-70.

Couchman K, Grothe B, Felmy F (2010) Medial superior olivary neurons receive surprisingly few excitatory and inhibitory inputs with balanced strength and short-term dynamics. *J Neurosci* 30:17111-17121.

Covey E, Casseday JH (1991) The monaural nuclei of the lateral lemniscus in an echolocating bat: parallel pathways for analyzing temporal features of sound. *J Neurosci* 11:3456-3470.

Dahan M, Levi S, Luccardini C, Rostaing P, Riveau B, Triller A (2003) Diffusion dynamics of glycine receptors revealed by single-quantum dot tracking. *Science* 302:442-445.

De No RL (1933) Anatomy of the eighth nerve: III.—General plan of structure of the primary cochlear nuclei. *The Laryngoscope* 43:327-350.

Deleuze C, Alonso G, Lefevre IA, Duvoid-Guillou A, Hussy N (2005a) Extrasynaptic localization of glycine receptors in the rat supraoptic nucleus: further evidence for their involvement in glia-to-neuron communication. *Neuroscience* 133:175-183.

Deleuze C, Runquist M, Orcel H, Rabie A, Dayanithi G, Alonso G, Hussy N (2005b) Structural difference between heteromeric somatic and homomeric axonal glycine receptors in the hypothalamo-neurohypophysial system. *Neuroscience* 135:475-483.

Dorrn AL, Yuan K, Barker AJ, Schreiner CE, Froemke RC (2010) Developmental sensory experience balances cortical excitation and inhibition. *Nature* 465:932-936.

Drescher MJ, Drescher DG (1992) Glutamate, of the endogenous primary alpha-amino acids, is specifically released from hair cells by elevated extracellular potassium. *J Neurochem* 59:93-98.

Eder M, Rammes G, Zieglgansberger W, Dodt HU (2001) GABA(A) and GABA(B) receptors on neocortical neurons are differentially distributed. *Eur J Neurosci* 13:1065-1069.

Eder M, Becker K, Rammes G, Schierloh A, Azad SC, Zieglgansberger W, Dodt HU (2003) Distribution and properties of functional postsynaptic kainate receptors on neocortical layer V pyramidal neurons. *J Neurosci* 23:6660-6670.

Englitz B, Tolnai S, Typlt M, Jost J, Rubsamen R (2009) Reliability of synaptic transmission at the synapses of Held in vivo under acoustic stimulation. *PLoS One* 4:e7014.

Farrant M, Nusser Z (2005) Variations on an inhibitory theme: phasic and tonic activation of GABA(A) receptors. *Nat Rev Neurosci* 6:215-229.

Ferragamo MJ, Oertel D (2002) Octopus cells of the mammalian ventral cochlear nucleus sense the rate of depolarization. *J Neurophysiol* 87:2262-2270.

Fitzpatrick DC, Kuwada S, Batra R (2000) Neural sensitivity to interaural time differences: beyond the Jeffress model. *J Neurosci* 20:1605-1615.

Flint AC, Liu X, Kriegstein AR (1998) Nonsynaptic glycine receptor activation during early neocortical development. *Neuron* 20:43-53.

Forsythe ID (1994) Direct patch recording from identified presynaptic terminals mediating glutamatergic EPSCs in the rat CNS, *in vitro*. *J Physiol* 479 (Pt 3):381-387.

Friauf E, Hammerschmidt B, Kirsch J (1997) Development of adult-type inhibitory glycine receptors in the central auditory system of rats. *J Comp Neurol* 385:117-134.

Fuchs PA (2005) Time and intensity coding at the hair cell's ribbon synapse. *J Physiol* 566:7-12.

Futai K, Okada M, Matsuyama K, Takahashi T (2001) High-fidelity transmission acquired via a developmental decrease in NMDA receptor expression at an auditory synapse. *J Neurosci* 21:3342-3349.

Gai Y, Carney LH (2008) Influence of inhibitory inputs on rate and timing of responses in the anteroventral cochlear nucleus. *J Neurophysiol* 99:1077-1095.

Galambos R, Schwartzkopff J, Rupert A (1959) Microelectrode study of superior olivary nuclei. *Am J Physiol* 197:527-536.

Gardner MB, Gardner RS (1973) Problem of localization in the median plane: effect of pinnae cavity occlusion. *J Acoust Soc Am* 53:400-408.

Gardner SM, Trussell LO, Oertel D (2001) Correlation of AMPA receptor subunit composition with synaptic input in the mammalian cochlear nuclei. *J Neurosci* 21:7428-7437.

Glendenning KK, Brunso-Bechtold JK, Thompson GC, Masterton RB (1981) Ascending auditory afferents to the nuclei of the lateral lemniscus. *J Comp Neurol* 197:673-703.

Glowatzki E, Fuchs PA (2002) Transmitter release at the hair cell ribbon synapse. *Nat Neurosci* 5:147-154.

Godfrey DA, Carter JA, Berger SJ, Matschinsky FM (1976) Levels of putative transmitter amino acids in the guinea pig cochlea. *J Histochem Cytochem* 24:468-470.

Goldberg JM, Brown PB (1969) Response of binaural neurons of dog superior olivary complex to dichotic tonal stimuli: some physiological mechanisms of sound localization. *J Neurophysiol* 32:613-636.

Golding NL, Robertson D, Oertel D (1995) Recordings from slices indicate that octopus cells of the cochlear nucleus detect coincident firing of auditory nerve fibers with temporal precision. *J Neurosci* 15:3138-3153.

Golding NL, Khurana S, Pena JL, Rosa K (2009) Developmental Changes in Hyperpolarization-Activated Cation Channels Control the Resolution of Coincidence Detection in MSO Principal Neurons In: *Assoc. Res. Otolaryngol. Abs.*, p 128. Baltimore, Maryland, USA.

Grau-Serrat V, Carr CE, Simon JZ (2003) Modeling coincidence detection in nucleus laminaris. *Biol Cybern* 89:388-396.

Griffin SJ, Bernstein LR, Ingham NJ, McAlpine D (2005) Neural sensitivity to interaural envelope delays in the inferior colliculus of the guinea pig. *J Neurophysiol* 93:3463-3478.

Groc L, Heine M, Cognet L, Brickley K, Stephenson FA, Lounis B, Choquet D (2004) Differential activity-dependent regulation of the lateral mobilities of AMPA and NMDA receptors. *Nat Neurosci* 7:695-696.

Grothe B (2003) New roles for synaptic inhibition in sound localization. *Nat Rev Neurosci* 4:540-550.

Grothe B, Sanes DH (1993) Bilateral inhibition by glycinergic afferents in the medial superior olive. *J Neurophysiol* 69:1192-1196.

Haider B, Duque A, Hasenstaub AR, McCormick DA (2006) Neocortical network activity in vivo is generated through a dynamic balance of excitation and inhibition. *J Neurosci* 26:4535-4545.

Handford CA, Lynch JW, Baker E, Webb GC, Ford JH, Sutherland GR, Schofield PR (1996) The human glycine receptor beta subunit: primary structure, functional characterisation and chromosomal localisation of the human and murine genes. *Brain Res Mol Brain Res* 35:211-219.

Hassfurth B, Grothe B, Koch U The mammalian interaural time difference detection circuit is differentially controlled by GABAB receptors during development. *J Neurosci* 30:9715-9727.

Hassfurth B, Grothe B, Koch U (2010) The mammalian interaural time difference detection circuit is

differentially controlled by GABAB receptors during development. *J Neurosci* 30:9715-9727.

Heffner RS, Heffner HE (1988) Sound localization and use of binaural cues by the gerbil (*Meriones unguiculatus*). *Behav Neurosci* 102:422-428.

Held H (1893) Die centrale Gehörleitung. *Arch Anat Physiol Anat Abt* 1893:201-247.

Inbody SB, Feng AS (1981) Binaural response characteristics of single neurons in the medial superior olfactory nucleus of the albino rat. *Brain Res* 210:361-366.

Jarsky T, Roxin A, Kath WL, Spruston N (2005) Conditional dendritic spike propagation following distal synaptic activation of hippocampal CA1 pyramidal neurons. *Nat Neurosci* 8:1667-1676.

Jeffress LA (1948) A place theory of sound localization. *J Comp Physiol Psychol* 41:35-39.

Jercog PE, Svirskis G, Kotak VC, Sanes DH, Rinzel J (2010) Asymmetric excitatory synaptic dynamics underlie interaural time difference processing in the auditory system. *PLoS Biol* 8:e1000406.

Johnson JW, Ascher P (1987) Glycine potentiates the NMDA response in cultured mouse brain neurons. *Nature* 325:529-531.

Johnston J, Forsythe ID, Kopp-Scheinpflug C (2010) Going native: voltage-gated potassium channels controlling neuronal excitability. *J Physiol* 588:3187-3200.

Joris PX, Yin TC (1995) Envelope coding in the lateral superior olive. I. Sensitivity to interaural time differences. *J Neurophysiol* 73:1043-1062.

Joris PX, Schreiner CE, Rees A (2004) Neural processing of amplitude-modulated sounds. *Physiol Rev* 84:541-577.

Joris PX, Carney LH, Smith PH, Yin TC (1994) Enhancement of neural synchronization in the anteroventral cochlear nucleus. I. Responses to tones at the characteristic frequency. *J Neurophysiol* 71:1022-1036.

Joseph AW, Hyson RL (1993) Coincidence detection by binaural neurons in the chick brain stem. *J Neurophysiol* 69:1197-1211.

Joshi I, Wang LY (2002) Developmental profiles of glutamate receptors and synaptic transmission at a single synapse in the mouse auditory brainstem. *J Physiol* 540:861-873.

Kampa BM, Stuart GJ (2006) Calcium spikes in basal dendrites of layer 5 pyramidal neurons during action potential bursts. *J Neurosci* 26:7424-7432.

Kapfer C, Seidl AH, Schweizer H, Grothe B (2002) Experience-dependent refinement of inhibitory inputs to auditory coincidence-detector neurons. *Nat Neurosci* 5:247-253.

Kellerhals B (1967) [The morphology of the ganglion spirale cochleae]. *Acta Otolaryngol:Suppl* 226:221-278.

Kempter R, Gerstner W, van Hemmen JL (1998) How the threshold of a neuron determines its capacity for coincidence detection. *Biosystems* 48:105-112.

Khimich D, Nouvian R, Pujol R, Tom Dieck S, Egner A, Gundelfinger ED, Moser T (2005) Hair cell synaptic ribbons are essential for synchronous auditory signalling. *Nature* 434:889-894.

Kiang NY, Rho JM, Northrop CC, Liberman MC, Ryugo DK (1982) Hair-cell innervation by spiral ganglion cells in adult cats. *Science* 217:175-177.

Kil J, Kageyama GH, Semple MN, Kitzes LM (1995) Development of ventral cochlear nucleus projections to the superior olivary complex in gerbil. *J Comp Neurol* 353:317-340.

Kiss A, Majorossy K (1983) Neuron morphology and synaptic architecture in the medial superior olivary nucleus. Light- and electron microscope studies in the cat. *Exp Brain Res* 52:315-327.

Klumpp RG, Eady HR (1957) Some measurements of interaural time difference thresholds. *J Acoust Soc Am* 28:859-860.

Koch U, Braun M, Kapfer C, Grothe B (2004) Distribution of HCN1 and HCN2 in rat auditory brainstem nuclei. *Eur J Neurosci* 20:79-91.

Koike-Tani M, Saitoh N, Takahashi T (2005) Mechanisms underlying developmental speeding in AMPA-EPSC decay time at the calyx of Held. *J Neurosci* 25:199-207.

Konig P, Engel AK, Singer W (1996) Integrator or coincidence detector? The role of the cortical neuron revisited. *Trends Neurosci* 19:130-137.

Kopp-Scheinplug C, Dehmel S, Dorrscheidt GJ, Rubsamen R (2002) Interaction of excitation and inhibition in anteroventral cochlear nucleus neurons that receive large endbulb synaptic endings. *J Neurosci* 22:11004-11018.

Koss M, Vater M (1989) Noradrenaline enhances temporal auditory contrast and neuronal timing precision in the cochlear nucleus of the mustached bat. *J Neurosci* 9:4169-4178.

Kotak VC, Sanes DH (1996) Developmental influence of glycinergic transmission: regulation of NMDA receptor-mediated EPSPs. *J Neurosci* 16:1836-1843.

Kotak VC, Korada S, Schwartz IR, Sanes DH (1998) A developmental shift from GABAergic to glycinergic transmission in the central auditory system. *J Neurosci* 18:4646-4655.

Kros CJ, Ruppersberg JP, Rusch A (1998) Expression of a potassium current in inner hair cells during development of hearing in mice. *Nature* 394:281-284.

Kuba H (2007) Cellular and molecular mechanisms of avian auditory coincidence detection. *Neurosci Res* 59:370-376.

Kuba H, Koyano K, Ohmori H (2002a) Synaptic depression improves coincidence detection in the nucleus laminaris in brainstem slices of the chick embryo. *Eur J Neurosci* 15:984-990.

Kuba H, Koyano K, Ohmori H (2002b) Development of membrane conductance improves coincidence detection in the nucleus laminaris of the chicken. *J Physiol* 540:529-542.

Kuba H, Yamada R, Ohmori H (2003) Evaluation of the limiting acuity of coincidence detection in nucleus laminaris of the chicken. *J Physiol* 552:611-620.

Kuba H, Ishii TM, Ohmori H (2006) Axonal site of spike initiation enhances auditory coincidence detection. *Nature* 444:1069-1072.

Kuba H, Yamada R, Fukui I, Ohmori H (2005) Tonotopic specialization of auditory coincidence detection in nucleus laminaris of the chick. *J Neurosci* 25:1924-1934.

Kuhse J, Laube B, Magalei D, Betz H (1993) Assembly of the inhibitory glycine receptor: identification of amino acid sequence motifs governing subunit stoichiometry. *Neuron* 11:1049-1056.

Kushmerick C, Price GD, Taschenberger H, Puente N, Renden R, Wadiche JI, Duvoisin RM, Grandes P, von Gersdorff H (2004) Retroinhibition of presynaptic Ca^{2+} currents by endocannabinoids released via postsynaptic mGluR activation at a calyx synapse. *J Neurosci* 24:5955-5965.

Kuwabara N, Zook JM (1992) Projections to the medial superior olive from the medial and lateral nuclei of the trapezoid body in rodents and bats. *J Comp Neurol* 324:522-538.

Kuwabara N, DiCaprio RA, Zook JM (1991) Afferents to the medial nucleus of the trapezoid body and their collateral projections. *J Comp Neurol* 314:684-706.

Kuwada S, Fitzpatrick DC, Batra R, Ostapoff EM (2006) Sensitivity to interaural time differences in the dorsal nucleus of the lateral lemniscus of the unanesthetized rabbit: comparison with other structures. *J Neurophysiol* 95:1309-1322.

Langosch D, Thomas L, Betz H (1988) Conserved quaternary structure of ligand-gated ion channels: the postsynaptic glycine receptor is a pentamer. *Proc Natl Acad Sci U S A* 85:7394-7398.

Larkum ME, Zhu JJ, Sakmann B (1999) A new cellular mechanism for coupling inputs arriving at different cortical layers. *Nature* 398:338-341.

Leao RM, Von Gersdorff H (2002) Noradrenaline increases high-frequency firing at the calyx of Held synapse during development by inhibiting glutamate release. *J Neurophysiol* 87:2297-2306.

Lenzi D, Runyon JW, Crum J, Ellisman MH, Roberts WM (1999) Synaptic vesicle populations in saccular

hair cells reconstructed by electron tomography. *J Neurosci* 19:119-132.

Lesica NA, Lingner A, Grothe B (2010) Population coding of interaural time differences in gerbils and barn owls. *J Neurosci* 30:11696-11702.

Levi S, Schweizer C, Bannai H, Pascual O, Charrier C, Triller A (2008) Homeostatic regulation of synaptic GlyR numbers driven by lateral diffusion. *Neuron* 59:261-273.

Li Y, Krupa B, Kang JS, Bolshakov VY, Liu G (2009) Glycine site of NMDA receptor serves as a spatiotemporal detector of synaptic activity patterns. *J Neurophysiol* 102:578-589.

Liberman MC, Dodds LW, Pierce S (1990) Afferent and efferent innervation of the cat cochlea: quantitative analysis with light and electron microscopy. *J Comp Neurol* 301:443-460.

Lim R, Alvarez FJ, Walmsley B (2000) GABA mediates presynaptic inhibition at glycinergic synapses in a rat auditory brainstem nucleus. *J Physiol* 525 Pt 2:447-459.

Lindsey BG (1975) Fine structure and distribution of axon terminals from the cochlear nucleus on neurons in the medial superior olfactory nucleus of the cat. *J Comp Neurol* 160:81-103.

Liu J, Wu DC, Wang YT Allosteric potentiation of glycine receptor chloride currents by glutamate. *Nat Neurosci* 13:1225-1232.

Liu J, Wu DC, Wang YT (2010) Allosteric potentiation of glycine receptor chloride currents by glutamate. *Nat Neurosci* 13:1225-1232.

Lorteije JA, Rusu SI, Kushmerick C, Borst JG (2009) Reliability and precision of the mouse calyx of Held synapse. *J Neurosci* 29:13770-13784.

Losonczy A, Makara JK, Magee JC (2008) Compartmentalized dendritic plasticity and input feature storage in neurons. *Nature* 452:436-441.

Magnusson AK, Kapfer C, Grothe B, Koch U (2005) Maturation of glycinergic inhibition in the gerbil medial superior olive after hearing onset. *J Physiol* 568:497-512.

Magnusson AK, Park TJ, Pecka M, Grothe B, Koch U (2008) Retrograde GABA signaling adjusts sound localization by balancing excitation and inhibition in the brainstem. *Neuron* 59:125-137.

Malenka RC, Nicoll RA (1993) NMDA-receptor-dependent synaptic plasticity: multiple forms and mechanisms. *Trends Neurosci* 16:521-527.

Manis PB, Marx SO (1991) Outward currents in isolated ventral cochlear nucleus neurons. *J Neurosci* 11:2865-2880.

Mathews PJ, Jercog PE, Rinzel J, Scott LL, Golding NL (2010) Control of submillisecond synaptic timing in

binaural coincidence detectors by K(v)1 channels. *Nat Neurosci*.

Matsubara A, Laake JH, Davanger S, Usami S, Ottersen OP (1996) Organization of AMPA receptor subunits at a glutamate synapse: a quantitative immunogold analysis of hair cell synapses in the rat organ of Corti. *J Neurosci* 16:4457-4467.

McAlpine D, Grothe B (2003) Sound localization and delay lines--do mammals fit the model? *Trends Neurosci* 26:347-350.

McAlpine D, Jiang D, Palmer AR (2001) A neural code for low-frequency sound localization in mammals. *Nat Neurosci* 4:396-401.

Meier J, Vannier C, Serge A, Triller A, Choquet D (2001) Fast and reversible trapping of surface glycine receptors by gephyrin. *Nat Neurosci* 4:253-260.

Mihalek RM, Banerjee PK, Korpi ER, Quinlan JJ, Firestone LL, Mi ZP, Lagenaur C, Tretter V, Sieghart W, Anagnostaras SG, Sage JR, Fanselow MS, Guidotti A, Spigelman I, Li Z, DeLorey TM, Olsen RW, Homanics GE (1999) Attenuated sensitivity to neuroactive steroids in gamma-aminobutyrate type A receptor delta subunit knockout mice. *Proc Natl Acad Sci U S A* 96:12905-12910.

Mills A (1958) On the Minimum Audible Angle. *Journal of the Acoustical Society of America* 30:237-246.

Mody I (2001) Distinguishing between GABA(A) receptors responsible for tonic and phasic conductances. *Neurochem Res* 26:907-913.

Moore MJ, Caspary DM (1983) Strychnine blocks binaural inhibition in lateral superior olivary neurons. *J Neurosci* 3:237-242.

Moore RY, Goldberg JM (1966) Projections of the inferior colliculus in the monkey. *Exp Neurol* 14:429-438.

Moser T, Beutner D (2000) Kinetics of exocytosis and endocytosis at the cochlear inner hair cell afferent synapse of the mouse. *Proc Natl Acad Sci U S A* 97:883-888.

Nabekura J, Katsurabayashi S, Kakazu Y, Shibata S, Matsubara A, Jinno S, Mizoguchi Y, Sasaki A, Ishibashi H (2004) Developmental switch from GABA to glycine release in single central synaptic terminals. *Nat Neurosci* 7:17-23.

Nicol MJ, Walmsley B (2002) Ultrastructural basis of synaptic transmission between endbulbs of Held and bushy cells in the rat cochlear nucleus. *J Physiol* 539:713-723.

Nusser Z, Sieghart W, Somogyi P (1998) Segregation of different GABA(A) receptors to synaptic and extrasynaptic membranes of cerebellar granule cells. *J Neurosci* 18:1693-1703.

Oertel D (1983) Synaptic responses and electrical properties of cells in brain slices of the mouse

anteroventral cochlear nucleus. *J Neurosci* 3:2043-2053.

Oertel D (1985) Use of brain slices in the study of the auditory system: spatial and temporal summation of synaptic inputs in cells in the anteroventral cochlear nucleus of the mouse. *J Acoust Soc Am* 78:328-333.

Oertel D, Bal R, Gardner SM, Smith PH, Joris PX (2000) Detection of synchrony in the activity of auditory nerve fibers by octopus cells of the mammalian cochlear nucleus. *Proc Natl Acad Sci U S A* 97:11773-11779.

Oleskevich S, Youssoufian M, Walmsley B (2004) Presynaptic plasticity at two giant auditory synapses in normal and deaf mice. *J Physiol* 560:709-719.

Osen KK (1969) Cytoarchitecture of the cochlear nuclei in the cat. *J Comp Neurol* 136:453-484.

Overholt EM, Rubel EW, Hyson RL (1992) A circuit for coding interaural time differences in the chick brainstem. *J Neurosci* 12:1698-1708.

Palmer AR, Russell IJ (1986) Phase-locking in the cochlear nerve of the guinea-pig and its relation to the receptor potential of inner hair-cells. *Hear Res* 24:1-15.

Parks TN, Rubel EW (1975) Organization and development of brain stem auditory nuclei of the chicken: organization of projections from n. magnocellularis to n. laminaris. *J Comp Neurol* 164:435-448.

Pecka M, Brand A, Behrend O, Grothe B (2008) Interaural time difference processing in the mammalian medial superior olive: the role of glycinergic inhibition. *J Neurosci* 28:6914-6925.

Peng Z, Huang CS, Stell BM, Mody I, Houser CR (2004) Altered expression of the delta subunit of the GABA_A receptor in a mouse model of temporal lobe epilepsy. *J Neurosci* 24:8629-8639.

Perney TM, Kaczmarek LK (1997) Localization of a high threshold potassium channel in the rat cochlear nucleus. *J Comp Neurol* 386:178-202.

Perrott DR, Saberi K (1990) Minimum audible angle thresholds for sources varying in both elevation and azimuth. *J Acoust Soc Am* 87:1728-1731.

Pettit DL, Augustine GJ (2000) Distribution of functional glutamate and GABA receptors on hippocampal pyramidal cells and interneurons. *J Neurophysiol* 84:28-38.

Pfeiffer RR (1966) Classification of response patterns of spike discharges for units in the cochlear nucleus: tone-burst stimulation. *Exp Brain Res* 1:220-235.

Pliss L, Yang H, Xu-Friedman MA (2009) Context-dependent effects of NMDA receptors on precise timing information at the endbulb of Held in the cochlear nucleus. *J Neurophysiol* 102:2627-2637.

Polsky A, Mel BW, Schiller J (2004) Computational subunits in thin dendrites of pyramidal cells. *Nat Neurosci* 7:621-627.

Pribilla I, Takagi T, Langosch D, Bormann J, Betz H (1992) The atypical M2 segment of the beta subunit confers picrotoxinin resistance to inhibitory glycine receptor channels. *EMBO J* 11:4305-4311.

Rautenberg PL, Grothe B, Felmy F (2009) Quantification of the three-dimensional morphology of coincidence detector neurons in the medial superior olive of gerbils during late postnatal development. *J Comp Neurol* 517:385-396.

Ravindranathan A, Donevan SD, Sugden SG, Greig A, Rao MS, Parks TN (2000) Contrasting molecular composition and channel properties of AMPA receptors on chick auditory and brainstem motor neurons. *J Physiol* 523 Pt 3:667-684.

Rayleigh (1907) XII. On our perception of sound direction. *Philosophical Magazine Series* 6 13:214 - 232.

Reyes AD, Rubel EW, Spain WJ (1996) In vitro analysis of optimal stimuli for phase-locking and time-delayed modulation of firing in avian nucleus laminaris neurons. *J Neurosci* 16:993-1007.

Rhode WS, Oertel D, Smith PH (1983) Physiological response properties of cells labeled intracellularly with horseradish peroxidase in cat ventral cochlear nucleus. *J Comp Neurol* 213:448-463.

Rice JJ, May BJ, Spirou GA, Young ED (1992) Pinna-based spectral cues for sound localization in cat. *Hear Res* 58:132-152.

Robertson D, Paki B (2002) Role of L-type Ca²⁺ channels in transmitter release from mammalian inner hair cells. II. Single-neuron activity. *J Neurophysiol* 87:2734-2740.

Rose JE, Gross NB, Geisler CD, Hind JE (1966) Some neural mechanisms in the inferior colliculus of the cat which may be relevant to localization of a sound source. *J Neurophysiol* 29:288-314.

Rose JE, Brugge JF, Anderson DJ, Hind JE (1967) Phase-locked response to low-frequency tones in single auditory nerve fibers of the squirrel monkey. *J Neurophysiol* 30:769-793.

Rothman JS, Young ED, Manis PB (1993) Convergence of auditory nerve fibers onto bushy cells in the ventral cochlear nucleus: implications of a computational model. *J Neurophysiol* 70:2562-2583.

Ruel J, Bobbin RP, Vidal D, Pujol R, Puel JL (2000) The selective AMPA receptor antagonist GYKI 53784 blocks action potential generation and excitotoxicity in the guinea pig cochlea. *Neuropharmacology* 39:1959-1973.

Rusznak Z, Szucs G (2009) Spiral ganglion neurones: an overview of morphology, firing behaviour, ionic channels and function. *Pflugers Arch* 457:1303-1325.

Ryan A (1976) Hearing sensitivity of the mongolian gerbil, *Meriones unguiculatis*. *J Acoust Soc Am*

Ryugo DK, Weinberger NM (1976) Corticofugal modulation of the medial geniculate body. *Exp Neurol* 51:377-391.

Ryugo DK, Sento S (1991) Synaptic connections of the auditory nerve in cats: relationship between endbulbs of held and spherical bushy cells. *J Comp Neurol* 305:35-48.

Saldana E, Feliciano M, Mugnaini E (1996) Distribution of descending projections from primary auditory neocortex to inferior colliculus mimics the topography of intracollicular projections. *J Comp Neurol* 371:15-40.

Satzler K, Sohl LF, Bollmann JH, Borst JG, Frotscher M, Sakmann B, Lubke JH (2002) Three-dimensional reconstruction of a calyx of Held and its postsynaptic principal neuron in the medial nucleus of the trapezoid body. *J Neurosci* 22:10567-10579.

Saxena NC, Macdonald RL (1994) Assembly of GABA_A receptor subunits: role of the delta subunit. *J Neurosci* 14:7077-7086.

Saxena NC, Macdonald RL (1996) Properties of putative cerebellar gamma-aminobutyric acid A receptor isoforms. *Mol Pharmacol* 49:567-579.

Schiller J, Schiller Y, Stuart G, Sakmann B (1997) Calcium action potentials restricted to distal apical dendrites of rat neocortical pyramidal neurons. *J Physiol* 505 (Pt 3):605-616.

Schmidt-Hieber C, Jonas P, Bischofberger J (2007) Subthreshold dendritic signal processing and coincidence detection in dentate gyrus granule cells. *J Neurosci* 27:8430-8441.

Schneggenburger R, Meyer AC, Neher E (1999) Released fraction and total size of a pool of immediately available transmitter quanta at a calyx synapse. *Neuron* 23:399-409.

Schofield PR, Lynch JW, Rajendra S, Pierce KD, Handford CA, Barry PH (1996) Molecular and genetic insights into ligand binding and signal transduction at the inhibitory glycine receptor. *Cold Spring Harb Symp Quant Biol* 61:333-342.

Scott LL, Mathews PJ, Golding NL (2005) Posthearing developmental refinement of temporal processing in principal neurons of the medial superior olive. *J Neurosci* 25:7887-7895.

Scott LL, Mathews PJ, Golding NL (2010) Perisomatic voltage-gated sodium channels actively maintain linear synaptic integration in principal neurons of the medial superior olive. *J Neurosci* 30:2039-2050.

Semyanov A, Walker MC, Kullmann DM, Silver RA (2004) Tonically active GABA_A receptors: modulating gain and maintaining the tone. *Trends Neurosci* 27:262-269.

Sento S, Ryugo DK (1989) Endbulbs of held and spherical bushy cells in cats: morphological correlates with physiological properties. *J Comp Neurol* 280:553-562.

Sewell WF (1984) The relation between the endocochlear potential and spontaneous activity in auditory nerve fibres of the cat. *J Physiol* 347:685-696.

Shinn-Cunningham BG, Santarelli S, Kopco N (2000) Tori of confusion: binaural localization cues for sources within reach of a listener. *J Acoust Soc Am* 107:1627-1636.

Silver RA, Cull-Candy SG, Takahashi T (1996) Non-NMDA glutamate receptor occupancy and open probability at a rat cerebellar synapse with single and multiple release sites. *J Physiol* 494 (Pt 1):231-250.

Singer JH, Berger AJ (1999) Contribution of single-channel properties to the time course and amplitude variance of quantal glycine currents recorded in rat motoneurons. *J Neurophysiol* 81:1608-1616.

Sjostrom PJ, Rancz EA, Roth A, Häusser M (2008) Dendritic excitability and synaptic plasticity. *Physiol Rev* 88:769-840.

Skottun BC (1998) Sound localization and neurons. *Nature* 393:531.

Smith AJ, Owens S, Forsythe ID (2000) Characterisation of inhibitory and excitatory postsynaptic currents of the rat medial superior olive. *J Physiol* 529 Pt 3:681-698.

Smith CA, Sjostrand FS (1961) Structure of the nerve endings on the external hair cells of the guinea pig cochlea as studied by serial sections. *J Ultrastruct Res* 5:523-556.

Smith PH, Joris PX, Yin TC (1993) Projections of physiologically characterized spherical bushy cell axons from the cochlear nucleus of the cat: evidence for delay lines to the medial superior olive. *J Comp Neurol* 331:245-260.

Smith PH, Joris PX, Yin TC (1998) Anatomy and physiology of principal cells of the medial nucleus of the trapezoid body (MNTB) of the cat. *J Neurophysiol* 79:3127-3142.

Smith PH, Joris PX, Carney LH, Yin TC (1991) Projections of physiologically characterized globular bushy cell axons from the cochlear nucleus of the cat. *J Comp Neurol* 304:387-407.

Sobolevsky AI, Rosconi MP, Gouaux E (2009) X-ray structure, symmetry and mechanism of an AMPA-subtype glutamate receptor. *Nature* 462:745-756.

Spangler KM, Warr WB, Henkel CK (1985) The projections of principal cells of the medial nucleus of the trapezoid body in the cat. *J Comp Neurol* 238:249-262.

Spassova MA, Avissar M, Furman AC, Crumling MA, Saunders JC, Parsons TD (2004) Evidence that rapid vesicle replenishment of the synaptic ribbon mediates recovery from short-term adaptation at the

hair cell afferent synapse. *J Assoc Res Otolaryngol* 5:376-390.

Spigelman I, Li Z, Banerjee PK, Mihalek RM, Homanics GE, Olsen RW (2002) Behavior and physiology of mice lacking the GABA_A-receptor delta subunit. *Epilepsia* 43 Suppl 5:3-8.

Spirou GA, Rager J, Manis PB (2005) Convergence of auditory-nerve fiber projections onto globular bushy cells. *Neuroscience* 136:843-863.

Spitzer MW, Semple MN (1995) Neurons sensitive to interaural phase disparity in gerbil superior olive: diverse monaural and temporal response properties. *J Neurophysiol* 73:1668-1690.

Spoendlin H (1985) Anatomy of cochlear innervation. *Am J Otolaryngol* 6:453-467.

Srinivasan Y, Guzikowski AP, Haugland RP, Angelides KJ (1990) Distribution and lateral mobility of glycine receptors on cultured spinal cord neurons. *J Neurosci* 10:985-995.

Steinert JR, Postlethwaite M, Jordan MD, Chernova T, Robinson SW, Forsythe ID (2010) NMDAR-mediated EPSCs are maintained and accelerate in time course during maturation of mouse and rat auditory brainstem in vitro. *J Physiol* 588:447-463.

Stotler WA (1953) An experimental study of the cells and connections of the superior olfactory complex of the cat. *J Comp Neurol* 98:401-431.

Stuart G, Schiller J, Sakmann B (1997) Action potential initiation and propagation in rat neocortical pyramidal neurons. *J Physiol* 505 (Pt 3):617-632.

Sun YJ, Wu GK, Liu BH, Li P, Zhou M, Xiao Z, Tao HW, Zhang LI (2010) Fine-tuning of pre-balanced excitation and inhibition during auditory cortical development. *Nature* 465:927-931.

Swanson GT, Kamboj SK, Cull-Candy SG (1997) Single-channel properties of recombinant AMPA receptors depend on RNA editing, splice variation, and subunit composition. *J Neurosci* 17:58-69.

Szabo ZS, Harasztsosi CS, Sziklai I, Szucs G, Rusznak Z (2002) Ionic currents determining the membrane characteristics of type I spiral ganglion neurons of the guinea pig. *Eur J Neurosci* 16:1887-1895.

Takahashi T (2005) Postsynaptic receptor mechanisms underlying developmental speeding of synaptic transmission. *Neurosci Res* 53:229-240.

Takahashi T, Momiyama A, Hirai K, Hishinuma F, Akagi H (1992) Functional correlation of fetal and adult forms of glycine receptors with developmental changes in inhibitory synaptic receptor channels. *Neuron* 9:1155-1161.

Taschenberger H, von Gersdorff H (2000) Fine-tuning an auditory synapse for speed and fidelity: developmental changes in presynaptic waveform, EPSC kinetics, and synaptic plasticity. *J Neurosci* 20:9162-9173.

Taschenberger H, Leao RM, Rowland KC, Spirou GA, von Gersdorff H (2002) Optimizing synaptic architecture and efficiency for high-frequency transmission. *Neuron* 36:1127-1143.

Thompson AM, Thompson GC (1987) Efferent projections from posteroventral cochlear nucleus to lateral superior olive in guinea pig. *Brain Res* 421:382-386.

Thompson SP (1882) LI. On the function of the two ears in the perception of space. *Philosophical Magazine Series 5* 13:406 - 416.

Tsuchitani C, Boudreau JC (1966) Single unit analysis of cat superior olive S segment with tonal stimuli. *J Neurophysiol* 29:684-697.

Typlt M, Haustein MD, Dietz B, Steinert JR, Witte M, Englitz B, Milenkovic I, Kopp-Scheinpflug C, Forsythe ID, Rubsam R (2010) Presynaptic and postsynaptic origin of multicomponent extracellular waveforms at the endbulb of Held-spherical bushy cell synapse. *Eur J Neurosci* 31:1574-1581.

Von Békésy G (1960) Experiments in hearing. New York,: McGraw-Hill.

Wang Y, Manis PB (2008) Short-term synaptic depression and recovery at the mature mammalian endbulb of Held synapse in mice. *J Neurophysiol* 100:1255-1264.

Warr WB (1966) Fiber degeneration following lesions in the anterior ventral cochlear nucleus of the cat. *Experimental Neurology* 14:453-474.

Warr WB (1972) Fiber degeneration following lesions in the multipolar and globular cell areas in the ventral cochlear nucleus of the cat. *Brain Res* 40:247-270.

Wei W, Zhang N, Peng Z, Houser CR, Mody I (2003) Perisynaptic localization of delta subunit-containing GABA(A) receptors and their activation by GABA spillover in the mouse dentate gyrus. *J Neurosci* 23:10650-10661.

Werthat F, Alexandrova O, Grothe B, Koch U (2008) Experience-dependent refinement of the inhibitory axons projecting to the medial superior olive. *Dev Neurobiol* 68:1454-1462.

Williams SR, Mitchell SJ (2008) Direct measurement of somatic voltage clamp errors in central neurons. *Nat Neurosci* 11:790-798.

Wohlfarth KM, Bianchi MT, Macdonald RL (2002) Enhanced neurosteroid potentiation of ternary GABA(A) receptors containing the delta subunit. *J Neurosci* 22:1541-1549.

Wu LG, Borst JG (1999) The reduced release probability of releasable vesicles during recovery from short-term synaptic depression. *Neuron* 23:821-832.

Xu-Friedman MA, Regehr WG (2005) Dynamic-clamp analysis of the effects of convergence on spike

timing. II. Few synaptic inputs. *J Neurophysiol* 94:2526-2534.

Yamada R, Kuba H, Ishii TM, Ohmori H (2005) Hyperpolarization-activated cyclic nucleotide-gated cation channels regulate auditory coincidence detection in nucleus laminaris of the chick. *J Neurosci* 25:8867-8877.

Yang H, Xu-Friedman MA (2008) Relative roles of different mechanisms of depression at the mouse endbulb of Held. *J Neurophysiol* 99:2510-2521.

Yin TC, Chan JC (1990) Interaural time sensitivity in medial superior olive of cat. *J Neurophysiol* 64:465-488.

Zhou N, Parks TN (1993) Maintenance of pharmacologically-immature glutamate receptors by aberrant synapses in the chick cochlear nucleus. *Brain Res* 628:149-156.

Zhou Y, Carney LH, Colburn HS (2005) A model for interaural time difference sensitivity in the medial superior olive: interaction of excitatory and inhibitory synaptic inputs, channel dynamics, and cellular morphology. *J Neurosci* 25:3046-3058.

Zook JM, Casseday JH (1982) Origin of ascending projections to inferior colliculus in the mustache bat, *Pteronotus parnellii*. *J Comp Neurol* 207:14-28.

Acknowledgements

From a long and deserving list of people, the first thank you is for Felix. Thank you for the endless support and for your patience in the face of my ignorance. You let me set my own rhythm and kicked me right when it got too slow. One day, I hope to be able to replicate your favourite magic trick, of transforming a blank sheet of paper into the design for an exciting new experiment (or ten), all in the blink of an eye. Thanks, Doktorvater.

Thank you also to Benedikt, for your solid, supportive presence these past few years. Thanks for sharing a good story over beer and for making time for me whenever I popped my head around the door, or chased you down the corridor.

Thanks to Walter Zieglgänsberger and Christian Leibold for making my TAC meetings such a great place for discussion and to the GRK and GSN for funding and support.

To my family: Mum and Dad, Chris, Fi, Gin, Ash, Nat, Micky and Ant (and my lovely ladies). Thanks for answering my phone calls at the strangest hours and sending the world's most welcome care packages year after year. Most of all, thank you for being proud of me.

When my Australian family was sleeping, my German family was there for me, with large amounts of both coffee and patience. Thanks to my lab homeys Christian and Julian (and honorary lab homey Hanna), for the burgers and the beers, and most importantly for putting up with the crazy. For those who had to share an office with me (Andrea, Ben, Leila and Misku, as if you would forget), thanks for developing so quickly a tolerance for the constant background mumbling and occasional ranting outbursts. Although it might well have been at the cost of your own sanity, you helped me keep mine.

Merci Olive.

To all of these people, and a thousand others in the lab here and around the world, thanks. There is a piece of each of you somewhere in this thesis.

CURRICULUM VITAE



PERSONAL DETAILS

Name	Couchman, Kiri
Address	Karwendelstrasse 40 81369 München
Telephone	+49 (0)89 2180 74369
E-Mail	couchman@bio.lmu.de
Nationality	Australian
Date of birth	26 th of September, 1984

EDUCATION AND STUDIES

2007 – present	PhD student at the Graduate School of Systemic Neurosciences (GSN ^{LMU}) Ludwig-Maximilians Universität, Munich, Germany Division of Neurobiology: Prof. Dr. Benedikt Grothe, Dr. Felix Felmy
Project and Methods	<i>Basal mechanisms underlying dendritic integration in gerbil medial superior olive neurons</i> • electrophysiology in acute brain slices (whole-cell patch-clamp) • single-photon UV-uncaging • immunohistochemistry • confocal microscopy
2005 – 2006	Honours (First Class) in Neuroscience at the John Curtin School of Medical Research, Australian National University, Canberra, Australia Synapses and Hearing Laboratory: Prof. Dr. Bruce Walmsley, Dr. Richardson Leão
Project and Methods	<i>Activity-dependent development of inhibition in auditory brainstem neurons</i> • calcium and voltage-sensitive dye imaging • electrophysiology in acute brain slices (whole-cell patch-clamp) • immunohistochemistry • confocal microscopy
2001 – 2005	B.Sc. (Cell and Molecular Biology) Australian National University, Canberra, Australia
2001 – 2005	B.A. (History and Philosophy) Australian National University, Canberra, Australia

ADDITIONAL QUALIFICATIONS

2009 – 2010	Student representative and member of the Scientific Board of the GSN ^{LMU}
2009 – 2010	Organiser & Participant, 'Talking Science' round table discussion and distinguished speaker programme for PhD students Prof. Markus Meister (2009), Prof. Karel Svoboda (2010)
2009	Teaching, AMGEN Scientific Poster Presentation Course
2009	Organiser & Participant, LMU-Harvard Young Scientist's Forum: From Molecules to Organisms
2008	Supervisor, "Basispraktikum" Practical Course in Neurophysiology (LMU)
2006 – 2007	Laboratory technical officer, Grade 2 Synapse and Hearing Laboratory, Division of Neuroscience (JCSMR, ANU)

FELLOWSHIPS AND FUNDING

2008 – 2011	Stipend of the Deutschen Forschungsgemeinschaft (DFG) and member of the Graduiertenkolleg 1091 "Orientation and Motion in Space"
2007 – 2008	Stipend of the GSN ^{LMU}

ADDITIONAL SKILLS

Languages	English: mother tongue German: good
Computer Skills	Igor (programming), ImageJ, Patchmaster, Axograph, CorelDraw, MS-Office

REFEREES

Prof. Benedikt Grothe	Chair, Dean of Biology Division of Neurobiology, Department Biology II Ludwig-Maximilians-Universität, München, Germany ph: +49 (0) 89 218074300 email: neurobio@lmu.de
Dr. Felix Felmy	Scientific Assistant, Auditory Processing Lab Division of Neurobiology, Department Biology II Ludwig-Maximilians-Universität, München, Germany ph: +49 (0) 89 218074316 email: felmy@bio.lmu.de
Dr. Richardson N Leão	Postdoctoral Scientist, Neural Oscillations Laboratory Nobel Institute for Neurophysiology, Department of Neuroscience Karolinska Institute, Stockholm, Sweden ph: +46 (0) 8 52487354 email: Richardson.Leao@ki.se

LIST OF PUBLICATIONS

in preparation	Couchman K, Grothe B, Felmy F, <i>Functional localization of neurotransmitter receptors and synaptic inputs to mature neurons of the medial superior olive.</i>
published	Couchman K, Garrett A, Deardoff AS, Rattay F, Resatz S, Fyffe R, Walmsley B, Leão RN, (2011) <i>Lateral superior olive function in congenital deafness</i> , Hear. Res.
published	Couchman K, Grothe B, Felmy F, (2010) <i>Medial superior olivary neurons receive surprisingly few excitatory and inhibitory inputs with balanced strength and short-term dynamics</i> , J Neuro.
published	Youssoufian M*, Couchman K*, Shivedasani MN, Paolini AG, Walmsley B, (2008) <i>Maturation of auditory brainstem projections and calyces in the congenitally deaf (dn/dn) mouse</i> , J Comp Neurol. *co-first authorship.

OTHER PRESENTATIONS

poster	Couchman K, Grothe B, Felmy F, (2010) <i>Receptor and synaptic input distribution on neurons of the medial superior olive of the Mongolian gerbil</i> , Poster, Federation of European Neuroscience Society, Amsterdam, Netherlands.
poster	Couchman K, Grothe B, Felmy F, (2009) <i>Distribution and kinetics of synaptic AMPA receptors in adult MSO neurons</i> , Poster, 8 th Göttingen Meeting of the German Neuroscience Society, Göttingen, Germany.
oral presentation	Couchman K, Grothe B, Felmy F, (2009) <i>The distribution of neurotransmitter receptors in neurons of the medial superior olive</i> , LMU-Harvard Young Scientist's Forum, Center for Advanced Studies LMU, Munich, Germany.
poster	Couchman K, Grothe B, Felmy F, (2008) <i>Quantifying the components of glycinergic synaptic transmission to the medial superior olive</i> , Poster, 38 th Annual Meeting of the Society for Neuroscience, Washington DC, USA.
poster	Couchman K, Walmsley B, and Leão RN, (2007) <i>Activity-dependent development of inhibition in auditory brainstem neurons</i> , Poster, 7 th IBRO World Congress of Neuroscience, Melbourne, Australia.

Ehrenwörtliche Erklärung

Hiermit versichere ich, Kiri Couchman, dass die vorliegende Arbeit von mir selbstständig und nur unter Verwendung der angegebenen Hilfsmittel angefertigt wurde.

Kiri Couchman

14th Februar 2011

